VESTAL JR., RICHARD D., Ph.D. Targeting the Atypical Chemokine Receptor ACKR3/CXCR7 for the Treatment of Cancer and Other Diseases. (2015) Directed by Dr. Ethan W. Taylor. 108 pp.

One of the greatest challenges in fighting cancer is cell targeting and biomarker selection. The Atypical Chemokine Receptor ACKR3/CXCR7 is expressed on many cancer cell types, including breast cancer and glioblastoma, and binds the endogenous ligands SDF1/CXCL12 and ITAC/CXCL11. A 20 amino acid region of the ACKR3/CXCR7 N-terminus was synthesized and targeted with the NEB PhD™-7 Phage Display Peptide Library. Twenty-nine phages were isolated and heptapeptide inserts sequenced; of these, 23 sequences were unique. A 3D molecular model was created for the ACKR3/CXCR7 N-terminus by mutating the corresponding region of the crystal structure of CXCR4 with bound SDF1/CXCL12. A ClustalW alignment was performed on each peptide sequence using the entire SDF1/CXCL12 sequence as the template.

The 23-peptide sequences showed similarity to three distinct regions of the SDF1/CXCL12 molecule. A 3D molecular model was made for each of the phage peptide inserts to visually identify potential areas of steric interference of peptides that simulated CXCL12 regions not in contact with the receptor's N-terminus. An ELISA analysis of the relative binding affinity between the peptides identified 9 peptides with statistically significant results. The candidate pool of 9 peptides was further reduced to 3 peptides based on their affinity for the targeted N-terminus region peptide versus no target peptide present or a scrambled negative control peptide.

The results clearly show the Phage Display protocol can be used to target a synthesized region of the ACKR3/CXCR7 N-terminus. The 3 peptides chosen, P20, P3,

and P9, showed no effect on the viability or proliferation upon exposure to MCF-7 and U87-MG cells. Membrane binding, colocalization, and cellular uptake were confirmed by whole-cell ELISA and confocal microscopy. The recovered peptides did not activate the receptor as confirmed by a β-arrestin recruitment assay. The data shows that the peptide sequences recovered from the phage display protocol are viable candidates for targeting cancer cells and delivering material to them.

Keywords: atypical chemokine receptor, glioblastoma, Phage Display, targeted therapy

TARGETING THE ATYPICAL CHEMOKINE RECEPTOR ACKR3/CXCR7 FOR THE TREATMENT OF CANCER AND OTHER DISEASES

by

Richard D. Vestal Jr.

A Dissertation Submitted to
the Faculty of The Graduate School at
The University of North Carolina at Greensboro
in Partial Fulfillment
of the Requirements for the Degree
Doctor of Philosophy

Greensboro
2015

Approved by

_____
Committee Chair

APPROVAL PAGE

This dissertation written by Richard D. Vestal Jr. has been approved by the following committee of the Faculty of The Graduate School at The University of North Carolina at Greensboro.

Committee Chair _____

Committee Members _____

_____

_____

_____
Date of Acceptance by Committee

_____
Date of Final Oral Examination

ACKNOWLEDGEMENTS

I would like to acknowledge the guidance and assistance of my advisor, Dr. Ethan Will Taylor, my committee members, Dr. Dennis R. LaJeunesse, Dr. Jianjun Wei and Dr. Jan Ruzicka and the support provided by the University of North Carolina at Greensboro (UNCG) and the Joint School of Nanoscience and Nanoengineering (JSNN). I would like to acknowledge the assistance of the following JSNN faculty and graduate students: Dr. Chris Kepley, Adam Boseman, Anthony Dellinger, Jesse Plotkin, Kristen Rhinehardt, Stephen Vance, Lee Williams, and Effat Zeidan for their assistance in laboratory techniques and experimental design. I would also like to acknowledge the love and support of my wife Ann Vestal, my mom Gerry Browning and step-dad Steve Browning.

TABLE OF CONTENTS

Page

LIST OF FIGURES viii

CHAPTER

I. INTRODUCTION 1

Current Cancer Treatments and Challenges to Delivery 1
Bypassing the Blood Brain Barrier (BBB) 3
Chemokines and their Receptors 5
The ACKR3/CXCR7 Receptor as a Target 7

II. IDENTIFYING TARGETING MOIETIES 9

Introduction 9
A Promising Duo: MRI and FUS 10
TCGA and the Identification of ACKR3/CXCR7 13
Materials and Methods 16
Comparison and Identification of Sequence Similarities 16
Epitope Mapping of ACKR3/CXCR7 and CXCR4 N-terminus Regions 16
Scrambled Negative Control Sequence Generation 16
Phage Display (Ph.D. ™-7 Phage Display Peptide Library Kit) 17
DNA Sequencing of Phage and Phage Targeting Peptide Sequence Identification 17
Phage Peptide Insert Sequence Characterization 18
Phage ELISA Assay 18
Statistical Analysis of ELISA Data 19
3D Homology Modeling of the CXCR7 N-terminus and Recovered Phage Peptide Structures 20
Results 21
Selection and Generation of ACKR3/CXCR7 Test Peptide and Epitope Mapping 21
Selection and Generation of Scrambled Negative Control Sequence 23
Phage Targeting Peptide Sequence Characterization 23
Comparison with SDF1 26
Phage ELISA Assay 27
3D Homology Modeling of the ACKR3/CXCR7 N-terminus and Recovered Phage Peptide Structures 28

Discussion 29

III. CELL LINE STUDIES WITH SELECTED TARGETING MOIETIES 33

Introduction to Cell Lines 33
Materials and Methods 37
The Effect of Phage Peptide Incubation on the Viability of a Small Population of MCF-7 Cells 37
The Effect of Phage Peptide Incubation on the Viability of a Large Population of MCF-7 Cells 37
The Effect of Phage Peptide Incubation on the Cell Proliferation of MCF-7 Cells 38
Whole-Cell ELISA Confirmation of MCF-7 Cell Membrane Binding by Phage Peptides Using an HRP Conjugated Anti-M13 Antibody with a TMB Substrate and STOP-450 Solution 38
MCF-7 Cells - Membrane Receptor Binding and Cellular Uptake of Phage Display Derived Peptides 39
Negative Control Cell Line THP-1 Cells - Membrane Receptor Binding and Cellular Uptake of Phage Display Derived Peptides 40
The Effect of Phage Peptide Incubation and Length of Initial Growth Cycle on the Viability of U87-MG Cells 40
The Effect of Phage Peptide Incubation and Length of Initial Growth Cycle on the Viability of U87-MG Cells 41
The Effect of Phage Peptide Incubation on the Cell Proliferation of U87-MG Cells 41
Whole-Cell ELISA Confirmation of U87-MG Cell Membrane Binding by Phage Peptides Using an HRP Conjugated Anti-M13 Antibody with a TMB Substrate and STOP-450 Solution 42
U87-MG Cells - Confirmation of Co-Localization of Phage Display Derived Peptides and the Known ACKR3/CXCR7 Antibody, Anti-RDC1 43
Quantifying the Level of ACKR3/CXCR7 Activation Using a PathHunter β-Arrestin Assay (DiscoverX) with the Phage Peptides, the Endogenous Ligand SDF1α, and CHO-K1 Modified Cells 43
Results 44
The Effect of Phage Peptide Incubation on the Viability of a Small Population of MCF-7 Cells 44

The Effect of Phage Peptide Incubation on the Viability of a Large Population of MCF-7 Cells 44
The Effect of Phage Peptide Incubation on the Cell Proliferation of MCF-7 Cells 45
Whole-Cell ELISA Confirmation of MCF-7 Cell Membrane Binding by Phage Peptides Using an HRP Conjugated Anti-M13 Antibody with a TMB Substrate and STOP-450 Solution 45
MCF-7 Cells - Membrane Receptor Binding and Cellular Uptake of Phage Display Derived Peptides 45
Negative Control Cell Line THP-1 Cells - Membrane Receptor Binding and Cellular Uptake of Phage Display Derived Peptides 46
The Effect of Phage Peptide Incubation and Length of Initial Growth Cycle (24 hrs) on the Viability of U87-MG Cells 46
The Effect of Phage Peptide Incubation and Length of Initial Growth Cycle (48 hrs) on the Viability of U87-MG Cells 46
The Effect of Phage Peptide Incubation on the Cell Proliferation of U87-MG Cells 46
Whole-Cell ELISA Confirmation of U87-MG Cell Membrane Binding by Phage Peptides Using an HRP Conjugated Anti-M13 Antibody with a TMB Substrate and STOP-450 Solution 47
U87-MG Cells - Confirmation of Co-Localization of Phage Display Derived Peptides and the Known ACKR3/CXCR7 Antibody, Anti-RDC1 47
Quantifying the Level of ACKR3/CXCR7 Activation Using a PathHunter β-Arrestin Assay (DiscoverX) with the Phage Peptides, the Endogenous Ligand SDF1α, and CHO-K1 Modified Cells 48
Discussion 48

IV . CONCLUSIONS AND FUTURE APPLICATIONS 50

REFERENCES 77

APPENDIX A. 3D MOLECULAR MODELS OF THE LIPOSOME COMPONENTS (C-70 DERIVATIVE (ALM) AND EGG-PC) IN THIN-TUBE MODE AND CPK COLOR SCHEME 94

APPENDIX B. ALTERNATE VIEW OF THE 3D MOLECULAR MODELS OF THE LIPOSOME COMPONENTS IN

APPENDIX A (C-70 DERIVATIVE (ALM) AND EGG-PC)
IN SPACE-FILL MODE AND CPK COLOR SCHEME..... 95

APPENDIX C. 3D MOLECULAR MODELS OF THE LIPOSOME
COMPONENTS IN APPENDIX A AND THE SELECTED
PHAGE PEPTIDE SEQUENCES (P-3, P-9, AND P-20)
IN THIN-TUBE MODE AND CPK COLOR SCHEME..... 96

APPENDIX D. 3D MOLECULAR MODELS OF THE LIPOSOME
COMPONENTS IN APPENDIX A AND THE SELECTED
PHAGE PEPTIDE SEQUENCES (P-3, P-9, AND P-20)
IN APPENDIX C IN SPACE-FILL MODE AND CPK
COLOR SCHEME..... 97

LIST OF FIGURES

Page

Figure 1. CXCR4 and ACKR3/CXCR7 40 Amino Acid N-Terminus Comparison and Epitope Mapping 54

Figure 2. Selection of the Scrambled (Scr) Control Sequence for ELISA Analysis 55

Figure 3. Phage Peptides Insert Coding Sequence Comparison and Predicted Physical and Chemical Properties of the Putative CXCR7 Binding Phages 56

Figure 4. ClustalW Predicted Regions of Similarity for Phage Peptides with the Endogenous Ligand, SDF1 57

Figure 5. Normalized ELISA Results: Phage Peptide Binding to CXCR7 Target or the Scrambled (Scr) Negative Control Peptide 58

Figure 6. 3D Molecular Model of the ACKR3/CXCR7 N-Terminus (F6-D25) 59

Figure 7. 3D Model Representing the Physical Location of Ligand Residues Similar to Peptide P-20 60

Figure 8. 3D Model Representing the Physical Location of Ligand Residues Similar to Peptide P-9 61

Figure 9. 3D Model Representing the Physical Location of Ligand Residues Similar to Peptide P-3 62

Figure 10. 100 nm Liposome Synthesis Using C-70 Derivative (ALM) and Egg-PC (1:2) 63

Figure 11. The Effect of Phage Peptide Incubation on the Viability of a Small Population of MCF-7 Cells 64

Figure 12. The Effect of Phage Peptide Incubation on the Viability of a Large Population of MCF-7 Cells 65

Figure 13. The Effect of Phage Peptide Incubation on the Cell Proliferation of MCF-7 Cells 66

Figure 14. Whole-Cell ELISA Confirmation of MCF-7 Cell Membrane Binding by Phage Peptides Using an HRP Conjugated Anti-M13 Antibody with a TMB Substrate and STOP-450 Solution 67

Figure 15. MCF-7 Cells - Membrane Receptor Binding and Cellular Uptake of Phage Display Derived Peptides 68

Figure 16. Negative Control Cell Line THP-1 Cells - Membrane Receptor Binding and Cellular Uptake of Phage Display Derived Peptides 69

Figure 17. The Effect of Phage Peptide Incubation and Length of Initial Growth Cycle (24 hrs) on the Viability of U87-MG Cells 70

Figure 18. The Effect of Phage Peptide Incubation and Length of Initial Growth Cycle (48 hrs) on the Viability of U87-MG Cells 71

Figure 19. The Effect of Phage Peptide Incubation on the Cell Proliferation of U87-MG Cells 72

Figure 20. Whole-Cell ELISA Confirmation of U87-MG Cell Membrane Binding by Phage Peptides Using an HRP Conjugated Anti-M13 Antibody with a TMB Substrate and STOP-450 Solution 73

Figure 21A. U87-MG Cells - Confirmation of Co-Localization and Cellular Uptake of Phage Display Derived Peptides and the Known ACKR3/CXCR7 Antibody, Anti-RDC1 74

Figure 21B. U87-MG Cells - Confirmation of Co-Localization and Cellular Uptake of Phage Display Derived Peptides and the Known ACKR3/CXCR7 Antibody, Anti-RDC1 75

Figure 22. Quantifying the Level of ACKR3/CXCR7 Activation Using a PathHunter β-Arrestin Assay (DiscoverX) with the Phage Peptides, the Endogenous Ligand SDF1α, and CHO-K1 Modified Cells 76

CHAPTER I

INTRODUCTION

Current Cancer Treatments and Challenges to Delivery

Cancer is one word that no one wants to hear. Instantly images of the effects of chemotherapy and radiation appear in people's minds. Individuals losing their hair, becoming frail and nauseous from the treatments, the loss of energy, isolation from friends and family, trips to the hospital or and many times it ends in death. Standard chemotherapy using anthracyclines such as doxorubicin aka "Adriamycin" or daunorubicin aka "Daunomycin", a vinca alkaloid like vincristine aka "Oncovin", and paclitaxel aka "Taxol" has traditionally attacked the body in a systemic fashion and eventually some of it makes it to the site of the tumor [1]. The protocols typically require multiple applications due to their inefficiency and this in turn increases or prolongs the suffering of the patient.

The drugs used may even have limits on the amounts individuals are exposed to such as the cardiotoxicity associated with anthracycline therapy [2,3]. Researchers were able to show that incorporating the drug within a lipid bilayer, a liposome, for delivery reduces the systemic toxicity by increasing the amount of drug delivered directly to the tumor and reducing the amount available for the rest of the body [4]. Vincristine, an antineoplastic alkaloid, can be lethal or severely neurotoxic depending upon the injection site [5,6]. Paclitaxel can also cause death and hypersensitive reactions such as

hypotension, bradycardia, and hypertension [7]. As these particular examples have shown, sometimes the worst part of cancer is the actual treatment and not the disease itself.

One way to dramatically improve the efficiency of these anticancer treatments is to target membrane bound molecules such as glycoproteins and glycolipids or receptors expressed on the extracellular surface of cancer cells and deliver the material directly to the cells [8-12]. The purpose of these ligand-targeted therapeutics (LTTs) and drug delivery vehicles are to increase deliverability that would in turn decrease the overall amount of chemotherapeutics or other compounds the patient is exposed to and enhance the anti-cancer effect on the tumor cells [1,10,13,14]. The end result is a faster recovery from the reduced side effects and quicker elimination of the targeted tumor cells. The anti-cancer drugs can be allowed to be passively uptaken by the cancer cells or targeted by conjugating them directly to peptides or antibodies (LTTs) [1,10,13,14].

Relying on the passive mechanism requires that the tumor vasculature is present versus its absence in the necrotic regions and the size of your treatment is ~100nm-780 nm in order to make it through the gaps of the leaky endothelial cells [11]. This increased in size of the fenestrate or opening in the tumor blood vasculature from less than ~10nm to roughly 600nm or more is called the enhanced permeability and retention (EPR) effect. If the delivery component is a vehicle like the liposome mentioned for the delivery of doxorubicin and it is less than 200nm, it will be retained in the tumor environment for an extended period of time due to limited or missing drainage by the lymphatic system [15]. This method can not only deliver drugs, like apomorphine, throughout the body but can also deliver imaging agents such as quantum dots (QDs) encapsulated in a 140 nm

liposome across the brains primary defensive mechanism for seclusion and isolation, the blood brain barrier (BBB), for the treatment of CNS cancers and diseases [16].

The size of the molecules or compounds will have a dramatic effect on how the body handles them. Systemic application of liposomes greater than 400nm will typically result in opsonization in the blood followed by rapid uptake by macrophages of the reticuloendothelial system (RES). The uptaken liposomes then primarily accumulate in the liver and spleen; however this accumulation effect may present other problems by quickly lowering the levels of phagocytic cells in these organs while undergoing chemotherapy [17].

Bypassing the Blood Brain Barrier (BBB)

The EPR effect can be useful when targeting tumors outside the central nervous system (CNS). Unfortunately the blood brain barrier does not provide such access and is characterized by a lack of fenestrations and the presence of tight junctions between the endothelial cells. It also contains a combination of influx and efflux transport proteins that monitor the movement of molecules into and out of the brain and blood stream [18]. The continuity of the system can be compromised or altered in the most aggressive and terminal cases of brain cancer, glioblastoma (GBM). It has been shown that the blood brain barrier can remain intact, contain pores up to 3 μM, or have tumors with permeable cores and structurally intact fringes or edges [18].

Given this strong line of defense, without using a highly invasive surgical procedure, other means of crossing or disrupting the blood brain barrier to deliver anticancer compounds and imaging agents to the intracranial space are necessary. There

are several approaches to accomplish this task. The chemical method uses a hypertonic solution of Mannitol or Alkylglycerol to shrink the endothelial cells and create temporary openings [19]. The physical method uses electromagnetic radiation in the form of ultrasonic waves to induce cavitation or the thermal effects of focused ultrasound waves to induce temporary permeability [20,21]. Lastly, permeation enhancers such as the surfactants DMSO and Polysorbate (Tween-80) are used to increase transport across the blood brain barrier [19].

The ability to bypass the blood brain barrier is possible by utilizing intranasal delivery. Using a phage display protocol (Ph.D.-C7C), researchers found a disulfide-constrained heptapeptide that translocated to the brain within 30 minutes. This peptide targeted the brain at a level 50 times higher than non-specific phage peptides and was found in high concentrations along the olfactory nerve post nasal application [22]. The phage display protocol is ideal for this type of desired targeting specificity. Billions of candidate amino acid sequences can be tested simultaneously, and then separated down to the single phage. This provides the ability to isolate individual peptide sequences for further testing of their binding specificity and potential effects on cell proliferation, viability, and downstream signaling. Luckily short peptide sequences or small lipophilic molecules are not the only things that can be delivered via the nasal cavity.

Experimentation has also shown that it is possible to deliver whole cells, neural stem/progenitor cells (NSPCs), via the olfactory pathways and the microvasculature of the nasal mucosa. NSPCs had the ability to intranasally target the main site of glioblastoma xenografts within six hours of treatment as well as small satellite tumors

located away from the main tumor mass. The NSPCs did not accumulate in the brain most likely due the lack of chemotactic signaling molecules, chemokines, generated by the tumors and nearby brain parenchyma [23]. Given the ability to deliver something as large as whole cells, this noninvasive method of treatment deserves further study.

Chemokines and their Receptors

The 7-13 kDa protein signaling molecules or chemokines necessary for NSPC homing to tumor sites are a large family of small cytokines that can be functionally identified in three primary ways: pro-inflammatory for mediating the migration of leucocytes (CXCL11/interferon-inducible T cell alpha chemoattractant (I-TAC)), have critical roles in developmental vasculogenesis and cardiogenesis (CXCL12/stromal-derived factor (SDF-1)), and maintaining homeostasis via regulation of stem cell pools for tissue renewal and tissue repair (CXCL12/SDF-1) [24,25]. The chemokines are divided into five groups or families (CC, CXC, CX3C, CX, and XC) and named for the location of two N-terminal residues of four cysteines and the number of amino acids between them or lack of one of the cysteines. For example, in the CC chemokines the cysteines are next to each other with no amino acids between them. In the CXC chemokines, there is one amino acid between the cysteines and in CX3C there are three amino acids between the cysteines.

The CXC chemokines are also structurally considered ELR-positive or ELR+ due to the presence of a three amino acid motif (Glu-Leu-Arg or "ELR") just ahead of the first cysteine residue or ELR-negative (ELR-) if it is missing [26-30]. Typically the presence or absence of the ELR motif defines the role of the chemokine as pro-

angiogenic (+) or anti-angiogenic (-). This is not the case for CXCL12/SDF1 which is (ELR-) and pro-angiogenic and yet CXCL11/I-TAC is also (ELR-) and it is anti-angiogenic [26-30]. In glioblastomas (GBMs), the transformation of gliomas to malignant high-grade GBMs is characterized by a large increase in vasculature and is considered to be instrumental for tumor growth. This flipping of the "angiogenic switch" is influenced increased levels of pro-angiogenic factors including chemokines and their associated receptors [30-32]. Given that angiogenesis is considered a "hallmark" of cancer, the ability of ACKR3/CXCR7 to bind both of these chemokines and either promote or inhibit angiogenesis or vasculogenesis shows just how important it is to the maintenance of the tumor environment [26-35].

All of the receptors for chemokines are named for the class of chemokine they bind and all are known to be seven-transmembrane G protein coupled receptors due to their activation of intracellular signaling pathways via G proteins [24,25]. This can be seen in the receptors for the previously mentioned CXCL11 and CXCL12. The receptors for these two chemokines are CXCR4 and CXCR7. It is important to note that the CXCR7 receptor is classified as atypical, hence it`s renaming to ACKR3/CXCR7, due to its ability to activate signaling pathways via β-arrestin-2 proteins and not G coupled proteins [36]. The ACKR3/CXCR7 receptor still holds some secrets as there is evidence to show that it can activate the Erk1/2 and Akt pathways via $G_{i/o}$ proteins upon stimulation with either CXCL11/12 in primary rodent astrocytes and human glioma cells [37].

Although chemokines and their receptors are only found in vertebrates, there are homologues to these genes in some viral genomes implying the sequences have been

acquired by these viruses to increase their infectivity [24,25]. The seven transmembrane domain receptors for chemokines also contain a highly conserved sequence (DRYLAIV) in their second extracellular loop which is necessary for the coupling of G proteins and downstream activation of signaling pathways [38-40]. This is reflected in the altered sequence of ACKR3/CXCR7 (DRYLSIT) [34]. It would appear the divergent sequence is different enough to initiate β-arrestin-2 signaling in some cells and similar enough to initiate $G_{i/o}$ signaling in others [38-40]. Based on all of the previous information, it is easy to see that the atypical chemokine receptor ACKR3/CXCR7 is an important target for anti-cancer therapy.

The ACKR3/CXCR7 Receptor as a Target

The ideal candidate for targeting multiple cancer types would therefore be present in large numbers on the extracellular surface and have the ability to internalize drugs, compounds, or genetic material once they are bound to the surface [1,41]. ACKR3/CXCR7 is expressed at high levels on multiple cancer cell types and vasculature associated cells such as endothelial progenitor cells (EPCs). ACKR3/CXCR7 was shown to be necessary for increased EPC proliferation, anti-apoptotic effects, and cell-to-cell adhesion [42,43]. It has also been associated with angiogenesis in at least five types of cancer including prostate, hepatocellular carcinomas, bladder, kidney, and meningioma [33,44-50]. ACKR3/CXCR7 plays an integral role in the proliferation of roughly nine types of cancer that also include breast, lung, pancreatic adenocarcinoma, cervical, colorectal, and gliomas [51-61]. This receptor has also been implicated in the metastasis or migration

of over ten different type of cancer. Some of those not previously mentioned are liver, rhabdomyosarcoma, and neuroblastoma [62-64].

ACKR3/CXCR7 has the ability to recycle between the plasma membrane and the cytoplasm without the need for ligand binding and activation of the receptor making it a highly desirable target [65,66]. All of the previously mentioned properties were taken into consideration when we were identifying our target of interest the atypical chemokine receptor ACKR3/CXCR7. Additionally, the characteristics necessary for blood brain barrier passage was into consideration in order to determine the vehicles size and type of materials we wanted to use in the design of our delivery vehicle. We chose a 100 nm liposome made of a C-70 fullerene derivative and egg-PC for its drug loading capabilities and its ability to quench reactive oxygen species (ROS) [67]. Low levels of ROS in the extracellular environment are involved in carcinogenesis and the ensuing cancer progression. The ability to scavenge these particles may prove beneficial to the treatment by reducing the level of oxidative stress if inducing high levels of ROS are not part of the protocol [68]. The search for a targeting moiety specific to ACKR3/CXCR7 begins there.

CHAPTER II

IDENTIFYING TARGETING MOIETIES

Introduction

The identification of cancer cell biomarkers is a driving force in research today. The transformation of normal cells into cancerous ones makes the identification of cancer cell specific markers extremely difficult. Many of the cancer associated genes are not novel and will simply be overexpressed. The overexpression of a plasma membrane bound target such as a cell-surface receptor provides the opportunity to fine tune a targeted approach for the delivery of drugs, diagnostics, theranostics, and genetic material [69]. For the identification of cancer associated genes and biomarkers, a major source is The Cancer Genome Atlas (TCGA). The cancers chosen have reduced survival rates and a large impact on the health and well-being of the general public (www.cancergenome.nih.gov/).

The first cancer studied by TCGA was glioblastoma (GBM), the most common, aggressive, and lethal type of CNS cancer [70,71]. The average survival time post diagnosis is currently 15 months and there are no successful long-term treatments available (http://cancergenome.nih.gov). Treatment is limited due to the intracranial location and restrictive nature of the blood brain barrier [21]. Resection, chemotherapy, and radiation treatments have typically only slowed the progression of the disease by few months. Personal experience has seen the survival time to be less than 10 months. Over

14,000 people are expected to die in the United States from CNS tumors in 2014, a nearly 9% increase in just the last four years (www.cancer.gov/). At this rate in the United States in 2018, on average at least one person every single day in each of the 50 states will pass away from CNS tumors.

Breast cancer was also selected by TCGA for analysis. In the United States, this form of cancer primarily affects females and is diagnosed in males less than two percent of the time. In women, breast cancer is the most common form of cancer and only trails lung cancer in the number of cancer related deaths (www.cdc.gov/). There were over 207,000 cases of female breast cancer in 2010 and over 19% or approximately 40,000 related deaths (http://cancergenome.nih.gov). Years of research and early detection through education and mammograms have reduced the ratio of deaths per diagnosis.

The number of new female cases is expected to climb above 232,000 in 2014, with the number of predicted deaths near 17%, or again remaining at 40,000 (www.cancer.gov/). Although 40,000 deaths is significant, that number would be over 4,640 higher if the ratio had remained the same as in 2010. If the detection rate in women maintains its current pace, there will be over 260,000 newly diagnosed cases in 2018. As the numbers indicate, the ability to target and treat breast cancer and GBM cells would be extremely beneficial to hundreds of thousands of people in the United States alone.

A Promising Duo: MRI and FUS

The major drawbacks to current cancer therapy are the effects that chemotherapy and radiation have on the patients. The debilitating side-effects include loss of hair, appetite, and energy, a constant flu-like feeling, and the destruction of otherwise normal

cells due to the systemic application of treatments. Cancer patients would have a better chance of a quicker and less strenuous recovery if their bodies did not have to deal with the extra burden placed upon them by the administration of current anti-cancer therapies and invasive surgeries. An extremely promising noninvasive treatment option initially developed at Brigham and Women's Hospital, magnetic resonance imaging guided focused ultrasound surgery (MRgFUS), was first approved by the FDA in 2004 for the treatment of uterine fibroids and again in 2012 for alleviating the pain associated with bone metastases [72-74].

The incorporation of MRI allows for the 3D identification of the tumor volume and real-time monitoring of local temperature increases and the accumulation of necrotic regions. The technique utilizes multiple ultrasound transducers and focuses the beam paths to a cigar shaped central location of the tumor mass to induce localized rapid heating at>70^0C, to thermally ablate the cells or it can be used to induce cavitation and mechanically destroy the cells [75-77]. Research has shown the technique to be a viable option in multiple cancer types including liver, kidney, prostate, and breast [78-83]. These types of cancer are typically easier to access and the soft tissues are ideal for MRI. As with many things, location matters. The efficiency of the technique is affected by the location of the tumor and the surrounding environment.

Given the importance of location, intracranial cancers such as GBM make them some of the most difficult to attempt to treat. The MRgFUS protocol applied to GBM is referred to as transcranial MRI-guided focused ultrasound surgery (TcMRgFUS) and was used with limited success in 2010 [84]. The protocol allows for multiple applications with

none of the side effects of standard chemotherapy and radiation. Two of the major challenges associated with the treatment include properly identifying the tumor`s peripheral boundaries to target the focal point of the beam paths and beam distortion or secondary skull heating due to variations in skull`s thickness and density [85-87].

Attempts to handle the beam distortion and secondary heating have been made with the addition of multiple transducers and constant software monitoring of temperature changes. The highly invasive nature of GBM makes the identification of all of the tumor`s finger-like projections nearly impossible and will most likely require additional components such as chemotherapeutics or genetic material like siRNA in order to be a complete regimen [88,89]. The procedure could therefore be enhanced by delivering contrast agents to the tumor to more properly define the tumor periphery and thereby allow a more aggressive and/or more precise application of the ultrasound treatment.

The power of TcMRgFUS can also be harnessed to increase access to the intracranial space by temporarily making the blood brain barrier more permeable to compounds or molecules and it can also be used to activate or release certain thermo-sensitive components or make cells more susceptible to uptake chemotherapeutics, diagnostics or theranostics from the extracellular environment [20,21]. These additional properties can be used to reduce the systemic effect of chemotherapeutics and increase the efficiency of applied therapies. Targeting a plasma membrane component such as a receptor would allow for the delivery of these materials and thereby increase the overall efficiency of the procedure. Chemokine receptors are known to be associated with the enhanced progression, increased severity, elevated morbidity rates of different types of

cancers, and are typically overexpressed in these conditions [26,29,50,90]. For our purposes, the ideal target would then be an overexpressed plasma membrane receptor that upon binding a compound or molecule will internalize it and deliver material to the cytoplasm without requiring activation of the receptor.

TCGA and the Identification of ACKR3/CXCR7

Our search began with the datasets at TCGA due to their wealth of sequence data for multiple cancers and the pre-selection criteria for the cancers studied. TCGA has identified the 668 most overexpressed genes in glioblastoma and two plasma membrane associated chemokine receptors are in the top 200, CXCR4 and CXCR7 [70,73]. The endogenous ligand for this pair of receptors, SDF1/CXCL12, was not on the list of overexpressed genes [70,91-94]. These receptors have been associated with enhancing angiogenesis, tumor growth, intravasation, and metastasis of tumor cells in multiple types of cancer [61,95-101]. These receptors have also been shown to increase the progression of WHIM syndrome and the infectivity of several strains of immunodeficiency viruses (HIV-1, HIV-2, and SIV) [102-105]. CXCR7 is also associated with the increased infectivity and proliferation of cells infected with Epstein-Barr virus (EBV), Human T-lymphotropic virus type 1 (HTLV-1), Kaposi's sarcoma–associated herpes virus (KSHV), and human papillomavirus (HPV) [54,106-108]. The ability to target one or both of these receptors has broad implications for diagnostic, theranostic, and drug delivery capabilities.

The discovery of a CXC-chemokine, CXCL12 or stromal cell-derived factor 1 (SDF1), binding to the LESTR/fusin receptor resulted in the renaming of the receptor to

CXCR4 [109]. CXCR4 was presumed to be the sole receptor for SDF1 and has been well characterized including the elucidation of the receptor`s crystal structure bound to the SDF1/CXCL12 ligand [110]. The other receptor, CXCR7, was originally identified as RDC1 [111,112]. Shortly after discovery, the receptor was misidentified as a vasoactive intestinal peptide (VIP) receptor [113,114] and later reclassified as an orphan G-protein coupled receptor [115]. It was also known as RDC1/GPRN1 and predicted to exist as two tissue specific subtypes which bound an unknown ligand [116]. In 2005, the RDC1 receptor was shown to also bind SDF1 in the presence of CXCR4 and this resulted in the renaming of the receptor to CXCR7 [93]. Like other chemokine receptors, CXCR7 has more than one ligand and it has been shown to bind interferon-inducible T-cell alpha chemoattractant (I-TAC/CXCL11), a known ligand of CXCR3 [51,63].

The role of CXCR7 in cellular processes varies from the apparent scavenging of SDF1 and I-TAC as it constantly recycles between the plasma membrane and intracellular regions, due to atypical β-arrestin signaling instead of the G-protein signaling typically associated with GPCRs [37,61,65,117]. Additionally, CXCR4 and CXCR7 have been shown to heterodimerize and work together to mediate the response to the presence of SDF1/CXCL12 [94,95,101,118]. CXCR7 mRNA is typically expressed at low levels and often only intracellularly expressed in several types of normal tissues and cells, including several types of leukocytes, differentiated neurons, and vascular endothelial cells [93,119-121]. CXCR7 protein overexpression results in or increases expression at the plasma membrane and has been associated with multiple types of cancer, including breast, renal cell carcinoma, pancreatic, neuroblastoma, glioblastoma, papillary thyroid

carcinoma, lung, colon, melanoma, Schwann cell and meninges tumors, endometrial, prostate, and bladder [29,44,48,50,52,59,60,98,100,101,122-124]. The knowledge base of CXCR7 continues to evolve and the receptor was recently reclassified as the atypical chemokine receptor ACKR3 [125].

A highly specific and productive method for the identification of cell targeting moieties is the phage display protocol. This method allows for the rapid identification and isolation of peptides that will bind the target of interest. The peptides have the distinct advantages of being easily reproducible, inexpensive, and stable for long term storage, versus the production time and costs and potential immunogenicity of monoclonal antibodies (mAbs) [1]. The protocol has been successfully used to target a variety of cancers and membrane components including gliomas [126,127], prostate cancer [128,129], cancer stem cell-associated marker CD133/Prominin-1 [130], breast cancer [97,131,132], gastric cancer [133], ovarian cancer [134], endometrial cancer [98], and primary Medullary Thyroid Carcinoma [135].

The results of these experiments indicate that the phage display protocol could be used to target CXCR4 or CXCR7. Using a synthesized portion of the N-terminus region of ACKR3/CXCR7 and modified M-13 phages, we identified and characterized 23 candidate amino acid sequences with an affinity for this region. Further side by side ELISA comparison reduced that number to three. Our findings imply that the identified peptide sequences could be used to target the membrane bound form of ACKR3/CXCR7 and thereby regulate its response or availability to the endogenous ligand SDF1/CXCL12 and viral particles.

Materials and Methods

Comparison and Identification of Sequence Similarities

The amino acid sequences from ACKR3/CXCR7 (www.uniprot.org/uniprot/P25106) and CXCR4 (www.uniprot.org/uniprot/P61073) were recovered from UniProtKB and loaded into the sequence alignment editor BioEdit (www.mbio.ncsu.edu/bioedit/bioedit_backup.html) for alignment.

Epitope Mapping of ACKR3/CXCR7 and CXCR4 N-terminus Regions

Epitopes were identified using IEDB Analysis Resource Antibody Epitope Prediction tool <http://tools.immuneepitope.org/tools/bcell/iedb_input>. Three methods were used: Emini Surface Accessibility Prediction, Kolaskar & Tongaonkar Antigenicity, and Bepipred Linear Epitope Prediction. The sequences for the ACKR3/CXCR7 and CXCR4 N-terminus regions were analyzed independently of each other.

Scrambled Negative Control Sequence Generation

The scrambled negative control sequence was generated using EMBOSS 6.3.1: shuffleseq software (<http://mobyle.pasteur.fr/cgi-bin/portal.py?#forms::shuffleseq>). The ACKR3/CXCR720 amino acid N-terminus sequence (FDYSEPGNFSDISWPCNSSD) was entered and 100 runs were performed. The chosen scrambled sequence had the least sequence similarity. A cut-off value of no more than three identical amino acids in a row (sequence or group) in either the forward or backward direction with the ACKR3/CXCR7and CXCR4 N-terminus template regions was used to eliminate candidate sequences. The Scrambled peptide fragment was purchased from Bio-Synthesis (www.biosyn.com/).

Phage Display (Ph.D. ™-7 Phage Display Peptide Library Kit)

The target ACKR3/CXCR7 N-terminus region peptide was purchased from Bio-Synthesis (http://www.biosyn.com/). The Surface Panning Procedure (Direct Target Coating) was used following the manufacturers protocols for phage capture (Ph.D. ™-7 Phage Display Peptide Library Kit - New England BioLabs NEB). Three rounds of selection were performed. Individual phages (blue plaques) were then amplified separately at 37°C for 4.5 hours in an overnight ER2738 culture diluted 1:100 in LB. The solutions were centrifuged for 14,000 rpm for 30 seconds. The supernatants were transferred and respun. The upper 80% of each was retained, diluted 1:1 with sterile glycerol, numbered, and stored at -20°C. Prior to storage, the phage stocks were titered to confirm they were above the desired 10^{20} plaque forming units (pfu) per 10 µl level.

DNA Sequencing of Phage and Phage Targeting Peptide Sequence Identification

Eurofins MWG Operon (www.operon.com/default.aspx) sequenced 3 rounds of samples 3 times each, 29 samples total, and the nucleotide sequences were saved as .ab1 files on their website. The stored .ab1files were loaded into the assembly editor, BioLign (www.mbio.ncsu.edu/bioedit/bioedit_backup.html), for chromatogram analysis to identify unknown nucleotides in the region of interest. Any unnamed base calls, designated "N" in the.ab1files, were identified by systematically comparing multiple sequencing runs of the same sample, identifying and declaring the most probable nucleotide for that position, and then saving the updated sequence file as a .gb file. The .gb files were loaded into the sequence alignment editor BioEdit, reverse transcribed, NEB insert bookend sequences identified, and the inserted heptapeptide region of the

M13 genome used in targeting was identified. Identical amino acid sequences were analyzed for experimental procedure cross-contamination by comparing the original nucleotide sequences (.ab1 files) against each other.

Phage Peptide Insert Sequence Characterization

Each phage heptapeptide insert sequence was characterized with the EXPASY ProtParam tool (http://web.expasy.org/protparam/) for theoretical isoelectric point (pI), estimated half-life, instability index, aliphatic index, and grand average of hydropathicity (GRAVY). A ClustalW sequence alignment (BioEdit) was performed individually for each recovered peptide sequence against the endogenous ligand SDF1. Regions of the SDF1 ligand that showed similarity to the phage insert sequences were located and these residue positions identified and entered into an Excel spreadsheet. The identified SDF1 residues were then highlighted by themselves in Maestro alongside the mutated ACKR3/CXCR7 N-terminus 3D model in order to confirm that candidate SDF1 residues were in a position to bind the N-terminus target.

Phage ELISA Assay

To coat a 96-well microplate for ELISA, four wells were used to test each phage: 2 wells with ACKR3/CXCR7N-terminus (1 experimental well with phage and 1 blank no-phage negative control, 1 Scrambled peptide negative control well, and 1 BSA blocked/No-target negative control well. Individual wells were incubated overnight with50 µls of one of the following solutions: (2 wells) 10 µg/ml solution of the ACKR3/CXCR7N-terminus target, (1 well) a 10 µg/ml solution of the Scramble peptide, and (1 well) a BSA 5mg/ml solution, all solutions in 0.1 M $NaHCO_3$ pH 8.6, at 4°C with

gentle agitation. The coating solutions were removed; the plate was blocked with BSA, and then washed with TBST. The 23 phage samples were randomly divided into 3 groups for plating and these groups of phages were tested together on the same day using separate wells in a 96-well microplate.

Except for the Blank No-phage negative control, individual wells were incubated with 100 µl of a single phage stock at room temperature for 2 hours with gentle agitation. The phage solution was removed and the wells were washed with PBS(1X). A 100 µl solution of anti-M13 antibody (anti-M13-HRP conjugate, GE Healthcare #27-9421-01) diluted 1:1000 in PBS(1X) was added to each well and allowed to incubate for 2 hours at room temperature. The antibody was removed and the plate was washed with PBS(1X). 100 µls of the TMB ELISA Substrate Slowest Kinetic Rate (Abcam - ab171527) was added and allowed to develop for 40 minutes. The reaction was stopped by adding 100 µls of the 450 nm Stop Solution for TMB Substrate (Abcam - ab171529). Each phage was tested a total of three times over three different days. The plates were read on a BioTek microplate reader at 450 nm and the values were exported into an Excel spreadsheet.

Statistical Analysis of ELISA Data

The raw data was initially arraigned into 9 tables (3 sets x 3 trials) with 7 or 8 phage samples per table. The data was standardized using the average Blank No-Phage Negative Control values from trial 1 as the standard level of background noise. The standard No-Phage Negative Control value was divided by each of the remaining 8 Blank No-Phage Negative Control values on a plate by plate basis in order to determine the

conversion factor for each plate. The conversion factor for each plate was applied to all values within that plate. The new values were normalized by subtracting the standard background noise baseline value from all of the remaining values on that plate.

Individual normalized values for each phage were then grouped into 3 tables for statistical analysis (t-Test: Paired Two Sample for Means). The values from the 3 trials were then grouped as follows: (1) Experimental values vs No CXCR7 Negative Control values and (2) Scrambled peptide values vs No CXCR7 Negative Control values. The Level of Significance used was 5% (Alpha $\alpha = 0.05$). The threshold cutoff values used were: * t-test Critical one-tail = 2.92 and ** t-test Critical two-tail= 4.30. Vertical error bars in both directions were set based on the Standard Error Margin (SEM).

3D Homology Modeling of the CXCR7 N-terminus and Recovered Phage Peptide Structures

Maestro Version 9.2.112 - MMshare Version 2.0.111 - Windows-x64 software was used for 3D homology modeling and Phage Peptide construction. The 38 residue N-terminus of the CXCR4 crystal structure with endogenous ligand SDF1/CXCL12 bound to it (PDB ID: 2K04) served as the template model [[110]]. The N-terminus residues 1-38 of CXCR4 were trimmed to residues 6-25 (IYTSDNYTEEMGSGDYDSMK). This sequence was saved as a Maestro project or ".prj" file. This .prj file was reloaded and then mutated to the corresponding N-terminus residues (6-25) of ACKR3/CXCR7 (FDYSEPGNFSDISWPCNSSD) and saved as a separate .prj file. The transformation of the CXCR4 sequence into ACKR3/CXCR7 was accomplished by selecting individual residues of the CXCR4 sequence and then mutating them into the

ACKR3/CXCR7sequence using the “Mutate Residue” command. Due to identical sequence similarity at positions S9 (Ser9), S18, and S23 between CXCR4 and ACKR3/CXCR7, these Serine residues were used as anchor locations for the necessary sequence mutations into ACKR3/CXCR7.

The two individual .prj files (CXCR4 N-terminus and ACKR3/CXCR7 N-terminus) were imported into the same workspace and overlaid upon each other. Stacking the two individual chains of CXCR4 and ACKR3/CXCR7, using only Chain D for each (Ball and Stick or Tube Mode) in this manner made it possible to include the bound SDF1/CXCL12 residues 3-67 (Chain C in CPK mode) in their original positions. This method of stacking made it possible to identify potential steric conflicts due to mutation of the previously existing CXCR4 residues. Potential steric conflicts were resolved using commands such as “Adjust - Quick Torsion” or “Adjust - Angle” on each mutated residue. The 7-amino acid sequence of each of the identified 23 Phage Peptide sequences was transformed into a 3D model and saved as individual PDB (.pdb) files. The models were constructed using commands such as “Build - Fragments - Amino Acids.”

Results

Selection and Generation of ACKR3/CXCR7 Test Peptide and Epitope Mapping

There is no crystal structure of ACKR3/CXCR7 in the RCSB PDB database (www.rcsb.org/pdb/home/home.do); however there is a structure of the related receptor CXCR4. To generate a test target peptide that takes into consideration structural and domain elements that may be important for the selection of putative targeting peptides that work *in vivo*, we used the extra cellular N-terminal peptide sequence of CXCR4 as a

backbone model. The ACKR3/CXCR7N-terminus was numbered M1-K40 and the CXCR4 N-terminus was numbered M1-K38. As seen in Figure (1), both 20 amino acid N-terminus regions have a Serine (S) residue at positions 9, 18, and 23. The Ser18 residue in ACKR3/CXCR7and CXCR4 is the site of O-linked Glycosylation. In addition, CXCR4 has post-translationally modified residues (N-linked Glycosylation or Sulfonation) at Y7, N11, Y12, and Y21 and two β-sheet folds. One is at S9-N11 starting with a serine residue and ends with an asparagine residue. The other is at Y21-S23 starting with a tyrosine and ending with a serine (www.uniprot.org/uniprot/P61073). ACKR3/CXCR7 has predicted or verified corresponding similarly modified residues at Y8, N13, and N22 and a β-sheet fold at S9-N13 that also starts with a serine residue and ends with an asparagine residue (www.uniprot.org/uniprot/P25106).

To identify and characterize potentially important epitopes within the N-terminus of ACKR3/CXCR7, we performed comparisons on both CXCR4 and ACKR3/CXCR7 as shown in Figure (1). Analysis of the N-terminal CXCR4 region revealed four epitopes. Three of these (Kolaskar & Tongaonkar I4-D10 and M24-E31, Bepipred Linear Epitope S9-E31) spanned portions of the 20 amino acid region isolated and one (Bepipred Linear Epitope N33-A34) was outside this region. A complimentary analysis of the homologous region of ACKR3/CXCR7 examined contained three complete epitopes identified by sequence analysis and includes part of a fourth area as shown in Figure (1). The complete epitopes included the area identified by Emini Surface mapping F6-N13, the two regions identified by Bepipred Linear Epitope mapping S9-I17, and W19-N22. The fourth area identified by Kolaskar & Tongaonkar mapping spanned I17-P35 and extended 10 AA`s

beyond the targeted region. However, the first 9 AA`s (17-25) were included in the target region. From this analysis we selected a 20 amino acid sequence from ACKR3/CXCR7that we used for the phage display screen.

Selection and Generation of Scrambled Negative Control Sequence

Based on a comparison of the EMBOSS 6.3.1: shuffleseq software generated sequences and the corresponding (ACKR3/CXCR7)/CXCR4 regions; the sequence (SWESFPNDCSYGDNDFSPIS) was the only scrambled variation to meet the necessary criteria as seen in Figure (2). Scrambled regions that were identical or similar to ACKR3/CXCR7or CXCR4 were identified and highlighted. Three of the eliminated candidate sequences, Example 1, 2, and 3, and the legend for amino acid grouping and classification have been included for comparison in Figure (2).

Phage Targeting Peptide Sequence Characterization

Using this 20 amino acid region, we performed a phage display screen using a 7 amino acid M13 phage library (NEB). The initial phage display experiments produced over 100 candidate plaques and 30 of those were selected for analysis. Prior to sequence analysis; the 30 phages had been labeled P-01 to P-24 and C1-C6. The amino acid sequences for 29 of the 30 phage inserts were successfully identified as seen in Figure (3).No usable sequence data was recovered from phage P-12. Of these 29 amino acid sequences, 23 were unique. No evidence for cross-contamination for the identical sequences was found after a comparison of their nucleotide sequences as shown in a comparison of the coding sequences in Figure (3).The results of the EXPASY ProtParam analysis (Isoelectric point (pI), estimated half-life, Instability Index, Aliphatic Index, and

GRAVY) yielded a wide variety of values across the categories and are listed in Figure (3).

The pH at which these peptides would have a neutral charge, the isoelectric point or pI, showed values that ranged from 5.24 (P-08, P-C4, and P-06) up to 12.00 (P-18 and P-17). Of the 29 identified putative ACKR3/CXCR7 targeting peptides, 15 had pI values of less than 6.00 and 6 had a value of 9.77 (±0.02). The influence of the positively charged arginine (R) and lysine (K) residues versus the negatively charged aspartic acid (D) and glutamic acid (E) residues is reflected in the pI values. There were multiple peptides with an (R) or (K) residue and they had pI`s above 8.44, all but one was ≥9.75. The presence of 2 (R) residues increased the pI to 12.00. Peptides P-08 and C4, with a single (E) residue, had lower pI values of 5.24. Peptides P-02 and P-09 contained a (D) and an (R) residue and their values were slightly higher at 5.50 and 6.74 respectively.

To determine the potential lifespan *in-vivo* or the usable working time limit of the recovered peptide sequences, it was necessary to calculate the amount of time required to degrade the peptide. The estimated in-vivo half-life for each peptide sequence was calculated using the N-end rule [[136-138]]. The values were calculated using mammalian (rabbit reticulocytes) cells as the host organism. Peptides P-3 and P-5 showed the fastest overall degradation rates with a value of 0.8 hrs. Peptides P-07 with valine (V) or P-16 and C1with glycine (G) at the N-terminus had the slowest rate of degradation rates of 100 hrs and 30 hrs. Peptides with an arginine (R) or glutamine (Q) at the N-terminus had the fastest degradation rates, ≤1hr. Therefore, peptide P-7 could remain viable in the system for 100 times longer than peptides P-3 and P-5. Another representation of a peptides

intracellular stability is the Instability Index. This value takes into consideration the combinations of dipeptides within a sequence and not just the amino acid represented at the N-terminus. The Instability Index (II) was predicted for each peptide and values less than 40 were considered to indicate a stable protein [139]. The five peptide sequences predicted to be the most stable were P-08 (-7.67), C-2 (-10.36), P-07 (-12.90), C-1 (-17.01), and P-04 (8.80). Peptide P-18 was predicted to be the least stable with the highest II at 133.30 and would therefore break down the quickest. A peptide sequence such as C-1 would be expected to survive in the system for the longest period of time and be available in a larger time window for targeting the cells of interest.

The Aliphatic Index is indicative of the alanine (A), valine (V), isoleucine (I), and leucine (L) content of the recovered peptides and increasing values are considered to reflect increasing thermostability [140,141]. The hydrophobic natures of these residues are different from those of aromatic amino acids and are a primary contributing factor to the increase in thermostability. The calculated values range from 0.00 for peptides P-06, P-09, and C-2 that contained none of those residues up to 208.57 for peptide P-08 that contained one each of the (I) and (L) residues and two (L) residues. The majority of the values were ≥ 55.71 with only eight of the values ≤ 28.57. Peptide C-1 had a value of 14.29 and would be less stable than P-08 at elevated temperatures. The results here are indicative of the thermal relationship associated with the Aliphatic Index. The Aliphatic Index for P-08 is over 14.6 times higher than the value for C-1. The Instability Index (II) for C-1 was only 2.2 times higher than the value for P-08. The stability of these two peptides varies greatly when temperature is a concern.

Whether or not a particular peptide sequence is hydrophilic or hydrophobic will affect how it is modified or utilized later and may impact the number of ways it can be incorporated into a protocol. Hydrophobic components such as cholesterol are known to self-assemble and insert themselves in lipid bilayers such as those associated with cellular membranes and liposomes. Extremely hydrophobic peptide sequences functionalized to cholesterol could potentially interfere with their ability to self-assemble properly and orient the conjugated molecule with the peptide sequence exposed to the exterior environment and the cholesterol component imbedded within the bilayer. The hydrophilic or hydrophobic nature of the peptides was determined by calculating the grand average of hydropathicity (GRAVY). This same technique has been used to predict the location of membrane spanning portions of proteins and receptors based on the hydrophobic nature of the residues examined. The level of hydropathicity was based on using isoleucine (I) as the most hydrophobic at +4.50 and arginine(R) as the most hydrophilic at -4.50 [142].The scores varied from +1.143 for peptide P-08 to -2.543 for peptide P-09. The majority of the sequences were of a hydrophilic nature as there were only six peptides with positive values.

Comparison with SDF1

To determine whether the identified peptides mimicked the ligand of the ACKR3/CXCR7 receptor, SDF1, we performed a ClustalW analysis comparing the identified peptides to the protein sequence of SDF1 as seen in Figure (4). The entire 93 amino acid sequence of SDF1 (www.uniprot.org/uniprot/P48061) was used for the analysis to include all potential binding regions of the molecule [51,93,118,143,144]. A

ClustalW analysis indicates the recovered putative ACKR3/CXCR7 targeting peptides fell into three clusters. None of the peptides were predicted to mimic the first 20 residues of the endogenous ACKR3/CXCR7 ligand as seen in Figure (4). The three clusters consist of SDF1 residues 26-35, 51-55, and 71-85 and showed similarity with ≥25% of all peptide sequences tested.

The number of similar sequences was highlighted in yellow. Due to the presence of identical sequences, the sequence for peptide P-13 was used to represent P-13 and P-19. Also, the sequence for peptide P-24 was used to represent peptides P-24, P-14, P-15, P-21, P-22, and P-23. There were 23 sequences total subjected to analysis. Using the sequence data for SDF1, the sequence positions of the SDF1 activation motif, Heparin and receptor binding sites, and structural elements (turn, β-strand, α=Helix) were identified and noted above the SDF1 sequence in Figure (4). Peptides P-16 and P-20 were the only two sequences predicted to simulate the activation motif and only nine sequences were predicted to simulate regions outside those known to bind Heparin or a receptor.

Phage ELISA Assay

To determine the specificity and relative affinity of binding of our 23 putative ACKR3/CXCR7 targeting peptides to the original peptide target performed an ELSA assay using phage against the original target peptide. The values for each ELISA were normalized to a control plate with no target and to control with scrambled peptide Figure (5). The goal was to identify peptides which have specific binding to the target peptide and showed no non-specific-binding to either the BSA treatment polypropylene surface

or 20 amino acid peptide coated surfaces. When compared to a peptide binding a surface without a ACKR3/CXCR7 target, we found a broad range of relative binding efficiencies with Peptide P-20 having the highest value at 10.3 (ten times greater than no target alone) and P-08 had the lowest at 1 (no better than no target). A statistical analysis of the data reveal that only nine peptides had a value greater than 2.92 which was determined to be the significant difference from control (Figure 5). Paired Two Comparison of the binding of the putative ACKR3/CXCR7 targeting peptides to the scrambled peptide revealed that only eight peptides showed significant binding to the scrambled peptide (Figure 5). From these results, five identified peptides showed specific high binding to the target peptide versus the scrambled peptide: P20, P3, P9, P11, and P4.

3D Homology Modeling of the ACKR3/CXCR7 N-terminus and Recovered Phage Peptide Structures

The transformation of the CXCR4 N-terminus into the ACKR3/CXCR7N-terminus had very few instances of steric interference. The ACKR3/CXCR7 homology model generated with Maestro as seen in Figure (6) overlays very well with the known crystal structure of CXCR4 bound to the endogenous SDF1α/CXCL12 ligand. Highlighting the ACKR3/CXCR7N-terminus (F6-D25) in Multicolored BALL & STICK mode and overlaying it on top of the corresponding CXCR4 N-terminus (I6-K25) in RED thin-tube mode showed an extremely tight fit. The location of the matching serines 9, 18, and 23 was identified and then outlined in YELLOW Boxes. The predicted matching phage peptide versus SDF1/CXCL12 sequence similarity regions were identified as seen in Figures (7, 8, and 9).

Discussion

Targeted delivery of contrast agents, or anti-viral and anti-cancer compounds to cancerous or infected cells would increase the efficiency of current imaging techniques and treatment regimens and decrease all or many detrimental side effects. The associated fatigue, loss of appetite, treatment acquired infections, flu-like symptoms, and hair loss are typically the result of systemic application of chemotherapeutics, repeated radiation exposure, or prolonged use of antibiotics[1]. Overexpressed plasma membrane bound components that are accessible via the extracellular space are highly attractive targets for cell specific delivery. One of these components is the atypical chemokine receptor ACKR3/CXCR7. These receptors consist of intracellular and extracellular loop regions as well as an extracellular N-terminus tail and intracellular C-terminus tail region. The extracellular regions are the most promising areas for targeting.

The N-terminus tail region of the ACKR3/CXCR7 receptor consists of 40 amino acids (#1-40) with position #1 out in the extracellular space and position #40 next to the cellular membrane. We chose amino acids #6-25 as our target region. The first five amino acids (#1-5) are known to be involved in receptor dimerization (homo/hetero) and could be occupied in a dimerized state *in-vivo* and therefore inaccessible for targeting. Amino acid #26 is a cysteine and would have added a potential cysteine-loop formation to our target during synthesis. Amino acids #27-29 are hydrophobic and would have changed the hydrophilic characteristic of our selected sequence. Epitope mapping of the N-terminus region of ACKR3/CXCR7 identified four areas of interest and three of these would be completely in the region targeted. A portion of the fourth region would also be

located here. The importance of the selected 20 amino acid region is highlighted by the number of predicted sites in such a short span of amino acids and the presence of a structural element such as the β-sheet fold at S9-N13 (Figure 1). The NEB M-13 Phage Display protocol provides a cost effective mechanism to quickly and efficiently identify, isolate, and amplify protein sequences with target specific binding affinity for such a region of interest as this.

Our experimental data show that the peptides identified via phage display as P-20, P-9, and P-3 bound a synthesized portion (F6-D25) of the N-terminus region of ACKR3/CXCR7 with a statistically relevant degree of significance using ELISA data. They were physically and chemically different from each other based on multiple computed characteristics, and were predicted to mimic three different regions of the endogenous ligand SDF1/CXCL12 based on a ClustalW comparison against its entire sequence. We were also able to generate a 3D molecular model of the synthesized portion of the ACKR3/CXCR7 N-terminus region using the known crystal structure of the same region in CXCR4 with SDF1/CXCL12 bound to it [[110]]. Our modeling data show no areas of potential steric interference when this region is transformed from CXCR4 to ACKR3/CXCR7 and the spacing between the Serine residues found in both sequences at positions 9, 18, and 23 and the corresponding residues in the bound ligand SDF1/CXCL12 is identical.

Based on our data for these three peptides, peptide P-20 should have the highest affinity for the N-terminus region of membrane bound ACKR3/CXCR7and it also has the highest predicted potential to activate the receptor and trigger downstream signaling. In

total, our data supports the conclusion that peptides P-20, P-9, and P-3 are viable candidates for the Phase 2 cell line studies. It is important to note that the degradation times are based on the L-peptide form and stability could potentially be improved by synthesizing the more stable D-peptide form of the peptide sequence. The peptides were presented to the target without the benefit of prior folding by molecular chaperones or structural cofactors.

As previously mentioned, the MRgFUS technique shows great promise in the noninvasive treatment of cancer, but is currently limited by incomplete imaging of tumor periphery and the ability to deliver sufficient power to the targeted region to completely ablate the tumor [89,145]. Targeted peptide sequences such as we have discovered are ideal components of cell specific delivery systems. The peptide sequences can be functionalized with a glycine linker tail (G4) and attached to cholesterol for incorporation into liposomes [146,147]. We have synthesized potential candidate liposome structures from a functionalized C-70 fullerene derivative (ALM, a kind gift from LUNA and Dr. C. Kepley) and egg-PC [148]. These liposomes were optimized at 99 nanometers (+/- 16 nanometers) as seen in Figure (10). This type of delivery vehicle with a lipid bi-layer allows for the use of hydrophilic core compounds, hydrophobic intramembranous compounds, and functionalized membrane embedded compounds [10,20,149]. The synthesis of liposomes at less than 200 nm makes them ideal candidates for delivery across the blood brain barrier via intranasal delivery [23,150]. Comparative 3D molecular models of the liposomal components, ALM and egg-PC, plus the three phage peptides, P-20, P-9, and P-3 can be seen in Appendix A.

Modifying the liposomal components also incorporates the ability to control the release of included compounds through a temperature sensitive mechanism [151]. The identification of multiple peptide sequences allows for a multivalent approach to functionalization and targeting [152]. Additionally, a multivalent approach provides a means to continue to target the cell membrane bound receptor even if there are some slight mutations or modifications in the N-terminus amino acid sequence. The inclusion of contrast agents such as super-paramagnetic iron oxide nanoparticles (SPIONs) in a targeted liposome could greatly enhance the ability to visualize a tumor, influence the rate of flow of compounds through the use of a localized magnetic field, and also allow the use of magnetic hyperthermia therapy to ablate the tumor cells [153,154]. These same SPIONs could also be used to magnetically separate targeted cells, such as virus-infected cells, from the blood stream through a modified dialysis procedure. The addition of a gold coating to the SPIONs would further add the ability to use near infrared light to thermally ablate these same cells [155].

In summary, we have identified three heptameric peptide sequences that bind a synthesized portion of the N-terminus region of ACKR3/CXCR7, have different physical and chemical properties, and are predicted to mimic three different regions of the endogenous ligand SDF1/CXCL12. These peptide sequences have the potential to provide a new mechanism for targeting of multiple forms of cancer and chronically infected cells and thereby increase the efficacy of current treatment regimens, while greatly reducing the pain and suffering caused by standard procedures.

CHAPTER III

CELL LINE STUDIES WITH SELECTED TARGETING MOIETIES

Introduction to Cell Lines

For this study, MCF-7 breast cancer cells were used as the positive control cell line. The MCF-7 cell line has been used previously as the cell line of choice for experiments involving CXCR4 and ACKR3/CXCR7 [156]. Historically, the use of MCF-7 cells has been associated with the identification and characterization of the ACKR3/CXCR7 receptor. In September of 2004 US Patent #US 2004/0170634 A1 identified an unknown receptor expressed on the surface of MCF-7 cells. That receptor, CCX-CKR2, had the ability to bind the endogenous ligands CXL12/SDF-1 and CXCL11/I-TAC with high affinity [157]. In 2006, again using MCF-7 cells, the CCX-CXKR2 receptor would be shown to be the same as the previously identified RDC1 receptor [112,158]. The researchers in 2006 would then reclassify the two receptors, CCX-CKR2 and RDC1, as CXCR7 [51]. They would also state that targeting the ACKR3/CXCR7 receptor with antagonistic compounds would be beneficial in the treatment of roughly 48 types of cancer including breast cancer and glioblastoma [157].

The renaming of the RDC1 receptor to CXCR7 was already supported by another group in 2005 due to their competitive binding analysis in T-lymphocytes of the binding affinity of ACKR3/CXCR7 for the endogenous ligand SDF1 versus their newly discovered antibody, anti-RDC1 mAb 9C4 [93]. It is important to note that the region of

the ACKR3/CXCR7 N-terminus used to generate their anti-RDC1 mAb 9C4 was four amino acids, NSSD, shorter than the region used by our research group. We deemed these four missing residues as important due to their specific sequence location or their potential involvement in ligand binding and included them for our experimentation. The first two missing amino acids include an asparagine, Asn23 or N23, potentially involved in post-translational N-linked Glycosylation and a serine, Ser24 or S24, which served as the third serine anchor for our sequence analysis and molecular models. The Asn23 residue in ACKR3/CXCR7 has a corresponding tyrosine residue, Tyr22 or Y22, in CXCR4 and this residue has been implicated in cancer metastasis and considered a good target for cancer treatment [[159]].

The Tyr21 residue in CXCR4 not only enhances SDF1 binding but a corresponding Tyr21 residue is located in the N-terminus of all of the CXC receptors. Only CXCR6 is missing this particular Tyr21 residue [[110,160,161]]. Additionally, the four missing amino acids were identified as being components in two of the four epitopes discovered during our epitope mapping experiments of the selected ACKR3/CXCR7 N-terminus region [[67]]. The prior use of the T-lymphocytes to quantify SDF1 binding reemphasizes the importance of targeting the ACKR3/CXCR7 receptor and its potential use in treatment of HIV and other infectious diseases [[102]]. The ability to inhibit SDF1 binding has been shown to decrease the infectivity of some HIV strains [[103,104,109,162]]. Given the ability of CXCR4 and ACKR3/CXCR7 to bind SDF1 in roughly the same region on their N-terminus, the ideal positive control cell line would not express CXCR4.

Again the MCF-7 cell line is an excellent choice as our positive control cell line due the lack of expression of CXCR4 [51].

To further test the binding specificity of the three phage display derived peptides, P-20, P-9, and P-3; THP-1 monocytes were used as the negative control cell line. THP-1 cells and primary human monocytes have recently been shown to express high levels of CXCR4 but not ACKR3/CXCR7 [163]. Therefore, any binding of the phage display peptides to the THP-1 cells would potentially indicate a tendency for the peptides to bind CXCR4 as well as ACKR3/CXCR7 and thereby limit the specificity required to be used as a targeting moiety.

The choice of a glioblastoma (GBM) based experimental cell line is based on personal experience with the debilitating effects and aggressive nature of the disease. The suddenness of its appearance, the constant threat of imminent death that surrounds it, and the lack of viable treatments make the disease a high priority for our research. Based on the prior experience members of our facility have culturing glioma cells; U87-MG glioblastoma cells were used as the experimental cell line. One of the defining characteristics of glioblastoma is its propensity for invasiveness. Research has shown that the hypoxic conditions of gliomas upregulates the expression of ACKR3/CXCR7 and U87-MG cells migrate towards SDF1 under these conditions [57].

The U87-MG cell line was also use in a comparative study with infiltrative astrocytomas. The data from those experiments showed that the expression of the ACKR3/CXCR7 protein rose with malignancy and the receptor was primarily localized to the cellular membrane where it is accessible as a target [164]. The heterodimeric role of

the ACKR3/CXCR7 and CXCR4 membrane bound complex as it pertains to enhancing cell migration was investigated. The complex was shown to recruit β-arrestin and activate multiple signaling pathways that included ERK1/2, p38 MAPK, and SAPK [165]. The ability to limit or reduce cell proliferation and the invasiveness of U87-MG cells was also shown using a siRNA reduction technique against ACKR3/CXCR7 [58].

The detection of ACR3/CXCR7 on the plasma membrane has had some confounding results. Some research has shown large pools of intracellular ACKR3/CXCR7 with limited or nominal expression on the U87-MG cell surface [56,121]. The findings of limited membrane localization may be associated with the ability of ACKR3/CXCR7 to constitutively recycle between the cytoplasm and the cell membrane [65,66]. This can be compared with the large portion of CXCR4 receptors, roughly 70%, that are degraded by lysosomes upon internalization. The loss of such a vast number of CXCR4 receptors could lead to loss of signaling activity or saturation of CXCR4 and an increased role in ligand scavenging by ACKR3/CXCR7 [166].

Thus the utilization of MCF-7 cells that are ACKR3/CXCR7 (+) and CXR4 (-) versus THP-1 cells that are ACKR3/CXCR7 (-) and CXR4 (+) will provide a mechanism to identify whether or not our phage display peptides have an affinity for ACKR3/CXCR7 expressed on the surface of U87-MG cells. The following experiments will focus on characterizing the effects of targeting U87-MG cells with our phage display derived peptides and determining how the peptides affect cell proliferation, cell viability, membrane binding, cellular uptake, and receptor activation.

Materials and Methods

The Effect of Phage Peptide Incubation on the Viability of a Small Population of MCF-7 Cells

The populations consisted of 3 wells each containing 5,000 MCF-7 cells, 15,000 cells total. Cells were grown for 48 hrs in filter sterilized HyClone RPMI (GE Healthcare) Complete media (87% RPMI 1640 + 10% FBS (Fisher Scientific) + 1% Pen/Strep/Ampho-B 100X (Sigma) + 1% essential amino acids 100X (Sigma) + 1% L-glutamate 200 mM (Sigma) at 37^0C in 5% CO_2 and then incubated in a 90% media + 10% (phage stock 10^{18}/PBS (1X)) solution (for each phage peptide) for another 48 hrs. Control wells included the Standard which only contained media and the PBS (1X) well that had 90% media + 10% PBS (1X). Cells were trypsinized and harvested. Live/Dead staining was performed with a hemocytometer and Trypan Blue. The average of 10 counts was used for statistical analysis, t-test with $\alpha = 0.05$. All analysis were based on comparison with the Standard (t Critical one-tail = 1.833 and t Critical two-tail = 2.262).

The Effect of Phage Peptide Incubation on the Viability of a Large Population of MCF-7 Cells

The population consisted of 1 well each containing 100,000 cells. Cells were grown for 48 hrs in RPMI Complete media at 37^0C in 5% CO_2 and then incubated in a 90% media + 10% phage PBS (1X) solution (for each phage peptide) for another 48 hrs. Control wells included the Standard which only contained media and the PBS (1X) well that had 90% media + 10% PBS (1X). Cells were trypsinized and harvested. Live/Dead staining was performed with a hemocytometer and Trypan Blue. The average of 10

counts was used for statistical analysis, t-test with $\alpha = 0.05$. All analysis were based on comparison with the Standard (t Critical one-tail = 1.833 and t Critical two-tail = 2.262).

The Effect of Phage Peptide Incubation on the Cell Proliferation of MCF-7 Cells

The populations consisted of 6 wells each containing 25,000 cells. Cells were grown for 48 hrs in 100 µl of RPMI Complete media at 37^0C in 5% CO_2 and then incubated in a 90% media + 10% phage/PBS (1X) solution (for each phage peptide) for another 48 hrs. The negative control population received no phage exposure. A Vybrant® MTT assay (Fisher Scientific) was performed according to the manufacturers Quick Protocol Option. Briefly, 10 µL of the 12 mM MTT stock solution was added to each well and incubated at 37°C for 4 hours. Then 85 µl of media was removed, 50 µL of DMSO was added to each well and mixed thoroughly, cells were incubated at 37°C for 10 minutes, mixed again, absorbance was read on a BioTek microplate reader at 540 nm instead of 570 nm and the values were exported into an Excel spreadsheet. All analysis were based on comparison with the Standard (t Critical one-tail = 2.920 and t Critical two-tail = 4.302) ($\alpha = 0.05$).

Whole-Cell ELISA Confirmation of MCF-7 Cell Membrane Binding by Phage Peptides Using an HRP Conjugated Anti-M13 Antibody with a TMB Substrate and STOP-450 solution

The populations consisted of 6 wells each containing 25,000 cells. Cells were grown for 48 hrs at 37^0C in RPMI Complete at 5% CO_2 and washed thrice with PBS (1X) between each step. Cells were blocked for 2 hrs with 1% BSA, washed, and incubated in a 90% media + 10% (phage/0.5% BSA) solution (for each phage peptide) for 4 hrs at

room temperature or RT (a no-phage negative control was included with 0.5% BSA). Wells were washed, incubated with anti-M13 HRP conjugated mAb (GE Healthcare) 1:2500 for 1 hr, washed, incubated with the TMB substrate (Abcam) for 1 hr, and allowed to develop color for 45 minutes. The acidic 450 nm STOP Solution (Abcam) was added to stop the enzymatic reaction. Absorbance was read at 450 nm on a BioTek microplate reader and the values were exported into an Excel spreadsheet. All phage peptide results were compared to the no-phage negative control ($\alpha = 0.05$) (t Critical one-tail = 2.920 and t Critical two-tail = 4.302).

MCF-7 Cells - Membrane Receptor Binding and Cellular Uptake of Phage Display Derived Peptides

Cells were grown on cover slips for 48 hrs at 37^0C in RPMI Complete media in 5% CO_2 , incubated in a 90% media + 10% phage solution overnight (for each phage peptide) at 4^0C, and washed thrice with PBS (1X) between each step. All steps were performed at RT. Cells were fixed for 20 minutes in a 4% PFA solution (4% paraformaldehyde in PBS (1X)), washed, blocked for 20 minutes in PBT (PBS (1X) + 1% BSA + 0.1% Triton X-100), washed, incubated with phage for 20 minutes, washed, incubated with 1^0(anti-M13) 1:1000 for phage peptides, washed, incubated with 2^0(GAM/Cy3) 1:2000, washed, incubated with Alexa Fluor 488 Phalloidin 1:1000 and Hoescht 33342 1:5000 for 20 minutes, washed, and mounted on slides for confocal microscopy. A no-phage negative control was included for antibody binding specificity. Cells were imaged on a Carl Zeiss Axio Observer Z1 Spinning Disc Confocal Microscope.

Negative Control Cell Line THP-1 Cells - Membrane Receptor Binding and Cellular Uptake of Phage Display Derived Peptides

Cells were grown in flasks for 48 hrs at 37^0C in RPMI Complete media in 5% CO_2 , incubated in a 90% media + 10% phage solution overnight (for each phage peptide) at 4^0C, and washed thrice with PBS (1X) between each step. Cells were transferred to 15 ml centrifuge tubes and gently centrifuged and softly pelleted between each step. All steps were performed at RT. Cells were fixed for 20 minutes in a 4% PFA solution (4% paraformaldehyde in PBS (1X)), washed, blocked for 20 minutes in PBT (PBS (1X) + 1% BSA + 0.1% Triton X-100), washed, incubated with phage for 20 minutes, washed, incubated with 1^0(anti-M13) 1:1000 for phage peptides, washed, incubated with 2^0(GAM/Cy3) 1:2000, washed, incubated with Alexa Fluor 488 Phalloidin 1:1000 and Hoescht 33342 1:5000 for 20 minutes, and washed. Cells were resuspended in mounting media, transferred to cover slips, and mounted on slides for confocal microscopy. No negative controls were included. Cells were imaged on a Carl Zeiss Axio Observer Z1 Spinning Disc Confocal Microscope.

The Effect of Phage Peptide Incubation and Length of Initial Growth Cycle on the Viability of U87-MG Cells

The populations consisted of 1 well each containing 100,000 cells. Cells were grown for 24 hrs at 37^0C in 90% MEM (Fisher Scientific) + 10% FBS in 5% CO_2 and then incubated in a 90% media + 10% phage solution (for each phage peptide) for another 48 hrs. Control wells included the Standard which only contained media and the PBS (1X) well that had 90% media + 10% PBS (1X). Cells were trypsinized and

harvested. Live/Dead staining was performed with a hemocytometer and Trypan Blue. The average of 10 counts was used for statistical analysis, t-test with $\alpha = 0.05$. All analysis were based on comparison with the Standard (t Critical one-tail = 1.833 and t Critical two-tail = 2.262).

The Effect of Phage Peptide Incubation and Length of Initial Growth Cycle on the Viability of U87-MG Cells

The populations consisted of 4 wells, each containing 84,000 cells. Cells were grown for 24 hrs at 37^0C in 90% MEM + 10% FBS in 5% CO_2 and then incubated in a 90% media + 10% phage solution (for each phage peptide) for another 48 hrs. Control wells included the Standard which only contained media and the PBS (1X) well that had 90% media + 10% PBS (1X). Cells were trypsinized and harvested. Live/Dead staining was performed with a hemocytometer and Trypan Blue. The average of 10 counts was used for statistical analysis, t-test with $\alpha = 0.05$. All analysis were based on comparison with the Standard (t Critical one-tail = 1.833 and t Critical two-tail = 2.262).

The Effect of Phage Peptide Incubation on the Cell Proliferation of U87-MG Cells

The populations consisted of 6 wells each containing 25,000 cells. Cells were grown for 48 hrs at 37^0C in 90% MEM + 10% FBS in 5% CO_2 and then incubated in a 90% media + 10% phage solution (for each phage peptide) for another 48 hrs. The negative control population received no phage exposure. A Vybrant® MTT assay (Fisher Scientific) was performed according to the manufacturers Quick Protocol Option. Briefly, 10 µL of the 12 mM MTT stock solution was added to each well and incubated at 37°C for 4 hours. Then 85 µl of media was removed, 50 µL of DMSO was added to each well

and mixed thoroughly, cells were incubated at 37°C for 10 minutes, mixed again and absorbance was read on a BioTek microplate reader at 540 nm instead of 570 nm and the values were exported into an Excel spreadsheet. All analysis were based on comparison with the Standard (t Critical one-tail = 2.920 and t Critical two-tail = 4.302) ($\alpha = 0.05$).

Whole-Cell ELISA Confirmation of U87-MG Cell Membrane Binding by Phage Peptides Using an HRP Conjugated Anti-M13 Antibody with a TMB Substrate and STOP-450 Solution

The populations consisted of 6 wells each containing 25,000 cells. Cells were grown for 48 hrs at 37^0C in 90% MEM + 10% FBS in 5% CO_2 and washed thrice with PBS (1X) between each step. Cells were blocked for 2 hrs with 1% BSA, washed, and incubated in a 90% media + 10% (phage/0.5% BSA) solution (for each phage peptide) for 4 hrs at RT (a no-phage negative control was included with 0.5% BSA). Wells were washed, incubated with anti-M13 HRP conjugated mAb (GE Healthcare) 1:2500 for 1 hr, washed, incubated with the TMB substrate (Abcam) for 1 hr, and allowed to develop color for 45 minutes. The acidic 450 nm STOP Solution (Abcam) was added to stop the enzymatic reaction. Absorbance was read at 450 nm on a BioTek microplate reader and the values were exported into an Excel spreadsheet. All phage peptide results were compared to the no-phage negative control ($\alpha = 0.05$) (t Critical one-tail = 2.920 and t Critical two-tail = 4.302).

U87-MG Cells - Confirmation of Co-Localization of Phage Display Derived Peptides and the Known ACKR3/CXCR7 Antibody, Anti-RDC1

The populations consisted of U87-MG cells grown on cover slips. Experimental Cells were grown for 48 hrs at 37^0C in 90% MEM + 10% FBS in 5% CO_2 and then incubated in a 90% media + 10% phage solution (for each phage peptide) for 4 hours at RT. Cells were washed thrice with PBS (1X) between each step. All steps were performed at RT. Cells were fixed for 20 minutes in a 4% PFA solution (4% paraformaldehyde in PBS (1X)), washed, blocked for 20 minutes in PBT (PBS (1X) + 1% BSA + 0.1% Triton X-100), washed, incubated with phage for 20 minutes, washed, incubated with 1^0(anti-M13) 1:1000 for phage peptides or 1^0(anti-RDC1) for the ACKR3/CXCR7 receptor 1:1000, washed, incubated with 2^0(DAM/Alexa488) 1:2000 for phage peptides or 2^0(GAR/Cy3) for the ACKR3/CXCR7 receptor 1:2000, washed, incubated with Hoescht 33342 1:5000 for 20 minutes, washed, and mounted on slides for confocal microscopy. No-phage and no-1^0 antibody negative controls were included for 1^0 and 2^0 antibody binding specificity. Cells were imaged on a Carl Zeiss Axio Observer Z1 Spinning Disc Confocal Microscope.

Quantifying the Level of ACKR3/CXCR7 Activation Using a PathHunter β-Arrestin Assay (DiscoverX) with the Phage Peptides, the Endogenous Ligand SDF1α, and CHO-K1 Modified Cells

A 12-point dose response curve was performed according to the manufacturer's instructions. The CHO-K1 cells were seeded at 10,000 cells per well on a 96-well plate with AssayComplete Cell Plating Reagent and grown for 48hrs at 37^0C. The phage were

started at a concentration of 10^{18} PFU`s and diluted 10 times sequentially by 1/3 to a final concentration of 1.69 * $10^{13}$ PFU`s. The SDF1α ligand was started at a concentration of 20 μM and also diluted 10 times sequentially by 1/3 to a final concentration of 3.39 pM. There were two wells used per treatment for each dilution for eleven wells. A no-agonist (SDF1α) negative control and no-phage negative control wells were used for well twelve. The cells were incubated with the phage peptides or the agonist, SDF1α, for 90 minutes at 37^0C. Luminescence was read on a BioTek microplate reader and the RLU values were exported into an Excel spreadsheet. The rough approximation of the EC_{50} was calculated using the average value for all agonist treatments and then interpolating the molar value using the slope between the data points on either side of the average value, ($M=Y_2-Y_1/X_2-X_1$) where $X_1 \neq X_2$.

Results

The Effect of Phage Peptide Incubation on the Viability of a Small Population of MCF-7 Cells

The Live/Dead staining was performed and no statistical difference in viability was observed between the standard MEDIA treatment and the other treatments ($\alpha = 0.05$). The average live cell values for the different treatments were: MEDIA 82.24%, PBS (1X) 85.00%, P-20 81.82%, P-9 80.67%, and P-3 83.19% as seen in Figure (11).

The Effect of Phage Peptide Incubation on the Viability of a Large Population of MCF-7 Cells

The Live/Dead staining was performed and no statistical difference in viability was observed between the standard MEDIA treatment and the other treatments ($\alpha =$

0.05). The average live cell values for the different treatments were: MEDIA 87.50%, PBS (1X) 83.69%, P-20 85.53%, P-9 84.17%, and P-3 84.56% as seen in Figure (12).

The Effect of Phage Peptide Incubation on the Cell Proliferation of MCF-7 Cells

An MTT assay was performed and no statistical difference in viability was observed between the standard MEDIA treatment and the other treatments ($\alpha = 0.05$). The values for the different treatments were: MEDIA 0.398, PBS (1X) 0.386, P-20 0.383, P-9 0.387, and P-3 0.385 as seen in Figure (13).

Whole-Cell ELISA Confirmation of MCF-7 Cell Membrane Binding by Phage Peptides Using an HRP Conjugated Anti-M13 Antibody with a TMB Substrate and STOP-450 Solution

All phage peptide results were statistically significant compared to the no-phage negative control ($\alpha = 0.05$) (t Critical one-tail = 2.920 and t Critical two-tail = 4.302). The values for the different treatments were: Negative Control 0.073, P-20 0.254, P-9 0.256, and P-3 0.257 as seen in Figure (14). The experimental values were approximately 3.5 times higher than the negative control value.

MCF-7 Cells - Membrane Receptor Binding and Cellular Uptake of Phage Display Derived Peptides

The fluorescent dyes used were: [Hoechst-BLUE for Nucleus, Alexa488-GREEN for actin, 2^0(GAM/Cy3-RED) - 1^0(anti-M13) for Phage Peptides]. Negative controls were included and confirmed binding specificity. Membrane binding and cellular uptake of all three phage peptides was confirmed by the areas of fluorescence overlap indicated by YELLOW (Membrane) and PURPLE (Nucleus) as seen in Figure (15).

Negative Control Cell Line THP-1 Cells - Membrane Receptor Binding and Cellular Uptake of Phage Display Derived Peptides

The fluorescent dyes used were: [Hoechst-BLUE for Nucleus, Alexa488-GREEN for actin, 2^0(GAM/Cy3-RED) - 1^0(anti-M13) for Phage Peptides]. Any areas of location overlap would have been indicated by YELLOW (Membrane) and PURPLE (Nucleus). No phage binding was observed and therefore no negative controls were tested as seen in Figure (16).

The Effect of Phage Peptide Incubation and Length of Initial Growth Cycle (24 hrs) on the Viability of U87-MG Cells

The Live/Dead staining was performed and no statistical difference in viability was observed between the standard MEDIA treatment and the other treatments (α = 0.05). The average live cell values for the different treatments were: MEDIA 90.00%, PBS (1X) 87.80%, P-20 92.50%, P-9 86.84%, and P-3 87.18% as seen in Figure (17).

The Effect of Phage Peptide Incubation and Length of Initial Growth Cycle (48 hrs) on the Viability of U87-MG Cells

The Live/Dead staining was performed and no statistical difference in viability was observed between the standard MEDIA treatment and the other treatments (α = 0.05). The values for the different treatments were: MEDIA 92.57%, PBS (1X) 91.42%, P-20 91.67%, P-9 90.46%, and P-3 91.10% as seen in Figure (18).

The Effect of Phage Peptide Incubation on the Cell Proliferation of U87-MG Cells

An MTT assay was performed and no statistical difference in viability was observed between the standard MEDIA treatment and the other treatments (α = 0.05).

The average live cell values for the different treatments were: MEDIA 0.367, BSA 0.357, P-20 0.355, P-9 0.362, and P-3 0.361 as seen in Figure (19).

Whole-Cell ELISA Confirmation of U87-MG Cell Membrane Binding by Phage Peptides Using an HRP Conjugated Anti-M13 Antibody with a TMB Substrate and STOP-450 Solution

All phage peptide results were statistically significant compared to the no-phage negative control ($\alpha = 0.05$) (t Critical one-tail = 2.920 and t Critical two-tail = 4.302). The values for the different treatments were: Negative Control 0.110, P-20 0.330, P-9 0.328, and P-3 0.332 as seen in Figure (20). The experimental values were approximately 3 times higher than the negative control value.

U87-MG Cells - Confirmation of Co-Localization of Phage Display Derived Peptides and the Known ACKR3/CXCR7 Antibody, Anti-RDC1

The fluorescent dyes used were: [Hoechst-BLUE for Nucleus, 2^0(GAR/Cy3-RED) - 1^0(anti-RDC1) for ACKR3/CXCR7 receptor, 2^0(DAM/Alexa488-GREEN) - 1^0(anti-M13) for Phage Peptides]. All three phage peptides were shown to bind the extracellular membrane and be internalized by the U87-MG cells as seen in Figure (21-Continued). Negative control experiments verified the specificity of the 1^0 and 2^0 antibodies used in these experiments as seen in Figures (21A and 21B). The areas of colocalization at the extracellular membrane and in the cytoplasm are indicated by the YELLOW overlap (RDC1-RED + Phage Peptide-GREEN). Areas of intracellular colocalization in and around the nucleus are indicated by the GREEN + BLUE overlap as seen in Figure (21B).

Quantifying the Level of ACKR3/CXCR7 Activation Using a PathHunter β-Arrestin Assay (DiscoverX) with the Phage Peptides, the Endogenous Ligand SDF1α, and CHO-K1 Modified Cells

A 12-point dose response curve was performed according to the manufacturer's instructions. The Phage Peptides showed no effect compared to SDF1α as seen in Figure (22). The endogenous ligand SDF1α activated the receptor as expected. Activation was starting at dilution #5, ~915 pM, and began to plateau at dilution #10, 222 nM. The average value for the agonist treatments was 5,579 and this fell between data points #7 and #8. Data point #7 had an average value of 2,776 at a concentration of 8.23 x 10E-9 [M] and Data point #8 had an average value of 6,445 at 2.47 x 10E-8 [M]. The EC_{50} was roughly approximated at 20.89 nM and was slightly higher than but comparable to the manufacturer's stated EC_{50} of 3.5 nM.

Discussion

The ability to target cancer cells specifically allows for the delivery of chemotherapeutics, anti-cancer compounds, or contrast agents for imaging directly to the tumor region. These experiments have shown that the phage display peptides recovered from our previous experiments utilizing a synthesized portion of the N-terminus region of ACKR3/ CXCR7 were viable candidates for targeting MCF-7 breast cancer cells and U87-MG glioblastoma (GBM) cells [[67]]. The three peptides, P-20, P-9, and P-3 were shown to have no effect on the viability or proliferation of MCF-7 or U87-MG cells. Additionally, the peptides were observed to significantly bind these same cell lines using a whole-cell ELISA protocol. The ability of these cancer cell types to bind and internalize

the peptides was confirmed using confocal microscopy. The affinity of these peptides for the ACKR3/CXCR7 receptor was verified using a co-localization assay and the known anti-ACKR3/CXCR7 mAb RDC1.

The final piece of the peptide cell interaction puzzle was to quantify whether or not the peptides would activate the receptor upon binding. Utilizing a luminescent β-arrestin activation assay and a 12-point dose response curve, the peptides were shown to have no effect on the recruitment of β-arrestin and did not activate the receptor upon binding. Activation of the receptor was verified after exposure to the endogenous ligand SDF1α. The results of the SDF1α assay were validated when compared side-by-side with the published results from the manufacturer DiscoverX.

In conclusion, the three phage display derived peptides; P-20, P-9, and P-3 were shown to be viable candidates to be used as targeting moieties for ACKR3/CXCR7. The peptides showed no effect on cell viability or proliferation when used against MCF-7 breast cancer cells and U87-MG glioblastoma (GBM) cells. The peptides did bind the cell membrane of these same cell lines and were taken up intracellularly as seen in the whole-cell ELISA and confocal microscopy experiments. Lastly, the peptides had no effect on the activation of the receptor unlike the endogenous ligand CXCL12/SDF1as confirmed in the β-arrestin recruitment assay. These results show conclusively that our phage display protocol used against a synthesized portion of the N-terminus region of ACKR3/CXCR7 identified at least three valid candidates for targeting breast cancer and brain cancer cells.

CHAPTER IV

CONCLUSIONS AND FUTURE APPLICATIONS

In summary, we have identified three heptameric peptide sequences, P-20, P-9, and P-3, which bind a synthesized portion of the N-terminus region of ACKR3/CXCR7, have different physical and chemical properties, and are predicted to mimic three different regions of the endogenous ligand SDF1/CXCL12. These same three peptides were shown to have no effect on the viability or proliferation of MCF-7 or U87-MG cells. Additionally, the peptides were observed to significantly bind these same cell lines using a whole-cell ELISA protocol. The ability of these cancer cell types to bind and internalize the peptides was confirmed using confocal microscopy. The peptides were shown to bind the MCF-7 cells that express ACKR3/CXCR7 but not CXCR4. The peptides were also shown to have no affinity for THP-1 cells that do not express ACKR3/CXCR7 but do express CXCR4. The affinity of these peptides for the ACKR3/CXCR7 receptor was verified using a co-localization assay and the known anti-ACKR3/CXCR7 mAb RDC1.

The last bit of information needed was to quantify whether or not the peptides would activate the receptor upon binding. The peptides were shown to have no effect on the recruitment of β-arrestin and did not activate the receptor upon binding. Activation of the ACKR3/CXCR7 receptor was validated via exposure to its natural ligand SDF1α. The inability to activate the receptor is an integral part of our desired targeting moiety system.

Based on the data presented here, the three recovered peptides P-20, P-9, and P-3 are specific for the N-terminus of ACKR3/CXCR7.

The secondary component of the overall system, the liposome was also successfully completed. Liposomes comprised of a C-70 derivative (ALM) and a naturally occurring lipid (egg-PC) was consistently synthesized at the desired size of ~99 nm +/- ~12 nm [67]. Many of the characteristics of liposomes are controllable and can be modified for the desired effect. The use of cholesterol has been shown to be a required component for the uptake of liposomes into peripheral neurons and glial cells [167]. Conjugation of the discovered targeting moieties to the liposomal vehicle could be easily accomplished using cholesterol and this would provide the ability to deliver chemotherapeutics, contrast agents, genetic material, and other compounds directly to the targeted cells [147].

The cholesterol molecules themselves could be modified to change the surface charge of the liposome. A cholesterol hemisuccinate derivate (CHEMS) imparted a negative charge, a lysine-based cholesterol (CHYLS) derivative gave the system a positive charge, and the PEGylated cholesterol (Chol-PEG) provided no charge. All of their liposomes were in the 104 nm to 163 nm range. The anionic liposomes showed the greatest interaction with the cell membrane most likely due to electrostatic attractions between the positively charged liposome membrane and the negatively charged cancer cell membranes [168]. The inclusion of increasing concentrations of cholesterol in the lipid bilayer of liposomes has been shown to make them more rigid and susceptible to triggered release of their contents by induction of a magnetic field. This bit of

information is useful because these liposomes contained no metal particles and many cancers are imaged with MRI [169].

The targeting moieties could instead be conjugated to the polyethylene glycol–dioleoyl phosphatidylethanolamine (PEG–DOPE) amphiphilic copolymer and incorporated directly into the liposomes membrane. This method not only used PEG to escape the RES but it also used a short eight amino acid long peptide, similar to our seven amino acid long peptide, as its targeting moiety for breast cancer cells [10]. Another method to alter liposome characteristics is to change the pH of the solutions being used. Doxorubicin has been shown to have a positive charge below pH8 and this changed the loading capacity of the liposomes based on their charge, positive or negative [13].

Using a hydration medium with a pH of 4, the positively charged liposomes were limited in their ability to sequester Doxorubicin in the aqueous phase and into its core region. Due to this limitation, the negatively charged liposomes incorporated more than three times as much doxorubicin into its core region. The negatively charged liposomes only showed a modest 20% increase in loading capacity when the doxorubicin was dissolved in the methanol-chloroform solvent [13]. Thus it is possible to alter the amount of compound load based upon the pH of the solution used in the hydration buffers.

Finally, liposomes can be made sensitive to ultrasound stimulation, sonosensitive, by incorporating the proper lipid into the bilayer. Liposomes synthesized at 98 nm that have dioleoyl phosphatidylethanolamine (DOPE) in the membrane have been shown to have enhanced sonosensitivity [170]. Based on all of the information gathered about liposomal configurations, the optimum set up would be comprised of four components:

dioleoyl phosphatidylethanolamine (DOPE), the functionalized C70 derivative Amphiphilic Liposomal Malonylfullerene[70] (ALM), PEGylated-distearoylphosphatidylethanolamine (DSPE-PEG 2000), and cholesterol in a roughly 25:27:8:40 mol%. This particular configuration would allow for modifications to be made to the surface charge of the liposome, control loading capacities with pH, scavenge ROS with the empty cage fullerene derivative, and allow for the controlled release of encapsulated compounds via ultrasound and magnetic exposure. Combining our recovered peptide sequences with this liposomal configuration has the potential to provide a new mechanism for the targeting of multiple forms of cancer and chronically infected cells. This would accomplish our goal of increasing the efficacy of current treatment regimens, while greatly reducing the pain and suffering caused to patients by many of today`s standard procedures.

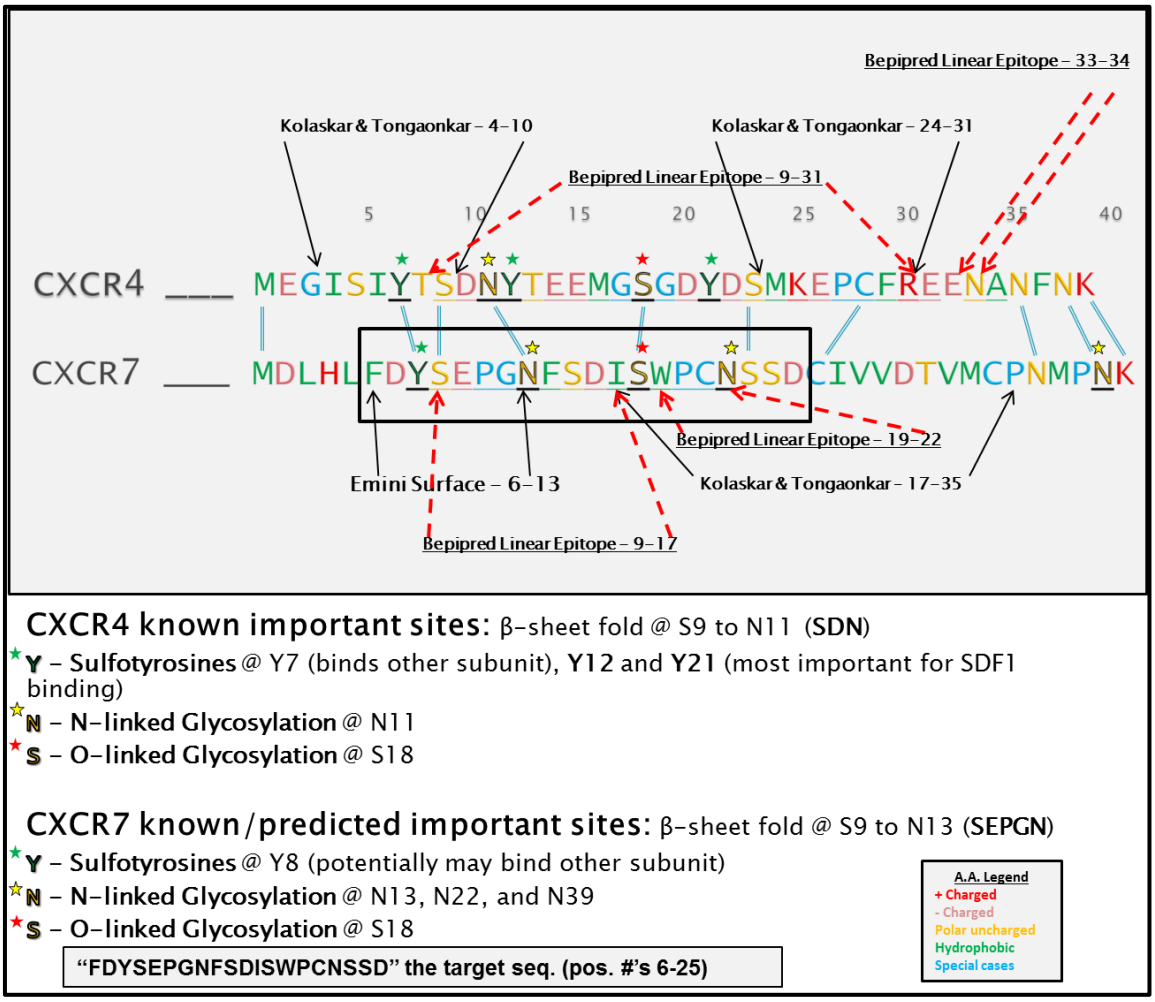

Figure 1. CXCR4 and ACKR3/CXCR7 40 Amino Acid N-Terminus Comparison and Epitope Mapping. The locations of posttranslationally modified residues are identified with a Red*, Yellow*, or Green* based on residue type. The locations of predicted epitope sites are identified by name (Bepipred, Kolaskar, or Emini) and the associated residue locations. The locations of residues identical to both receptors are linked together with a Blue line (i.e. M1-M1, Y7-Y8, etc.). Residues are colored based on the amino acid (A.A.) legend in the figure and the 20 ACKR3/CXCR7 residues chosen (F6-D25) for experimentation are outlined in the boxed region. The location of the β-sheet fold for each N-terminus is listed.

Scrambled: **SWESFPNDCSYGDNDFSPIS**	Legend for amino acid characterization: **Amino Acid Groups: aromatics are underlined** **Positive Charge (+): R (Arg), H (His), K (Lys)** **Negative Charge (-): D (Asp), E (Glu)** **Polar Uncharged: S (Ser), T (Thr), N (Asn), Q (Gln)** **Special Cases: C (Cys), G (Gly), and P (Pro)** **Hydrophobic: A (Ala), V (Val), I (Ile), L (Leu), M (Met), F (Phe), Y (Tyr), W (Trp)**
Example 1: **SSYGSIPNFSD NEDFSPCWD** ***GNFSD/ TEEM****	
Example 2: **NPWSIFSYEDDCG NSSSDFP** ****YTEEMG/ NSSD***	
Example 3: **SFPDCPENSGWDFNSSDISY** ***NSSD/DISW***	
CXCR7 seq: **FDYSEPGNFSDISWPCNSSD**	
CXCR4 seq: **IYTSDNYTEEMGSGDYDSMK**	

Figure 2. Selection of the Scrambled (Scr) Control Sequence for ELISA Analysis. The selected control sequence was labeled "Scrambled". Examples 1, 2, and 3 are representative of rejected scrambled sequence candidates due to their similarities with the sections of the ACKR3/CXCR7 and CXCR4 sequences listed below them. The symbol * = similarity to ACKR3/CXCR7 sequence and ** = similarity to CXCR4 sequence.

Id # P or C-__	Peptide sequence	DNA sequence	Isoelectric point (pI)	Estimated half-life	Instability Index	Aliphatic Index	GRAVY
P-16	GPLSRPG	GGTCCTCTTTCTCGTCCTGGT	9.75	30 hrs	63.60	55.71	-0.786
P-13	APLSRPG	GCTCCGCTGTCTCGGCCTGGT	9.79	4.4 hrs	91.11	70.00	-0.471
P-19	APLSRPG	GCTCCGCTGTCTCCTCCTGGG	9.79	4.4 hrs	91.11	70.00	-0.471
P-18	APLSRRG	GCTCCGCTTTCTCGTCGTGGT	12.00	4.4 hrs	133.30	70.00	-0.886
P-20	APLPRPG	GCTCCTCTTCCTCGTCCTGGT	9.79	4.4 hrs	80.34	70.00	-0.586
P-14	APLSPPG	GCTCCGCTGTCTCCTCCTGGG	5.57	4.4 hrs	126.37	70.00	-0.057
P-15	APLSPPG	GCTCCTCTTTCTCCTCCTGGT	5.57	4.4 hrs	126.37	70.00	-0.057
P-21	APLSPPG	GCTCCTCTTTCTCCTCCTGGG	5.57	4.4 hrs	126.37	70.00	-0.057
P-22	APLSPPG	GCTCCTCTGTCTCCTCCTGGG	5.57	4.4 hrs	126.37	70.00	-0.057
P-23	APLSPPG	GCTCCTCTTTCTCCTCCTGGT	5.57	4.4 hrs	126.37	70.00	-0.057
P-24	APLSPPG	GCTCCGCTTTCTCCTCCTGGG	5.57	4.4 hrs	126.37	70.00	-0.057
P-17	HPLMRRG	CATCCGCTGATGCGGCGTGGT	12.00	3.5 hrs	63.39	55.71	-1.214
P-08	HPLIVLE	CATCCGCTGATTGTTCTTGAG	5.24	3.5 hrs	-7.67	208.57	1.143
P-C5	AVLRTSP	GCTGTGCTTCGGACTTCTCCG	9.79	4.4 hrs	98.86	111.43	0.314
P-10	APSPMIW	GCGCCTTCGCCTATGATTTGG	5.57	4.4 hrs	115.60	70.00	0.471
P-C4	HSLELMP	CATAGTCTTGAGCTTATGCCG	5.24	3.5 hrs	71.34	11.43	0.057
P-11	RLPAFLH	CGTCTTCCTGCTTTTCTGCAT	9.76	1 hr	63.60	125.71	0.414
P-01	LMPARYH	CTTATGCCTGCGCGTTATCAT	8.75	5.5 hrs	105.71	70.00	-0.443
P-C6	HLWLTPP	CATTTGTGGTTGACGCCGCCT	6.74	3.5 hrs	87.54	111.43	-0.057
P-02	TYASDRS	ACGTATGCTTCTGATCGTAGT	5.50	7.2 hrs	94.40	14.29	-1.400
P-05	QYATPSA	CAGTATGCGACGCCGAGTGCG	5.52	0.8 hrs	59.14	28.57	-0.614
P-03	QMAQWPP	CAGATGGCGCAGTGGCCTCCG	5.52	0.8 hrs	53.71	14.29	-1.057
P-06	SWNMWSP	CAGTATGCGACGCCGAGTGCG	5.24	1.9 hrs	88.97	0.00	-0.943
P-C2	HWGMWSY	CATTGGGGGATGTGGAGTTAT	6.74	3.5 hrs	-10.36	0.00	-0.800
P-07	VNSAWTY	GTGAATTCGGCGTGGACGTAT	5.49	100 hrs	-12.90	55.71	-0.171
P-04	TTTWHLK	ACTACGACGTGGCATCTTAAG	8.44	7.2 hrs	8.80	55.71	-0.900
P-C3	NQSAVLP	AATCAGTCTGCTGTTTTGCCG	5.52	1.4 hrs	88.09	111.43	0.057
P-09	DSHTPQR	GATTCGCATACTCCGCAGAGG	6.74	1.1 hrs	52.83	0.00	-2.543
P-C1	GHWTRFA	GGTCATTGGACGAGGTTTGCG	9.76	30 hrs	-17.01	14.29	-0.729

Figure 3. Phage Peptides Insert Coding Sequence Comparison and Predicted Physical and Chemical Properties of the Putative CXCR7 Binding Phages. The DNA coding sequence for each 7 amino acid insert sequence is listed as well as the predicted values for the Isoelectric point (pI), Estimated Half-Life in reticulocytes, Instability index, Aliphatic index, and GRAVY index of each insert sequence. DNA coding sequences reveal no cross contamination.

Activation(Act), Receptor(Rec)/Heparin(Hep) Binding:			22-23 Act,		29-33 Rec/Hep ,	39-41 Rec ,		41-51 Hep , 48-50 Rec,			60----------70 Rec					
SDF1 2^0 structure: *T*=Turn, β=β-strand, *H*=Helix			*T*(24-26),	β(27-29),	β(31-34),	β(36-38),	H(41-43),	β(44-49),	T(53-55),		β(59-63),	T(64-66),	β(69-72),		H(79-86)	
SDF1 sequence with ClustalW alignment position			GKPVS	LSYRC	PCRFF	ESHVA	RANVK	HLKIL	NTPNC	ALQIV	ARLKN	NNRQV	CIDPK	LKWIQ	EYLEK	ALNKR	FKM
Peptide Id	**Peptide Seq**	**ClustalW Seq**	**21-25**	**26-30**	**31-35**	**36-40**	**41-45**	**46-50**	**51-55**	**56-60**	**61-65**	**66-70**	**71-75**	**76-80**	**81-85**	**86-90**	**91-93**
P_16	GPLSRPG	GPVSRPC	21, 23-25	29	31,32												
P_13	APLSRPG	CPLNTPN		30	31			50	51-54								
P_18	APLSRRG	TPVARKN							52,53	60	61,62,64,65						
P_20	APLPRPG	KPVPRPN	22-24		31, 33				53,54								
P_24	APLSPPG	CPLNTPN		30	31			50	51-54								
P_17	HPLMRRG	DPYLEKA											73,74		82-85	86	
P_8	HPLIVLE	TPLQIVA							52,53	57-60	61						
C_5	AVLRTSP	KILNTPP						48-50	51-53				74				
P_10	APSPMIW	TPDPLKW							52,53				73,74	76-78			
C_4	HSLELMP	KHLKILP					45	46-50	53								
P_11	RLPAFLH	RCPCFFE		29,30	31,32,34,35	36											
P_1	LMPARYH	LCPCRFH		26,30	31-34	38											
C_6	HLWLTPP	KLWIQEY											75	76,78-80	81,82		
P_2	TYASDRS	SYRCERA		27-30		36	41,42										
P_5	QYATPSA	SYRCPCR		27-30	31-33												
P_3	QMAQWPP	QVCKWIQ										69,70	71	77-80			
P_6	SWNMWSP	KWQEYLE												77,78,80	81-84		
C_2	HWGMWSY	KWIQEYL												77-80	81-83		
P_7	VNSAWTY	IDPKWIY											72-74	77-79	82		
P_4	TTTWHLK	KLKWYLE											75	76-78	82-84		
C_3	NQSAVLP	NRQVCIP										67-70	71,72,74				
P_9	DSHTPQR	ESHTPAR				36-38			52,53		61,62						
C_1	GHWTRFA	DKWIRFK											73	77-79		90	91,92
Number of peptides predicted to simulate each region			*2*	*7*	*7*	*4*	*2*	*4*	*8*	*2*	*3*	*2*	*9*	*8*	*6*	*2*	*1*

Figure 4. ClustalW Predicted Regions of Similarity for Phage Peptides with the Endogenous Ligand, SDF1. ClustalW analyses comparing the identified phage peptide insert sequences to the protein sequence of SDF1.The recovered putative ACKR3/CXCR7 targeting peptides fell into three clusters. None of the peptides were predicted to mimic the first 20 residues of SDF1.

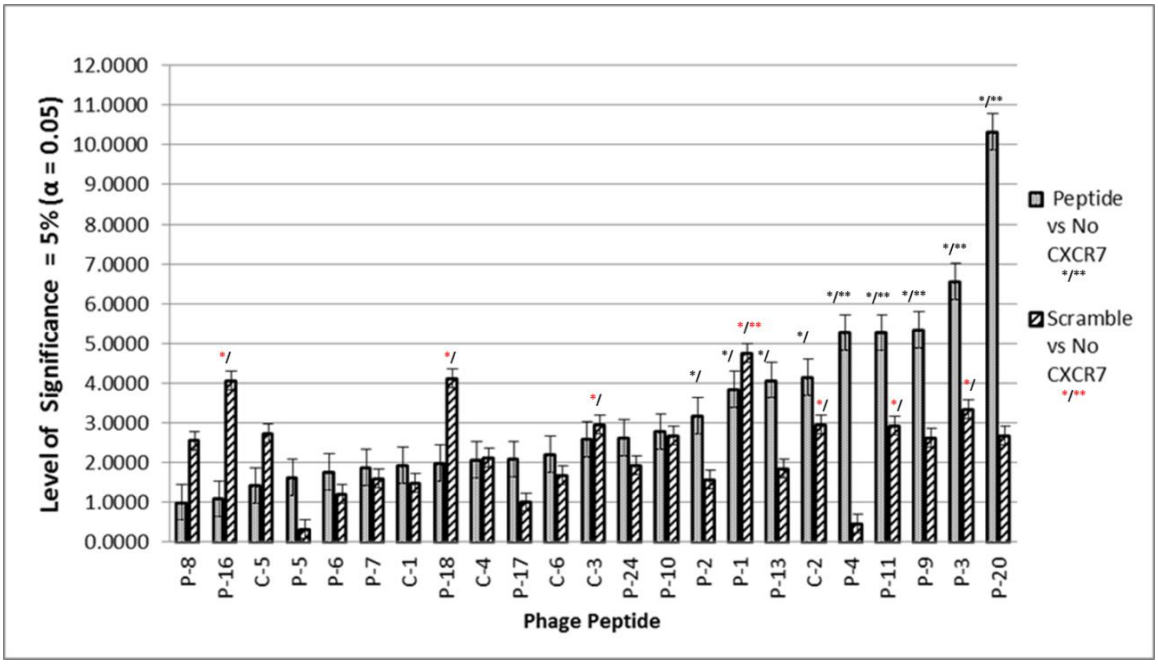

Figure 5. Normalized ELISA Results: Phage Peptide Binding to CXCR7 Target or the Scrambled (Scr) Negative Control Peptide. The Level of Significance used was 5% (Alpha α = 0.05). The threshold cutoff values used were: * t-test Critical one-tail = 2.91998558 and ** t-test Critical two-tail = 4.30265273. Vertical error bars in both directions were set based on the Standard Error Margin (SEM). Phage P-2 was the first peptide to exceed the 2.92 (α = 0.05) threshold value for significance in the experimental versus blank control series. Phage P-20 had the greatest affinity for CXCR7.

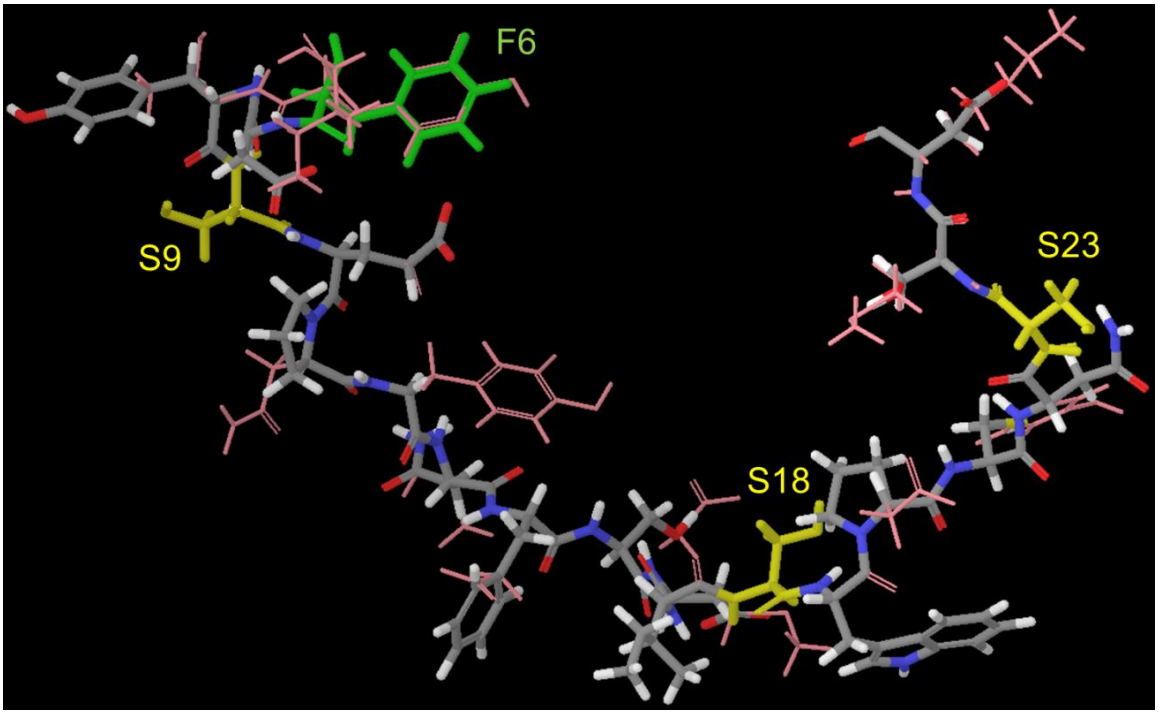

Figure 6. 3D Molecular Model of the ACKR3/CXCR7 N-Terminus (F6-D25). 3D model of the ACKR3/CXCR7 N-terminus F6-D25 (FDYSEPGNFSDISWPCNSSD) in CPK BALL & STICK mode overlaid on top of the corresponding CXCR4 N-terminus I6-K25 (IYTSDNYTEEMGSGDYDSMK) in PINK thin-tube mode. The residue phenylalanine-6 (F6) of the N-terminus of ACKR3/CXCR7 is highlighted in GREEN. The serine residues identical to both the ACKR3/CXCR7 and CXCR4 sequences, S9, S18, and S23, are highlighted in YELLOW.

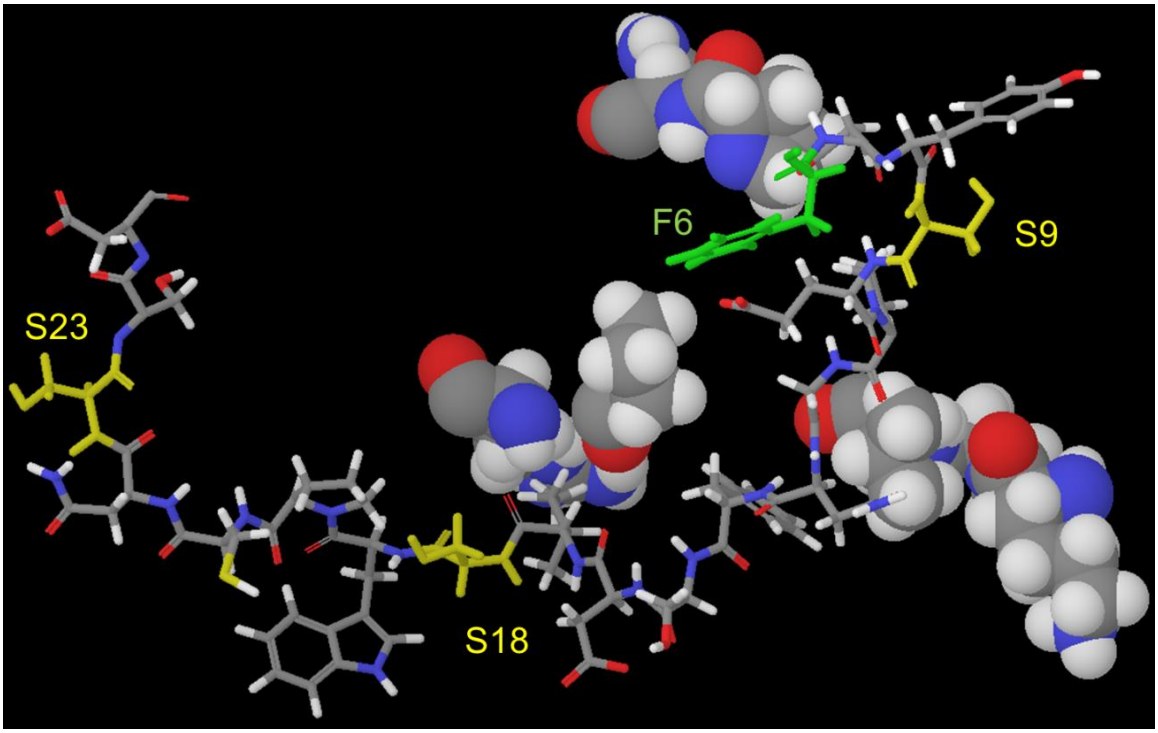

Figure 7. 3D Model Representing the Physical Location of Ligand Residues Similar to Peptide P-20. Amino acids from the endogenous ligand SDF1/CXCL12 ($K_{22}P_{23}V_{24}P_{31}R_{33}P_{53}N_{54}$) that were identified as the most similar to the sequence of Peptide P-20 (APLPRPG) are shown in Space-Fill mode interacting with the CXCR7 N-terminus (F6-D25) sequence model (CPK BALL & STICK mode). The residue phenylalanine-6 (F6) of the N-terminus of ACKR3/CXCR7 is highlighted in GREEN. The serine residues identical to both the ACKR3/CXCR7 and CXCR4 sequences, S9, S18, and S23, are highlighted in YELLOW.

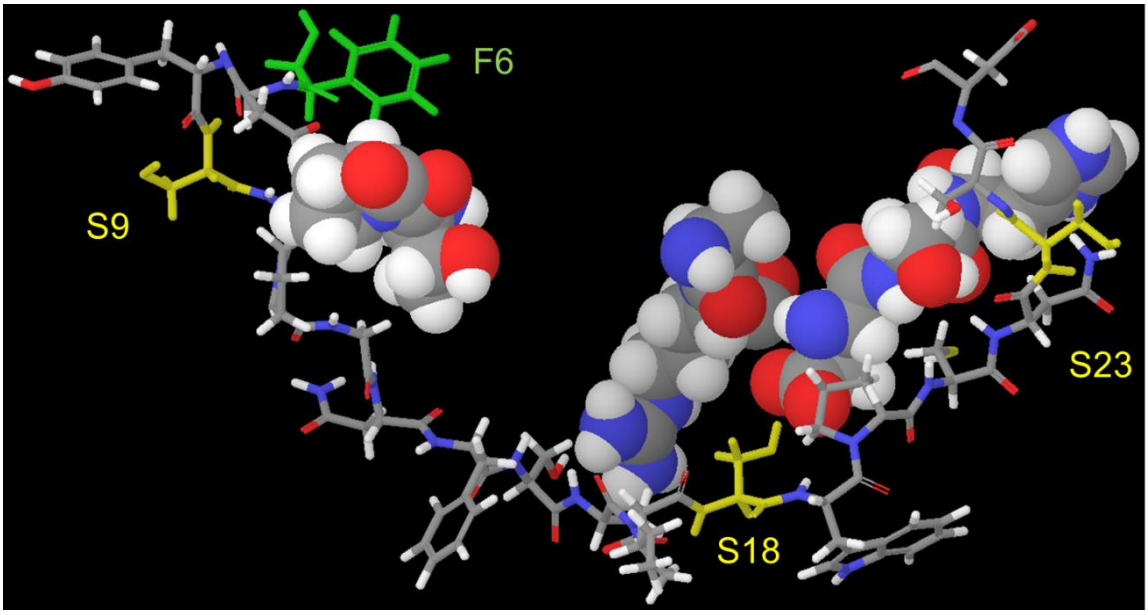

Figure 8. 3D Model Representing the Physical Location of Ligand Residues Similar to Peptide P-9. Amino acids from the endogenous ligand SDF1/CXCL12 ($E_{36}S_{37}H_{38}T_{52}P_{53}A_{61}R_{62}$) that were identified as the most similar to the sequence of Peptide P-9 (DSHTPQR) are shown in Space-Fill mode interacting with the CXCR7 N-terminus (F6-D25) sequence model (CPK BALL & STICK mode). The residue phenylalanine-6 (F6) of the N-terminus of ACKR3/CXCR7 is highlighted in GREEN. The serine residues identical to both the ACKR3/CXCR7 and CXCR4 sequences, S9, S18, and S23, are highlighted in YELLOW.

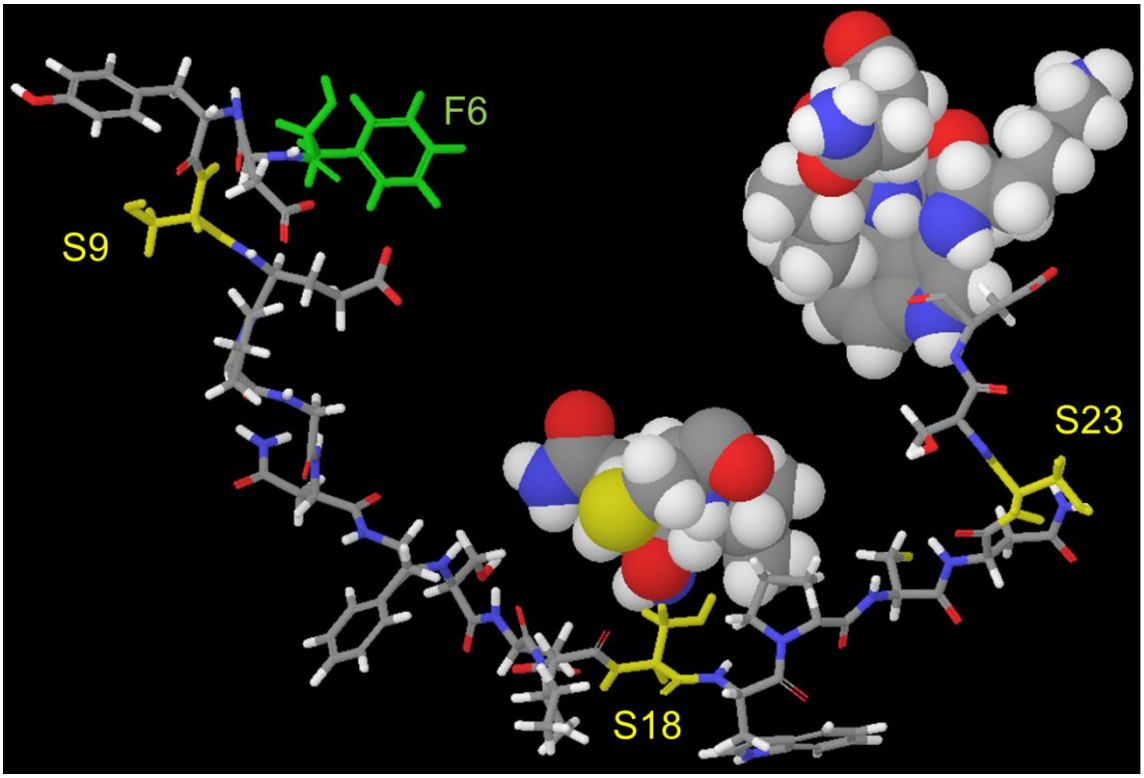

Figure 9. 3D Model Representing the Physical Location of Ligand Residues Similar to Peptide P-3. Amino acids from the endogenous ligand SDF1/CXCL12 ($Q_{69}V_{70}C_{71}K_{77}W_{78}I_{79}Q_{80}$) that were identified as the most similar to the sequence of Peptide P-3 (QMAQWPP) are shown in Space-Fill mode interacting with the CXCR7 N-terminus (F6-D25) sequence model (CPK BALL & STICK mode). The residue phenylalanine-6 (F6) of the N-terminus of ACKR3/CXCR7 is highlighted in GREEN. The serine residues identical to both the ACKR3/CXCR7 and CXCR4 sequences, S9, S18, and S23, are highlighted in YELLOW.

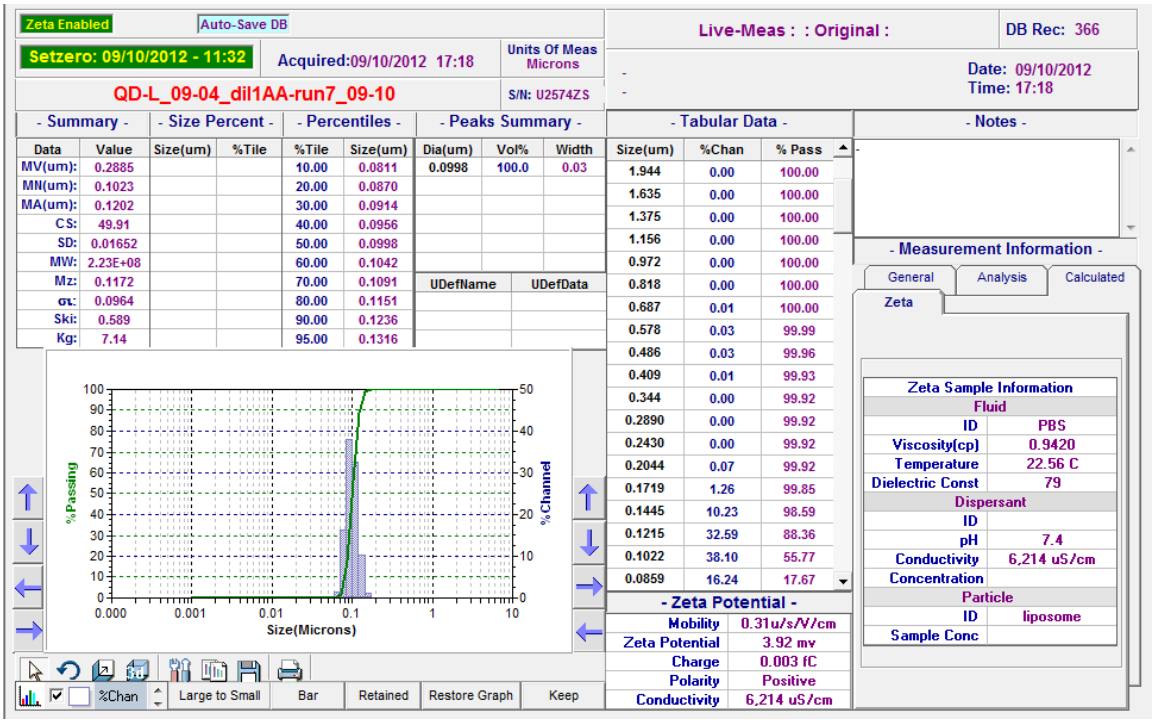

Figure 10. 100 nm Liposome Synthesis Using C-70 Derivative (ALM) and Egg-PC (1:2). ALM and egg-PC were dissolved in diethyl-ether in a round bottom flask suspended in an ice-water bath and sparged with Nitrogen to form a lipid film. The film was rehydrated with PBS (1X) for two hours at RT. The rehydrated PBS (1X) /ALM/egg-pc solution and extruder were maintained at 29°C. The solution was sequentially pushed through a 400nm, 200nm, and finally 100nm filter. The particle size and zeta potential were determined using a MicrotrakZetatrac.

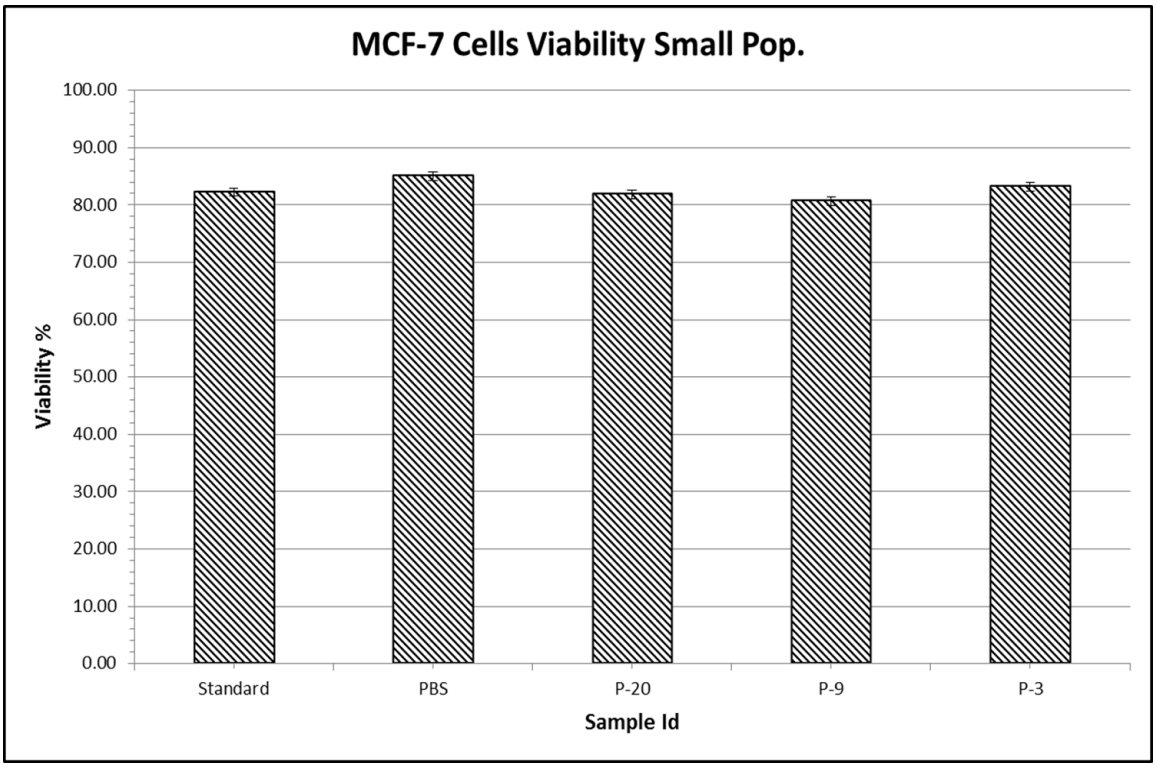

Figure 11. The Effect of Phage Peptide Incubation on the Viability of a Small Population of MCF-7 Cells. The populations consisted of 3 wells each containing 5,000 cells. Cells were grown for 48 hrs and then incubated in a 10% phage/PBS (1X) solution for another 48 hrs. Standard well received only media and PBS well received PBS (1X) instead of phage peptide. Live/Dead staining was performed with Trypan Blue and no statistical difference in viability was observed ($\alpha = 0.05$).

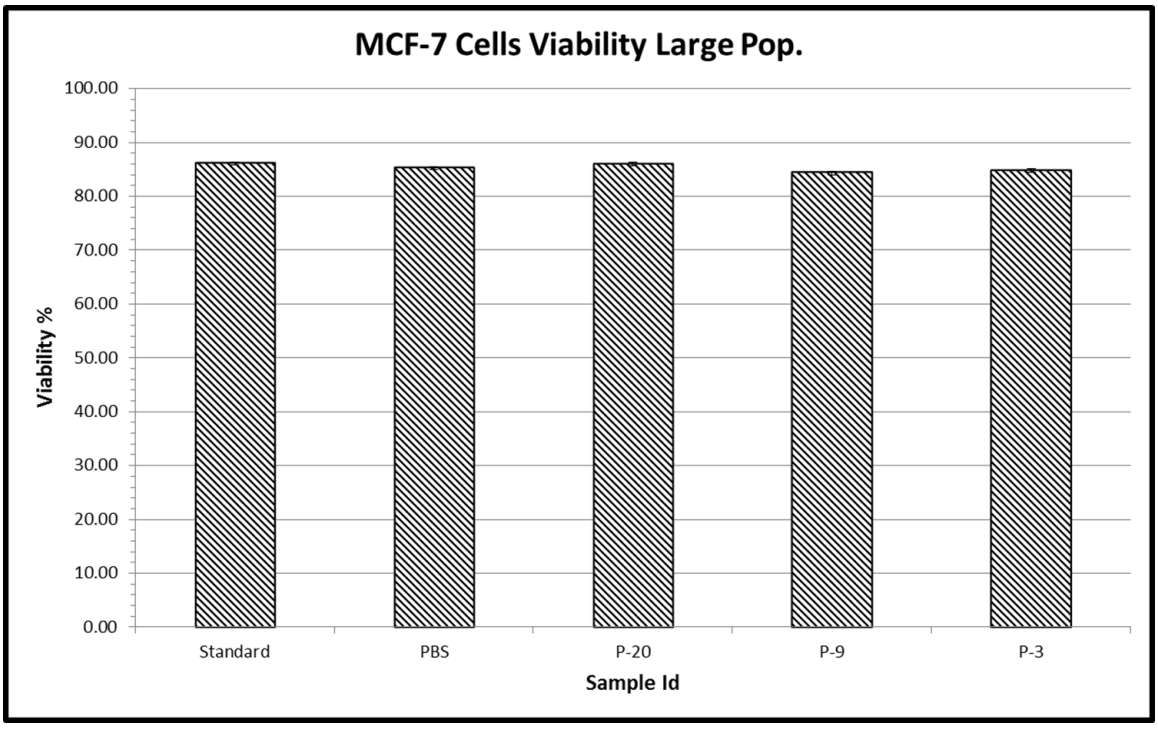

Figure 12. The Effect of Phage Peptide Incubation on the Viability of a Large Population of MCF-7 Cells. The populations consisted of 1 well each containing 100,000 cells. Cells were grown for 48 hrs and then incubated in a 10% phage/PBS (1X) solution for another 48 hrs. Standard well received only media and PBS well received PBS (1X) instead of phage peptide. Live/Dead staining was performed with Trypan Blue and no statistical difference in viability was observed ($\alpha = 0.05$).

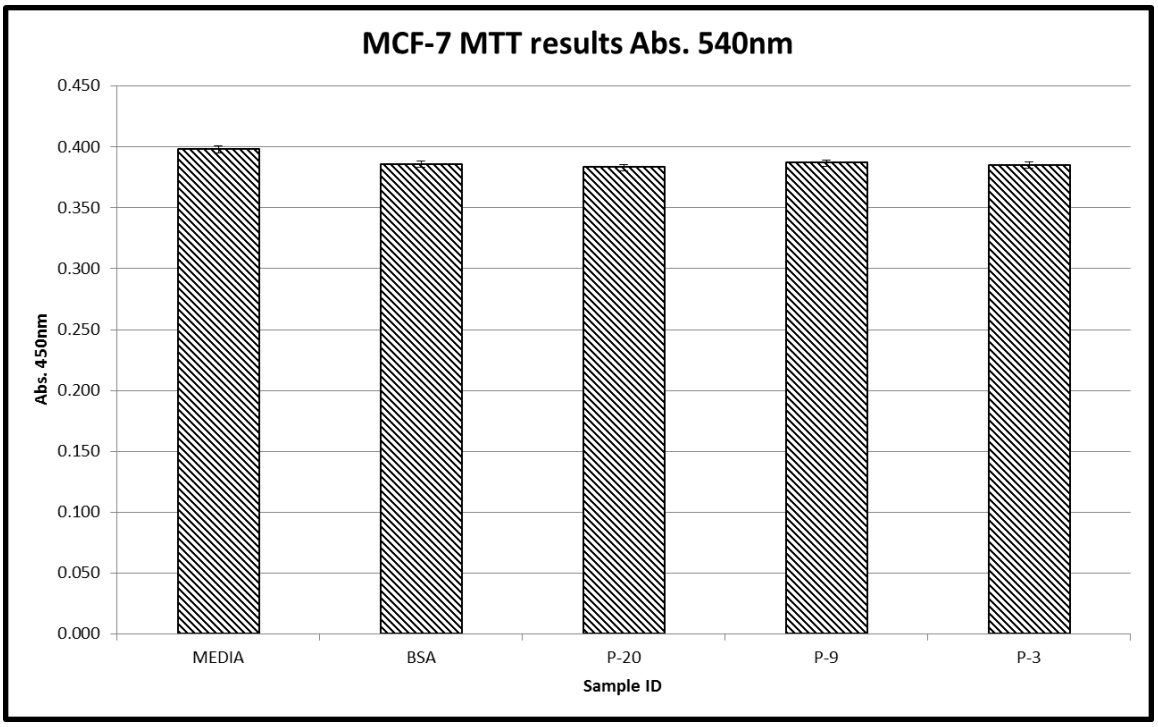

Figure 13. The Effect of Phage Peptide Incubation on the Cell Proliferation of MCF-7 Cells. The populations consisted of 6 wells each containing 25,000 cells. Cells were grown for 48 hrs and then incubated in a 10% phage/BSA (0.5%) solution for another 48 hrs. Standard well received only media and BSA well received BSA (0.5%) instead of phage peptide. An MTT assay was performed and no statistical difference in viability was observed ($\alpha = 0.05$).

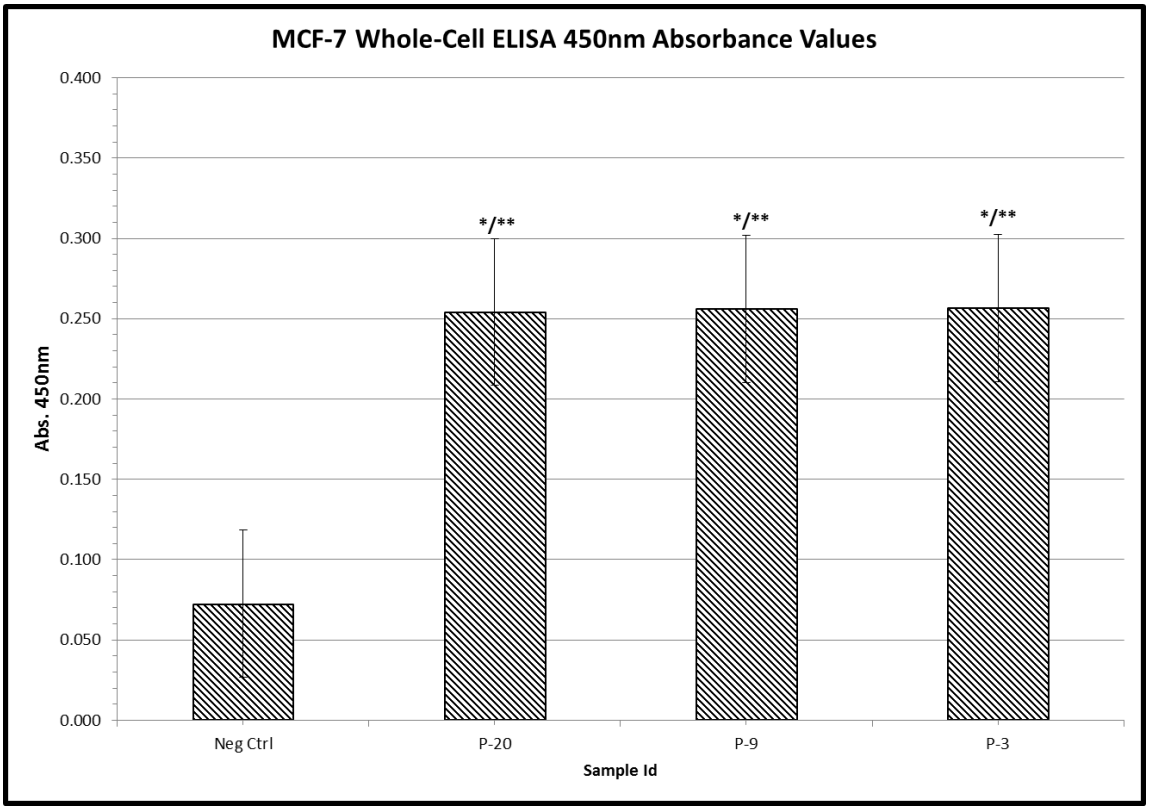

Figure 14. Whole-Cell ELISA Confirmation of MCF-7 Cell Membrane Binding by Phage Peptides Using an HRP Conjugated Anti-M13 Antibody with a TMB Substrate and STOP-450 Solution. The populations consisted of 6 wells each containing 25,000 cells. Cells were grown for 48 hrs at 37^0C and then incubated in a 10% phage/PBS (1X) solution for 2 hrs at 4^0C. All phage peptide results were statistically significant compared to the no-phage negative control ($\alpha = 0.05$).

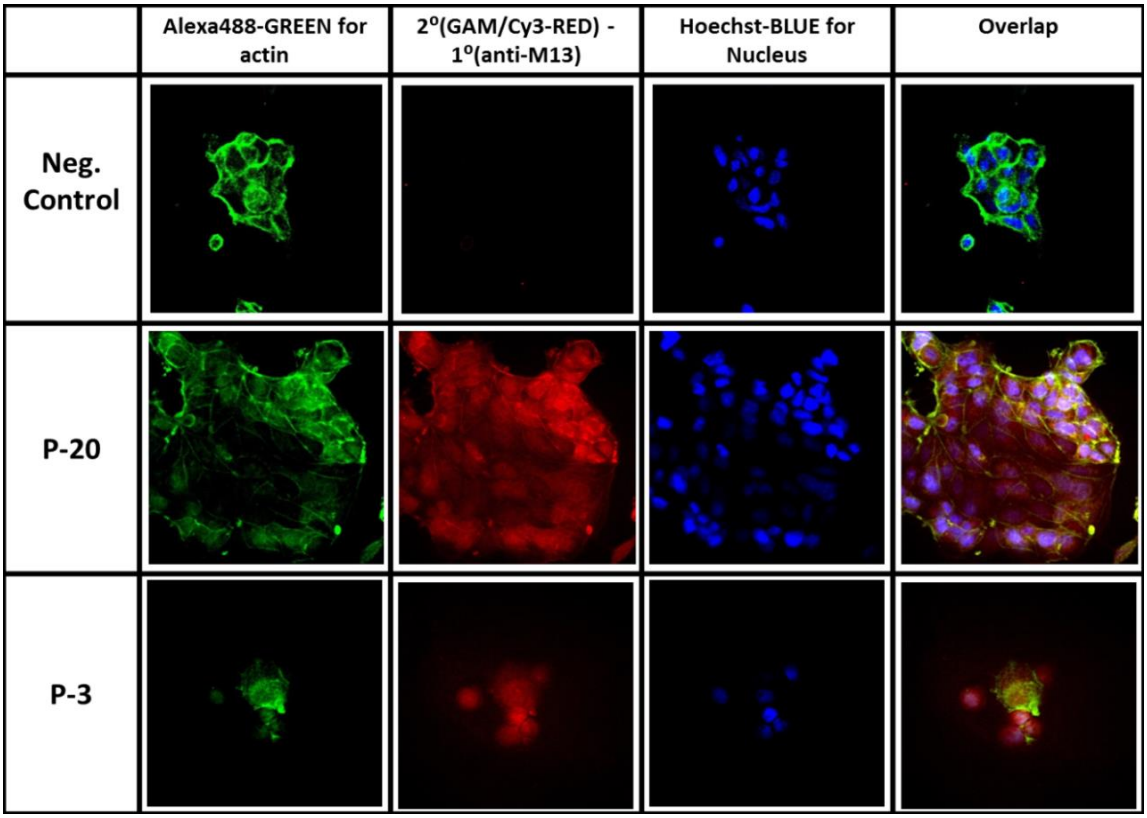

Figure 15. MCF-7 Cells - Membrane Receptor Binding and Cellular Uptake of Phage Display Derived Peptides. The fluorescent dyes used were: [Hoechst-BLUE for Nucleus, Alexa488-GREEN for actin, 2^0(GAM/Cy3-RED) - 1^0(anti-M13) for Phage Peptides]. Areas of location overlap are indicated by YELLOW (Membrane) and PURPLE (Nucleus).

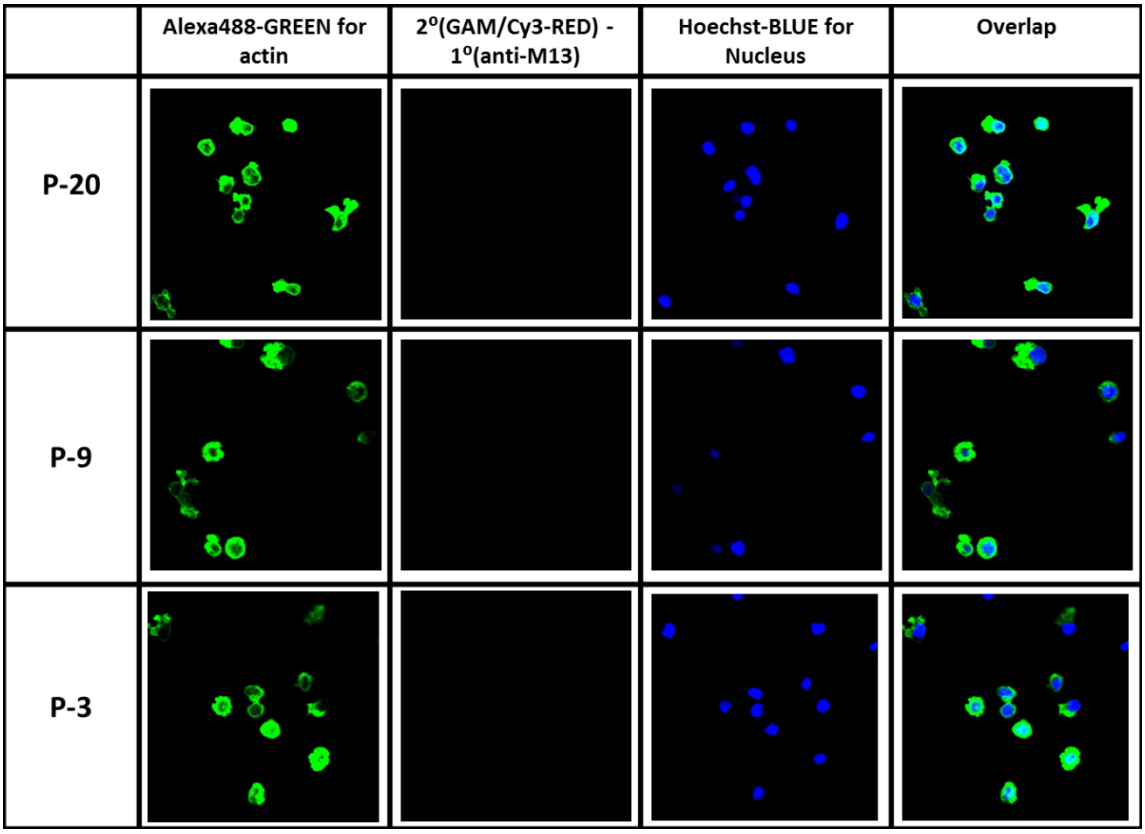

Figure 16. Negative Control Cell Line THP-1 Cells - Membrane Receptor Binding and Cellular Uptake of Phage Display Derived Peptides. The fluorescent dyes used were: [Hoechst-BLUE for Nucleus, Alexa488-GREEN for actin, 2^0(GAM/Cy3-RED) - 1^0(anti-M13) for Phage Peptides]. Areas of location overlap are indicated by YELLOW (Membrane) and PURPLE (Nucleus).

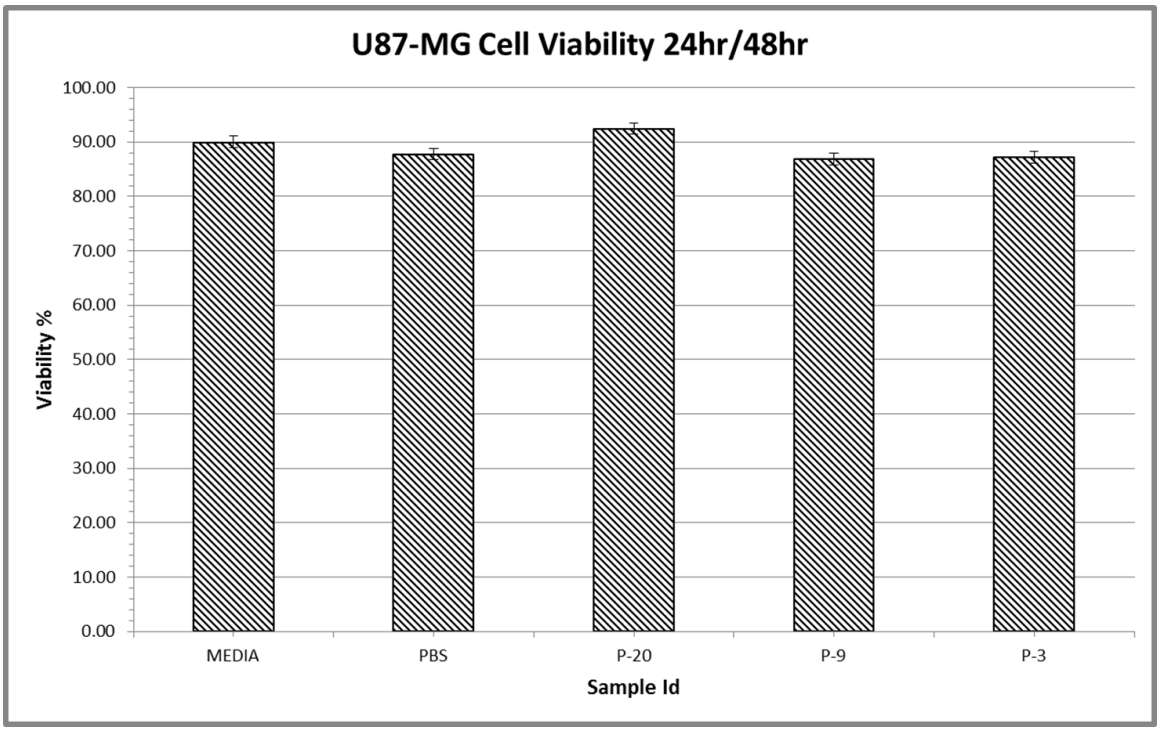

Figure 17. The Effect of Phage Peptide Incubation and Length of Initial Growth Cycle (24 hrs) on the Viability of U87-MG Cells. The populations consisted of 1 well each containing 100,000 cells. Cells were grown for 24 hrs and then incubated in a 10% phage/PBS (1X) for another 48 hrs. Standard well received only media and PBS well received PBS (1X) instead of phage peptide. Live/Dead staining was performed with Trypan Blue and no statistical difference in viability was observed ($\alpha = 0.05$).

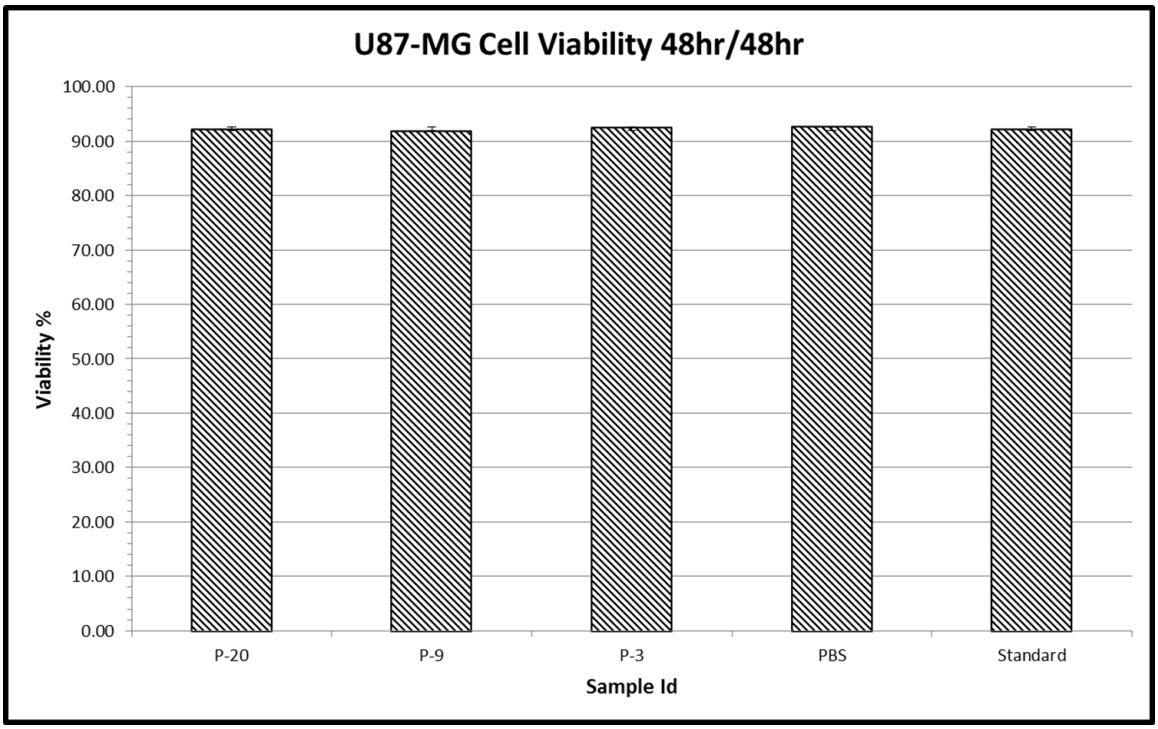

Figure 18. The Effect of Phage Peptide Incubation and Length of Initial Growth Cycle (48 hrs) on the Viability of U87-MG Cells. The populations consisted of 4 wells each containing 84,000 cells. Cells were grown for 48 hrs and then incubated in a 10% phage/PBS (1X) solution for another 48 hrs. Standard well received only media and PBS well received PBS (1X) instead of phage peptide. Live/Dead staining was performed with Trypan Blue and no statistical difference in viability was observed ($\alpha = 0.05$).

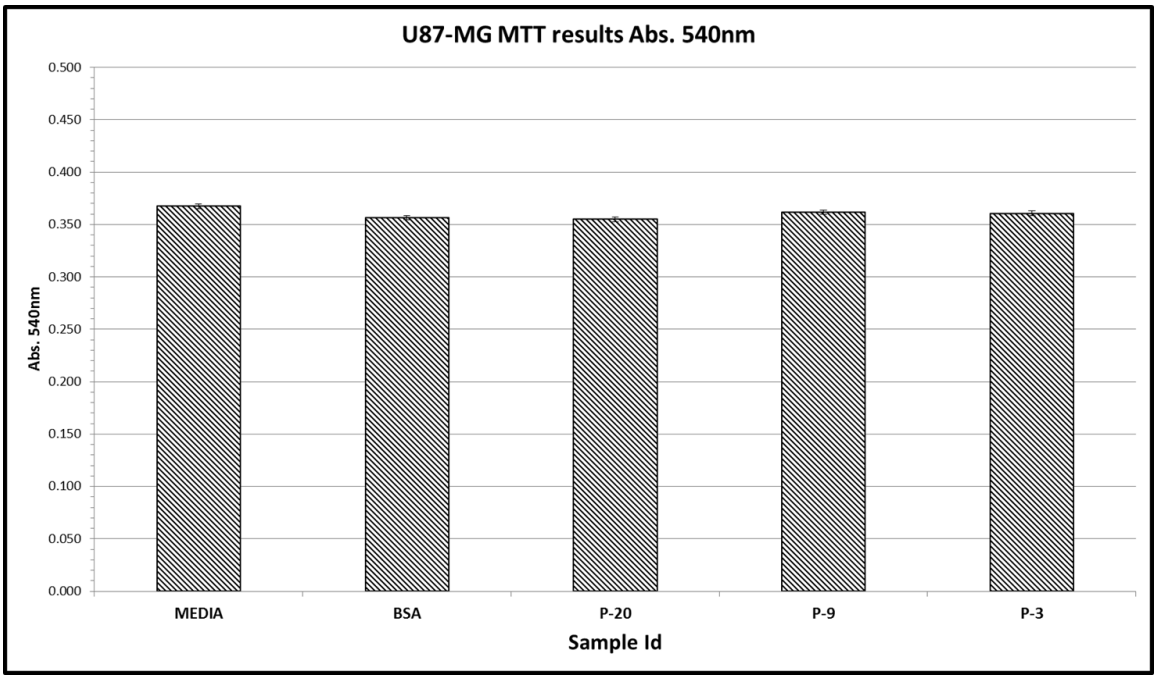

Figure 19. The Effect of Phage Peptide Incubation on the Cell Proliferation of U87-MG Cells. The populations consisted of 6 wells each containing 25,000 cells. Cells were grown for 48 hrs and then incubated in a 10% phage/BSA (0.5%) solution for another 48 hrs. Standard well received only media and BSA well received BSA (0.5%) instead of phage peptide. An MTT assay was performed and no statistical difference in viability was observed ($\alpha = 0.05$).

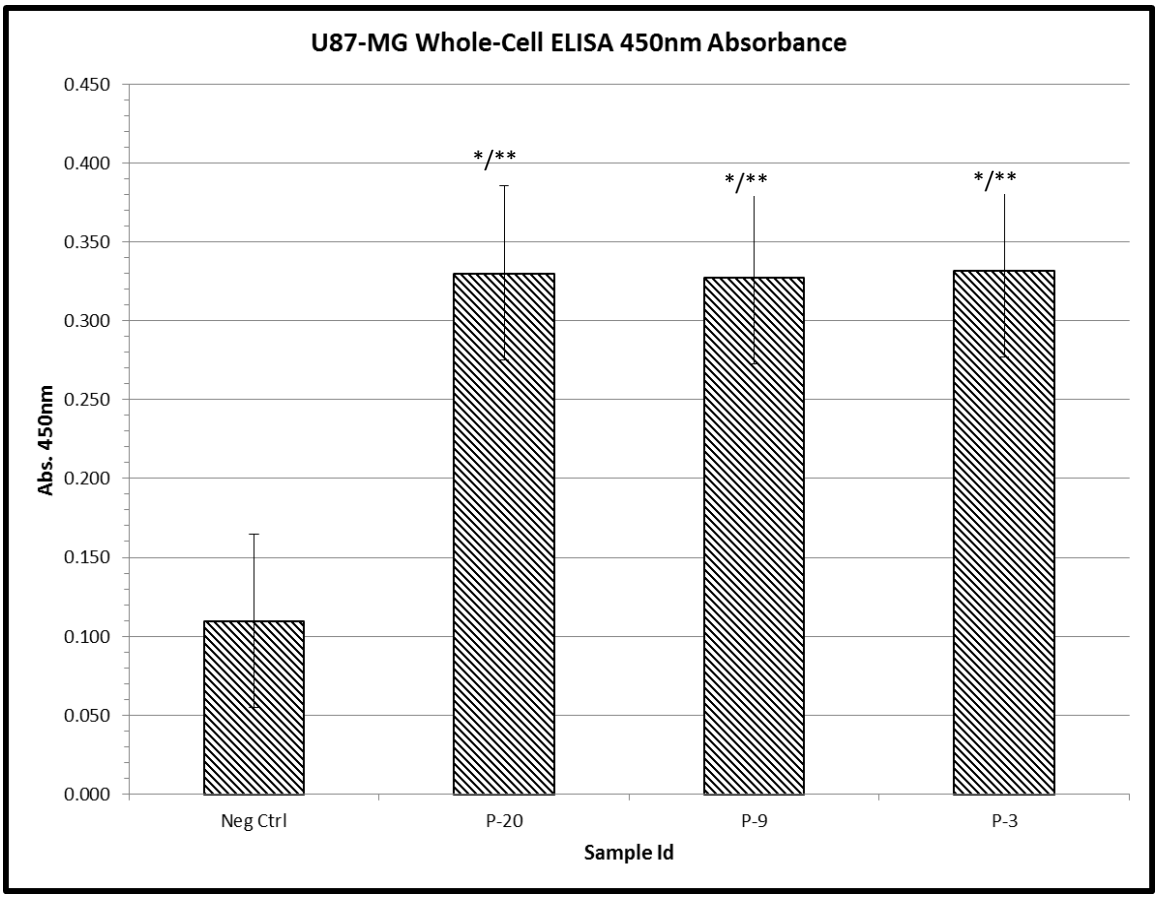

Figure 20. Whole-Cell ELISA Confirmation of U87-MG Cell Membrane Binding by Phage Peptides Using an HRP Conjugated Anti-M13 Antibody with a TMB Substrate and STOP-450 Solution. The populations consisted of 6 wells each containing 25,000 cells. Cells were grown for 48 hrs at 37^0C and then incubated in a 10% phage/BSA (0.5%) solution for 2 hrs at 4^0C. All phage peptide results were statistically significant compared to the no-phage negative control ($\alpha = 0.05$).

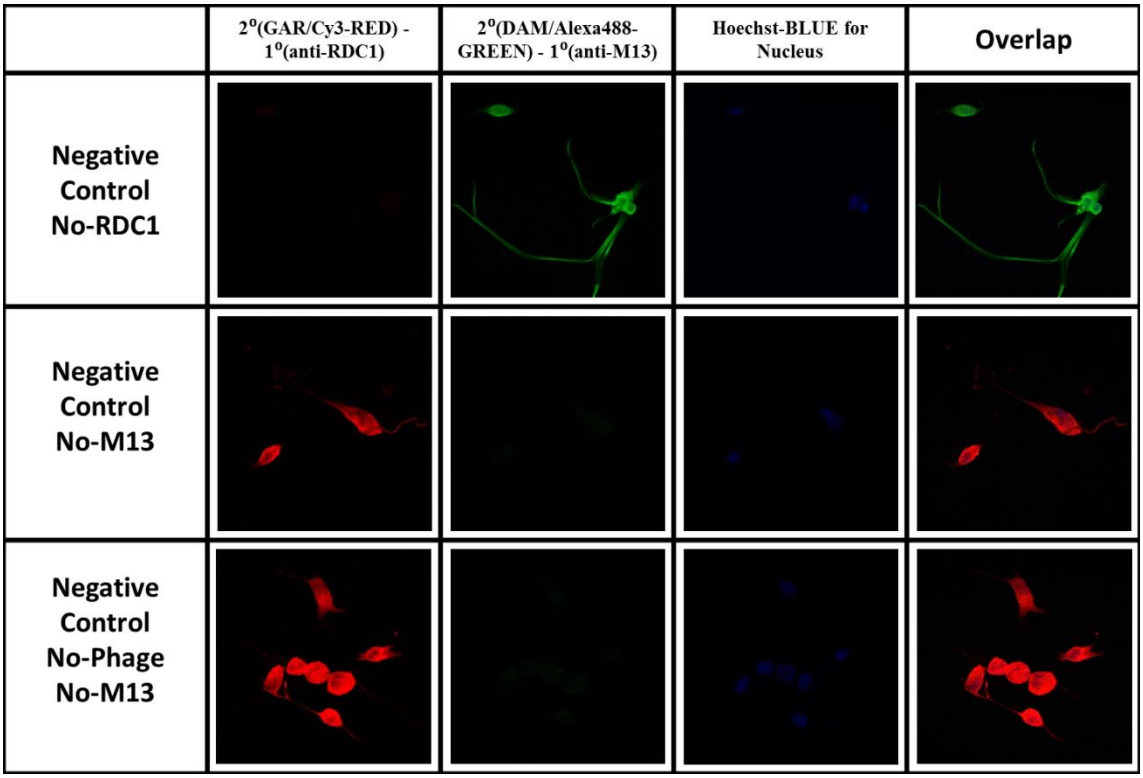

Figure 21A. U87-MG Cells - Confirmation of Co-Localization and Cellular Uptake of Phage Display Derived Peptides and the Known ACKR3/CXCR7 Antibody, Anti-RDC1. The fluorescent dyes used were: [Hoechst-BLUE for Nucleus, 2^0(GAR/Cy3-RED) - 1^0(anti-RDC1) for ACKR3/CXCR7 receptor, 2^0(DAM/Alexa488-GREEN) - 1^0(anti-M13) for Phage Peptides]. The areas of colocalization at the extracellular membrane and in the cytoplasm are indicated by the YELLOW overlap (RDC1-RED + Phage Peptide-GREEN). Areas of intracellular colocalization in and around the nucleus are indicated by the (Phage Peptide-GREEN + Nucleus-BLUE) overlap.

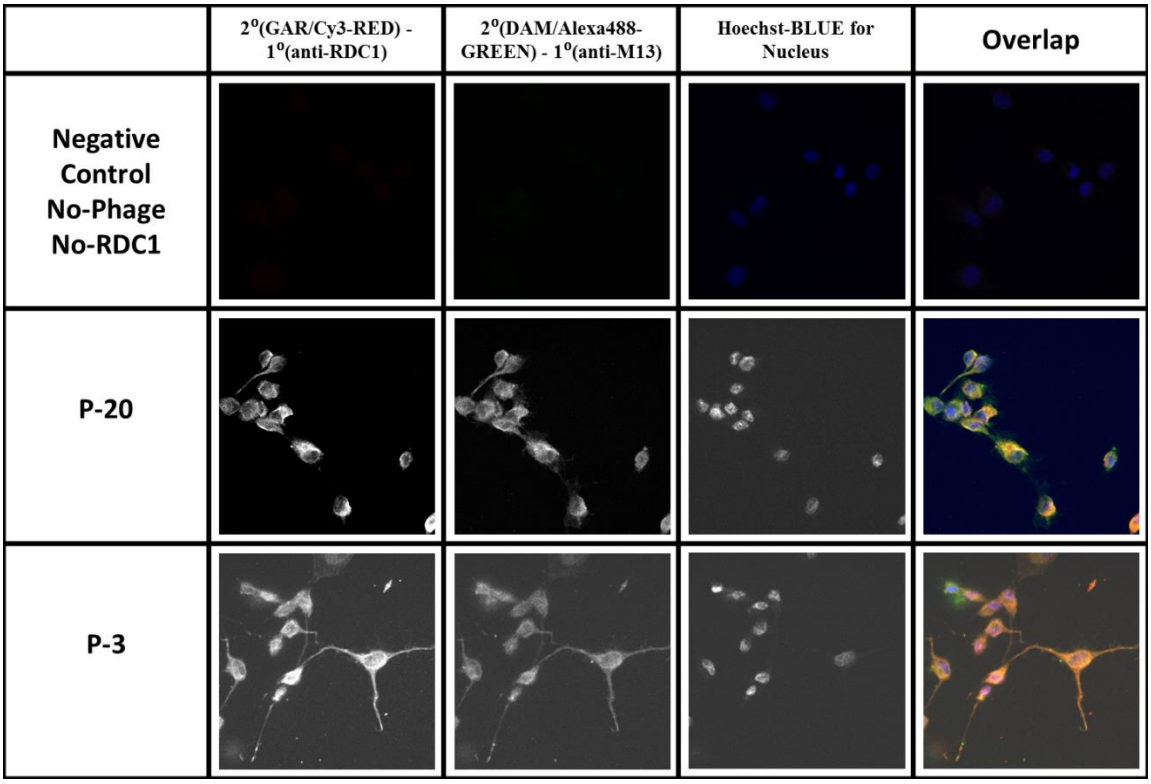

Figure 21B. U87-MG Cells - Confirmation of Co-Localization and Cellular Uptake of Phage Display Derived Peptides and the Known ACKR3/CXCR7 Antibody, Anti-RDC1. The fluorescent dyes used were: [Hoechst-BLUE for Nucleus, 2^0(GAR/Cy3-RED) - 1^0(anti-RDC1) for ACKR3/CXCR7 receptor, 2^0(DAM/Alexa488-GREEN) - 1^0(anti-M13) for Phage Peptides]. The areas of colocalization at the extracellular membrane and in the cytoplasm are indicated by the YELLOW overlap (RDC1-RED + Phage Peptide-GREEN). Areas of intracellular colocalization in and around the nucleus are indicated by the (Phage Peptide-GREEN + Nucleus-BLUE) overlap.

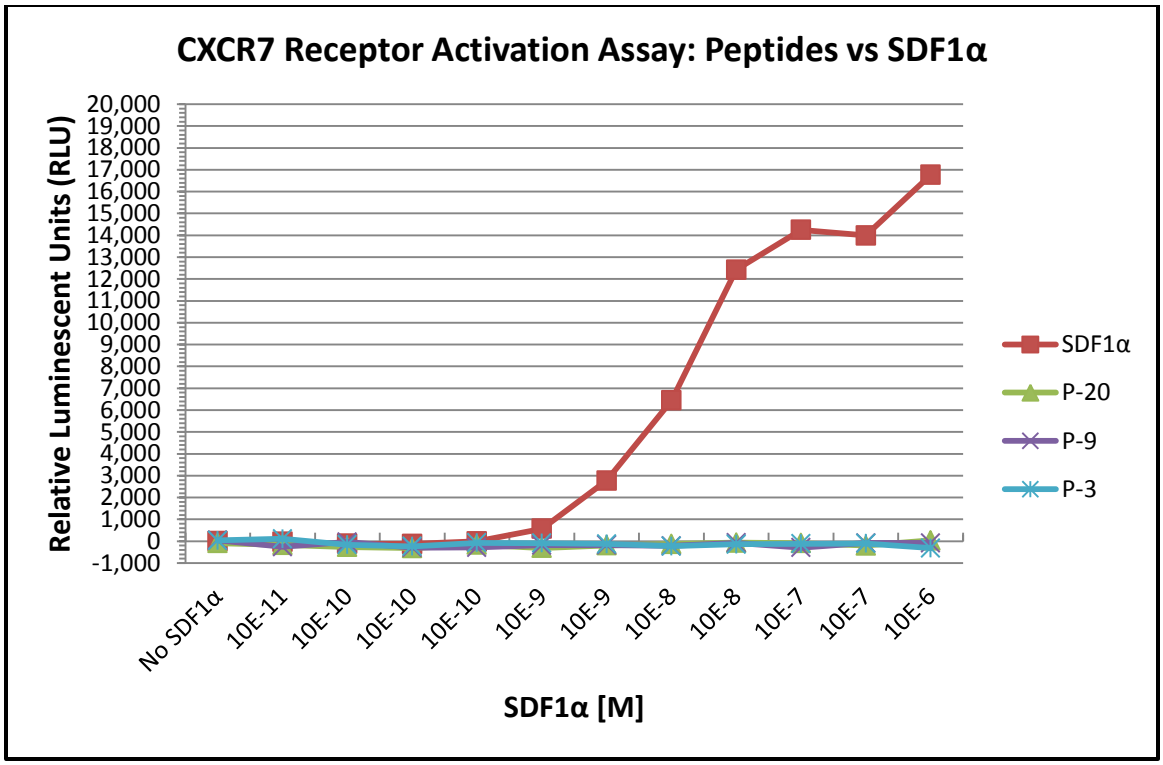

Figure 22. Quantifying the Level of ACKR3/CXCR7 Activation Using a PathHunter β-Arrestin Assay (DiscoverX) with the Phage Peptides, the Endogenous Ligand SDF1α, and CHO-K1 Modified Cells. A 12-point dose response curve was performed according to the manufacturer's instructions. The Phage Peptides showed no effect compared to SDF1α.

REFERENCES

1 Allen, T. M. Ligand-targeted therapeutics in anticancer therapy. *Nature reviews. Cancer* **2**, 750-763, doi:10.1038/nrc903 (2002).

2 Zhang, S. *et al.* Identification of the molecular basis of doxorubicin-induced cardiotoxicity. *Nature medicine* **18**, 1639-1642, doi:10.1038/nm.2919 (2012).

3 Minotti, G., Menna, P., Salvatorelli, E., Cairo, G. & Gianni, L. Anthracyclines: molecular advances and pharmacologic developments in antitumor activity and cardiotoxicity. *Pharmacological reviews* **56**, 185-229, doi:10.1124/pr.56.2.6 (2004).

4 Forssen, E. A. & Tőkés, Z. A. In vitro and in vivo studies with adriamycin liposomes. *Biochemical and biophysical research communications* **91**, 1295-1301, doi:http://dx.doi.org/10.1016/0006-291X(79)91207-5 (1979).

5 Maher Qweider, Joachim M. Gilsbach & Veit Rohde. Inadvertent intrathecal vincristine administration: a neurosurgical emergency. *Journal of Neurosurgery: Spine* **6**, 280-283, doi:doi:10.3171/spi.2007.6.3.280 (2007).

6 D'Addario, A. *et al.* Accidental intrathecal administration of vincristine. *The American journal of forensic medicine and pathology* **31**, 83-84, doi:10.1097/PAF.0b013e3181c21c10 (2010).

7 Weiss, R. B. *et al.* Hypersensitivity reactions from taxol. *Journal of clinical oncology : official journal of the American Society of Clinical Oncology* **8**, 1263-1268 (1990).

8 Park, J. W. *et al.* Anti-HER2 immunoliposomes: enhanced efficacy attributable to targeted delivery. *Clinical cancer research : an official journal of the American Association for Cancer Research* **8**, 1172-1181 (2002).

9 Carter, P. Improving the efficacy of antibody-based cancer therapies. *Nature reviews. Cancer* **1**, 118-129, doi:10.1038/35101072 (2001).

10 Biswas, S., Dodwadkar, N. S., Deshpande, P. P., Parab, S. & Torchilin, V. P. Surface functionalization of doxorubicin-loaded liposomes with octa-arginine for enhanced anticancer activity. *European journal of pharmaceutics and*

biopharmaceutics : official journal of Arbeitsgemeinschaft fur Pharmazeutische Verfahrenstechnik e.V **84**, 517-525, doi:10.1016/j.ejpb.2012.12.021 (2013).

11 Haley, B. & Frenkel, E. Nanoparticles for drug delivery in cancer treatment. *Urologic Oncology: Seminars and Original Investigations* **26**, 57-64, doi:http://dx.doi.org/10.1016/j.urolonc.2007.03.015 (2008).

12 Vivero-Escoto, J. L. Nanovehicles for Intracellular Protein Delivery. *J Biotechnol Biomater* **3**, e117 (2013).

13 Crommelin, D. J. A., Slaats, N. & van Bloois, L. Preparation and characterization of doxorubicin-containing liposomes: I. Influence of liposome charge and pH of hydration medium on loading capacity and particle size. *International Journal of Pharmaceutics* **16**, 79-92, doi:http://dx.doi.org/10.1016/0378-5173(83)90130-8 (1983).

14 Niu, G., Cogburn, B. & Hughes, J. Preparation and characterization of doxorubicin liposomes. *Methods in molecular biology (Clifton, N.J.)* **624**, 211-219, doi:10.1007/978-1-60761-609-2_14 (2010).

15 Maruyama, K. Intracellular targeting delivery of liposomal drugs to solid tumors based on EPR effects. *Advanced drug delivery reviews* **63**, 161-169, doi:10.1016/j.addr.2010.09.003 (2011).

16 Wen, C. J., Zhang, L. W., Al-Suwayeh, S. A., Yen, T. C. & Fang, J. Y. Theranostic liposomes loaded with quantum dots and apomorphine for brain targeting and bioimaging. *International journal of nanomedicine* **7**, 1599-1611, doi:10.2147/ijn.s29369 (2012).

17 Frank, M. M. The reticuloendothelial system and bloodstream clearance. *The Journal of laboratory and clinical medicine* **122**, 487-488 (1993).

18 Serwer, L. P. & James, C. D. Challenges in drug delivery to tumors of the central nervous system: an overview of pharmacological and surgical considerations. *Advanced drug delivery reviews* **64**, 590-597, doi:10.1016/j.addr.2012.01.004 (2012).

19 Alam, M. I. *et al.* Strategy for effective brain drug delivery. *European journal of pharmaceutical sciences : official journal of the European Federation for Pharmaceutical Sciences* **40**, 385-403, doi:10.1016/j.ejps.2010.05.003 (2010).

20 Gourevich, D. *et al.* Ultrasound activated nano-encapsulated targeted drug delivery and tumour cell poration. *Advances in experimental medicine and biology* **733**, 135-144, doi:10.1007/978-94-007-2555-3_13 (2012).

21 Meairs, S. *Topics in Medicinal Chemistry* Ch. 37, 1-16 (Springer Berlin Heidelberg, 2014).

22 Wan, X. M., Chen, Y. P., Xu, W. R., Yang, W. J. & Wen, L. P. Identification of nose-to-brain homing peptide through phage display. *Peptides* **30**, 343-350, doi:10.1016/j.peptides.2008.09.026 (2009).

23 Reitz, M. *et al.* Intranasal delivery of neural stem/progenitor cells: a noninvasive passage to target intracerebral glioma. *Stem cells translational medicine* **1**, 866-873, doi:10.5966/sctm.2012-0045 (2012).

24 Nomiyama, H., Osada, N. & Yoshie, O. Systematic classification of vertebrate chemokines based on conserved synteny and evolutionary history. *Genes to cells : devoted to molecular & cellular mechanisms* **18**, 1-16, doi:10.1111/gtc.12013 (2013).

25 Anders, H.-J., Romagnani, P. & Mantovani, A. Pathomechanisms: homeostatic chemokines in health, tissue regeneration, and progressive diseases. *Trends in molecular medicine* **20**, 154-165, doi:http://dx.doi.org/10.1016/j.molmed.2013.12.002 (2014).

26 Zhu, Q., Han, X., Peng, J., Qin, H. & Wang, Y. The role of CXC chemokines and their receptors in the progression and treatment of tumors. *J Mol Hist* **43**, 699-713, doi:10.1007/s10735-012-9435-x (2012).

27 Owen, J. L. & Mohamadzadeh, M. Macrophages and chemokines as mediators of angiogenesis. *Frontiers in physiology* **4**, 159, doi:10.3389/fphys.2013.00159 (2013).

28 Keeley, E. C., Mehrad, B. & Strieter, R. M. Chemokines as mediators of tumor angiogenesis and neovascularization. *Experimental cell research* **317**, 685-690, doi:10.1016/j.yexcr.2010.10.020 (2011).

29 Chew, A. L., Tan, W. Y. & Khoo, B. Y. Potential combinatorial effects of recombinant atypical chemokine receptors in breast cancer cell invasion: A research perspective. *Biomedical reports* **1**, 185-192, doi:10.3892/br.2013.57 (2013).

30 Ahn, B. J., Pollack, I. F. & Okada, H. Immune-checkpoint blockade and active immunotherapy for glioma. *Cancers* **5**, 1379-1412, doi:10.3390/cancers5041379 (2013).

31 Vartanian, A. *et al.* GBM's multifaceted landscape: highlighting regional and microenvironmental heterogeneity. *Neuro-oncology* **16**, 1167-1175, doi:10.1093/neuonc/nou035 (2014).

32 Goffart, N., Kroonen, J. & Rogister, B. Glioblastoma-initiating cells: relationship with neural stem cells and the micro-environment. *Cancers* **5**, 1049-1071, doi:10.3390/cancers5031049 (2013).

33 Wurth, R. *et al.* Expression of CXCR7 chemokine receptor in human meningioma cells and in intratumoral microvasculature. *Journal of neuroimmunology* **234**, 115-123, doi:10.1016/j.jneuroim.2011.01.006 (2011).

34 Wurth, R., Bajetto, A., Harrison, J. K., Barbieri, F. & Florio, T. CXCL12 modulation of CXCR4 and CXCR7 activity in human glioblastoma stem-like cells and regulation of the tumor microenvironment. *Frontiers in cellular neuroscience* **8**, 144, doi:10.3389/fncel.2014.00144 (2014).

35 Wani, N. *et al.* C-X-C motif chemokine 12/C-X-C chemokine receptor type 7 signaling regulates breast cancer growth and metastasis by modulating the tumor microenvironment. *Breast cancer research : BCR* **16**, R54, doi:10.1186/bcr3665 (2014).

36 Zweemer, A. J. M., Toraskar, J., Heitman, L. H. & Ijzerman, A. P. Bias in chemokine receptor signalling. *Trends in Immunology*, doi:http://dx.doi.org/10.1016/j.it.2014.02.004.

37 Odemis, V. *et al.* The presumed atypical chemokine receptor CXCR7 signals through G(i/o) proteins in primary rodent astrocytes and human glioma cells. *Glia* **60**, 372-381, doi:10.1002/glia.22271 (2012).

38 Graham, G. J., Locati, M., Mantovani, A., Rot, A. & Thelen, M. The biochemistry and biology of the atypical chemokine receptors. *Immunology letters* **145**, 30-38, doi:10.1016/j.imlet.2012.04.004 (2012).

39 Zhu, Y. & Murakami, F. Chemokine CXCL12 and its receptors in the developing central nervous system: emerging themes and future perspectives. *Developmental neurobiology* **72**, 1349-1362, doi:10.1002/dneu.22041 (2012).

40 Nomiyama, H. & Yoshie, O. Functional roles of evolutionary conserved motifs and residues in vertebrate chemokine receptors. *Journal of leukocyte biology* **97**, 39-47 (2015).

41 Wang, J. & Norcross, M. Dimerization of chemokine receptors in living cells: key to receptor function and novel targets for therapy. *Drug discovery today* **13**, 625-632, doi:10.1016/j.drudis.2008.04.004 (2008).

42 Dai, X. *et al.* The role of CXCR7 on the adhesion, proliferation and angiogenesis of endothelial progenitor cells. *Journal of cellular and molecular medicine* **15**, 1299-1309, doi:10.1111/j.1582-4934.2011.01301.x (2011).

43 Puchert, M. & Engele, J. The peculiarities of the SDF-1/CXCL12 system: in some cells, CXCR4 and CXCR7 sing solos, in others, they sing duets. *Cell and tissue research* **355**, 239-253, doi:10.1007/s00441-013-1747-y (2014).

44 Wang, J. *et al.* The role of CXCR7/RDC1 as a chemokine receptor for CXCL12/SDF-1 in prostate cancer. *The Journal of biological chemistry* **283**, 4283-4294, doi:10.1074/jbc.M707465200 (2008).

45 Singh, R. K. & Lokeshwar, B. L. The IL-8-regulated chemokine receptor CXCR7 stimulates EGFR signaling to promote prostate cancer growth. *Cancer research* **71**, 3268-3277, doi:10.1158/0008-5472.can-10-2769 (2011).

46 Zheng, K. *et al.* Chemokine receptor CXCR7 regulates the invasion, angiogenesis and tumor growth of human hepatocellular carcinoma cells. *Journal of experimental & clinical cancer research : CR* **29**, 31, doi:10.1186/1756-9966-29-31 (2010).

47 Hao, M. *et al.* Role of chemokine receptor CXCR7 in bladder cancer progression. *Biochemical pharmacology* **84**, 204-214, doi:10.1016/j.bcp.2012.04.007 (2012).

48 Yates, T. J. *et al.* C-X-C chemokine receptor 7: a functionally associated molecular marker for bladder cancer. *Cancer* **119**, 61-71, doi:10.1002/cncr.27661 (2013).

49 Maishi, N. *et al.* CXCR7: a novel tumor endothelial marker in renal cell carcinoma. *Pathology international* **62**, 309-317, doi:10.1111/j.1440-1827.2012.02792.x (2012).

50 Gahan, J. C. *et al.* Chemokine and chemokine receptor expression in kidney tumors: molecular profiling of histological subtypes and association with

metastasis. *The Journal of urology* **187**, 827-833, doi:10.1016/j.juro.2011.10.150 (2012).

51 Burns, J. M. *et al.* A novel chemokine receptor for SDF-1 and I-TAC involved in cell survival, cell adhesion, and tumor development. *The Journal of experimental medicine* **203**, 2201-2213, doi:10.1084/jem.20052144 (2006).

52 Miao, Z. *et al.* CXCR7 (RDC1) promotes breast and lung tumor growth in vivo and is expressed on tumor-associated vasculature. *Proceedings of the National Academy of Sciences* **104**, 15735-15740 (2007).

53 Marechal, R. *et al.* High expression of CXCR4 may predict poor survival in resected pancreatic adenocarcinoma. *British journal of cancer* **100**, 1444-1451 (2009).

54 Schrevel, M. *et al.* CXCR7 expression is associated with disease-free and disease-specific survival in cervical cancer patients. *British journal of cancer* **106**, 1520-1525, doi:10.1038/bjc.2012.110 (2012).

55 Xu, H. *et al.* Alteration of CXCR7 expression mediated by TLR4 promotes tumor cell proliferation and migration in human colorectal carcinoma. *PloS one* **6**, e27399, doi:10.1371/journal.pone.0027399 (2011).

56 Calatozzolo, C. *et al.* Expression of the new CXCL12 receptor, CXCR7, in gliomas. *Cancer biology & therapy* **11**, 242-253 (2011).

57 Esencay, M., Sarfraz, Y. & Zagzag, D. CXCR7 is induced by hypoxia and mediates glioma cell migration towards SDF-1alpha. *BMC cancer* **13**, 347, doi:10.1186/1471-2407-13-347 (2013).

58 Liu, Y., Carson-Walter, E. & Walter, K. A. Targeting chemokine receptor CXCR7 inhibits glioma cell proliferation and mobility. *Anticancer research* **35**, 53-64 (2015).

59 Liu, C. *et al.* Expression and functional heterogeneity of chemokine receptors CXCR4 and CXCR7 in primary patient-derived glioblastoma cells. *PloS one* **8**, e59750, doi:10.1371/journal.pone.0059750 (2013).

60 Tang, T., Xia, Q. J., Chen, J. B., Xi, M. R. & Lei, D. Expression of the CXCL12/SDF-1 chemokine receptor CXCR7 in human brain tumours. *Asian Pacific journal of cancer prevention : APJCP* **13**, 5281-5286 (2012).

61 Luker, K. E. *et al.* Scavenging of CXCL12 by CXCR7 promotes tumor growth and metastasis of CXCR4-positive breast cancer cells. *Oncogene* **31**, 4750-4758, doi:10.1038/onc.2011.633 (2012).

62 Guillemot, E. *et al.* CXCR7 receptors facilitate the progression of colon carcinoma within lung not within liver. *British journal of cancer* **107**, 1944-1949, doi:10.1038/bjc.2012.503 (2012).

63 Grymula, K. *et al.* Overlapping and distinct role of CXCR7-SDF-1/ITAC and CXCR4-SDF-1 axes in regulating metastatic behavior of human rhabdomyosarcomas. *International journal of cancer. Journal international du cancer* **127**, 2554-2568, doi:10.1002/ijc.25245 (2010).

64 Ma, M., Ye, J. Y., Deng, R., Dee, C. M. & Chan, G. C. Mesenchymal stromal cells may enhance metastasis of neuroblastoma via SDF-1/CXCR4 and SDF-1/CXCR7 signaling. *Cancer letters* **312**, 1-10, doi:10.1016/j.canlet.2011.06.028 (2011).

65 Luker, K. E., Steele, J. M., Mihalko, L. A., Ray, P. & Luker, G. D. Constitutive and chemokine-dependent internalization and recycling of CXCR7 in breast cancer cells to degrade chemokine ligands. *Oncogene* **29**, 4599-4610, doi:10.1038/onc.2010.212 (2010).

66 Canals, M. *et al.* Ubiquitination of CXCR7 Controls Receptor Trafficking. *PloS one* **7**, e34192, doi:10.1371/journal.pone.0034192 (2012).

67 Vestal, R. D., LaJeunesse, D.R., and Taylor, E.W. . Targeting the Atypical Chemokine Receptor ACKR3/CXCR7 for the Treatment of Cancer and Other Diseases: Phase 1 - Phage Display Peptide Identification and Characterization. *Current medicinal chemistry*, 42 (2015).

68 Yang, Y., Karakhanova, S., Werner, J. & Bazhin, A. V. Reactive oxygen species in cancer biology and anticancer therapy. *Current medicinal chemistry* **20**, 3677-3692 (2013).

69 Sergeeva, A., Kolonin, M. G., Molldrem, J. J., Pasqualini, R. & Arap, W. Display technologies: application for the discovery of drug and gene delivery agents. *Advanced drug delivery reviews* **58**, 1622-1654, doi:10.1016/j.addr.2006.09.018 (2006).

70 Network, T. C. G. A. T. R. Comprehensive genomic characterization defines human glioblastoma genes and core pathways. *Nature* **455**, 1061-1068, doi:10.1038/nature07385 (2008).

71 Brennan, C. W. *et al.* The somatic genomic landscape of glioblastoma. *Cell* **155**, 462-477, doi:10.1016/j.cell.2013.09.034 (2013).

72 Jolesz, F. in *Intraoperative Imaging and Image-Guided Therapy* (ed Ferenc A. Jolesz) Ch. 2, 25-45 (Springer New York, 2014).

73 Jolesz, F. A. & Tempany, C. M. C. in *MRI-Guided Focused Ultrasound Surgery* 81-99 (2007).

74 Schlesinger, D. *et al.* MR-guided focused ultrasound surgery, present and future. *Medical Physics* **40**, -, doi:doi:http://dx.doi.org/10.1118/1.4811136 (2013).

75 Wu, F. in *Tumor Ablation* Vol. 5 *The Tumor Microenvironment* (ed Yona Keisari) Ch. 4, 61-75 (Springer Netherlands, 2013).

76 Pfeffer, M. R., Rabin, T., Inbar, Y., Hananel, A. & Catane, R. in *Image-Guided Cancer Therapy* (eds Damian E. Dupuy, Yuman Fong, & William N. McMullen) Ch. 7, 79-99 (Springer New York, 2013).

77 Malietzis, G. *et al.* High-intensity focused ultrasound: advances in technology and experimental trials support enhanced utility of focused ultrasound surgery in oncology. *The British Journal of Radiology* **86**, 20130044, doi:doi:10.1259/bjr.20130044 (2013).

78 Senneville, B., Ries, M., Bartels, L. & Moonen, C. W. in *Interventional Magnetic Resonance Imaging Medical Radiology* (eds Thomas Kahn & Harald Busse) Ch. 394, 349-366 (Springer Berlin Heidelberg, 2012).

79 Schmitz, A. C., Gianfelice, D., Daniel, B. L., Mali, W. P. & van den Bosch, M. A. Image-guided focused ultrasound ablation of breast cancer: current status, challenges, and future directions. *European radiology* **18**, 1431-1441, doi:10.1007/s00330-008-0906-0 (2008).

80 Brenin, D. Focused Ultrasound Ablation for the Treatment of Breast Cancer. *Ann Surg Oncol* **18**, 3088-3094, doi:10.1245/s10434-011-2011-x (2011).

81 Lynch, J. & Loeb, S. The role of high-intensity focused ultrasound in prostate cancer. *Curr Oncol Rep* **9**, 222-225, doi:10.1007/s11912-007-0025-0 (2007).

82 Komura, K. *et al.* Single session of high-intensity focused ultrasound for localized prostate cancer: treatment outcomes and potential effect as a primary therapy. *World J Urol*, 1-7, doi:10.1007/s00345-013-1215-z (2013).

83 Kopelman, D. & Papa, M. Magnetic Resonance–Guided Focused Ultrasound Surgery for the Noninvasive Curative Ablation of Tumors and Palliative Treatments: A Review. *Ann Surg Oncol* **14**, 1540-1550, doi:10.1245/s10434-006-9326-z (2007).

84 McDannold, N., Clement, G., Black, P., Jolesz, F. & Hynynen, K. Transcranial MRI-guided focused ultrasound surgery of brain tumors: Initial findings in three patients. *Neurosurgery* **66**, 323 (2010).

85 Jolesz, F. A. & McDannold, N. J. Magnetic resonance-guided focused ultrasound: a new technology for clinical neurosciences. *Neurologic clinics* **32**, 253-269, doi:10.1016/j.ncl.2013.07.008 (2014).

86 Martin, E. & Jolesz, F. in *Tumors of the Central Nervous system, Volume 3* Vol. 3 *Tumors of the Central Nervous System* (ed M. A. Hayat) Ch. 23, 227-236 (Springer Netherlands, 2011).

87 Mylonas, N. & Damianou, C. MR compatible positioning device for guiding a focused ultrasound system for the treatment of brain deseases. *The International Journal of Medical Robotics and Computer Assisted Surgery* **10**, 1-10, doi:10.1002/rcs.1501 (2014).

88 Martin, E. & Werner, B. Focused ultrasound surgery of the brain. *Current Radiology Reports* **1**, 126-135 (2013).

89 Jolesz, F. & McDannold, N. in *Intraoperative Imaging and Image-Guided Therapy* (ed Ferenc A. Jolesz) Ch. 28, 403-412 (Springer New York, 2014).

90 Mentlein, R., Hattermann, K. & Held-Feindt, J. in *Trends in Stem Cell Proliferation and Cancer Research* (eds Rodrigo R. Resende & Henning Ulrich) Ch. 13, 339-358 (Springer Netherlands, 2013).

91 Network, T. C. Corrigendum: Comprehensive genomic characterization defines human glioblastoma genes and core pathways. *Nature* **494**, 506, doi:10.1038/nature11903 (2013).

92 Tamamis, P. & Floudas, C. A. Elucidating a Key Component of Cancer Metastasis: CXCL12 (SDF-1alpha) Binding to CXCR4. *Journal of chemical information and modeling* **54**, 1174-1188, doi:10.1021/ci500069y (2014).

93 Balabanian, K. *et al.* The chemokine SDF-1/CXCL12 binds to and signals through the orphan receptor RDC1 in T lymphocytes. *The Journal of biological chemistry* **280**, 35760-35766, doi:10.1074/jbc.M508234200 (2005).

94 Levoye, A., Balabanian, K., Baleux, F., Bachelerie, F. & Lagane, B. CXCR7 heterodimerizes with CXCR4 and regulates CXCL12-mediated G protein signaling. *Blood* **113**, 6085-6093, doi:10.1182/blood-2008-12-196618 (2009).

95 Sun, X. *et al.* CXCL12 / CXCR4 / CXCR7 chemokine axis and cancer progression. *Cancer metastasis reviews* **29**, 709-722, doi:10.1007/s10555-010-9256-x (2010).

96 Duda, D. G. *et al.* CXCL12 (SDF1alpha)-CXCR4/CXCR7 pathway inhibition: an emerging sensitizer for anticancer therapies? *Clinical cancer research : an official journal of the American Association for Cancer Research* **17**, 2074-2080, doi:10.1158/1078-0432.ccr-10-2636 (2011).

97 Hawkins, O. E. & Richmond, A. The dynamic yin-yang interaction of CXCR4 and CXCR7 in breast cancer metastasis. *Breast cancer research : BCR* **14**, 103, doi:10.1186/bcr3092 (2012).

98 Walentowicz-Sadlecka, M. *et al.* Stromal derived factor-1 (SDF-1) and its receptors CXCR4 and CXCR7 in endometrial cancer patients. *PloS one* **9**, e84629, doi:10.1371/journal.pone.0084629 (2014).

99 Hernandez, L., Magalhaes, M. A., Coniglio, S. J., Condeelis, J. S. & Segall, J. E. Opposing roles of CXCR4 and CXCR7 in breast cancer metastasis. *Breast cancer research : BCR* **13**, R128, doi:10.1186/bcr3074 (2011).

100 Romain, B. *et al.* Hypoxia differentially regulated CXCR4 and CXCR7 signaling in colon cancer. *Molecular cancer* **13**, 58, doi:10.1186/1476-4598-13-58 (2014).

101 Heinrich, E. L., Lee, W., Lu, J., Lowy, A. M. & Kim, J. Chemokine CXCL12 activates dual CXCR4 and CXCR7-mediated signaling pathways in pancreatic cancer cells. *Journal of translational medicine* **10**, 68, doi:10.1186/1479-5876-10-68 (2012).

102 Shimizu, N. *et al.* A putative G protein-coupled receptor, RDC1, is a novel coreceptor for human and simian immunodeficiency viruses. *Journal of virology* **74**, 619-626 (2000).

103 Feng, Y., Broder, C. C., Kennedy, P. E. & Berger, E. A. HIV-1 entry cofactor: functional cDNA cloning of a seven-transmembrane, G protein-coupled receptor. *Science (New York, N.Y.)* **272**, 872-877 (1996).

104 Endres, M. J. *et al.* CD4-independent infection by HIV-2 is mediated by fusin/CXCR4. *Cell* **87**, 745-756 (1996).

105 Chow, K. Y. *et al.* A pivotal role for CXCL12 signaling in HPV-mediated transformation of keratinocytes: clues to understanding HPV-pathogenesis in WHIM syndrome. *Cell host & microbe* **8**, 523-533, doi:10.1016/j.chom.2010.11.006 (2010).

106 Cancian, L., Bosshard, R., Lucchesi, W., Karstegl, C. E. & Farrell, P. J. C-terminal region of EBNA-2 determines the superior transforming ability of type 1 Epstein-Barr virus by enhanced gene regulation of LMP-1 and CXCR7. *PLoS pathogens* **7**, e1002164, doi:10.1371/journal.ppat.1002164 (2011).

107 Raggo, C. *et al.* Novel cellular genes essential for transformation of endothelial cells by Kaposi's sarcoma-associated herpesvirus. *Cancer research* **65**, 5084-5095, doi:10.1158/0008-5472.can-04-2822 (2005).

108 Jin, Z. *et al.* CXCR7 is inducible by HTLV-1 Tax and promotes growth and survival of HTLV-1-infected T cells. *International journal of cancer. Journal international du cancer* **125**, 2229-2235, doi:10.1002/ijc.24612 (2009).

109 Bleul, C. C. *et al.* The lymphocyte chemoattractant SDF-1 is a ligand for LESTR/fusin and blocks HIV-1 entry. *Nature* **382**, 829-833, doi:10.1038/382829a0 (1996).

110 Veldkamp, C. T. *et al.* Structural basis of CXCR4 sulfotyrosine recognition by the chemokine SDF-1/CXCL12. *Science signaling* **1**, ra4, doi:10.1126/scisignal.1160755 (2008).

111 Libert, F. *et al.* Selective amplification and cloning of four new members of the G protein-coupled receptor family. *Science (New York, N.Y.)* **244**, 569-572 (1989).

112 Libert, F., Parmentier, M., Lefort, A., Dumont, J. E. & Vassart, G. Complete nucleotide sequence of a putative G protein coupled receptor: RDC1. *Nucleic acids research* **18**, 1917 (1990).

113 Sreedharan, S. P., Robichon, A., Peterson, K. E. & Goetzl, E. J. Cloning and expression of the human vasoactive intestinal peptide receptor. *Proceedings of the National Academy of Sciences of the United States of America* **88**, 4986-4990 (1991).

114 Nagata, S. *et al.* RDC1 may not be VIP receptor. *Trends in pharmacological sciences* **13**, 102-103 (1992).

115 Cook, J. S. *et al.* Characterization of the RDC1 gene which encodes the canine homolog of a proposed human VIP receptor. Expression does not correlate with an increase in VIP binding sites. *FEBS letters* **300**, 149-152 (1992).

116 Law, N. M. & Rosenzweig, S. A. Characterization of the G-protein linked orphan receptor GPRN1/RDC1. *Biochemical and biophysical research communications* **201**, 458-465, doi:10.1006/bbrc.1994.1723 (1994).

117 Rajagopal, S. *et al.* Beta-arrestin- but not G protein-mediated signaling by the "decoy" receptor CXCR7. *Proceedings of the National Academy of Sciences of the United States of America* **107**, 628-632, doi:10.1073/pnas.0912852107 (2010).

118 Lipfert, J., Odemis, V., Wagner, D. C., Boltze, J. & Engele, J. CXCR4 and CXCR7 form a functional receptor unit for SDF-1/CXCL12 in primary rodent microglia. *Neuropathology and applied neurobiology* **39**, 667-680, doi:10.1111/nan.12015 (2013).

119 Infantino, S., Moepps, B. & Thelen, M. Expression and regulation of the orphan receptor RDC1 and its putative ligand in human dendritic and B cells. *Journal of immunology (Baltimore, Md. : 1950)* **176**, 2197-2207 (2006).

120 Sierro, F. *et al.* Disrupted cardiac development but normal hematopoiesis in mice deficient in the second CXCL12/SDF-1 receptor, CXCR7. *Proceedings of the National Academy of Sciences* **104**, 14759-14764, doi:10.1073/pnas.0702229104 (2007).

121 Shimizu, S., Brown, M., Sengupta, R., Penfold, M. E. & Meucci, O. CXCR7 protein expression in human adult brain and differentiated neurons. *PloS one* **6**, e20680, doi:10.1371/journal.pone.0020680 (2011).

122 Liberman, J. *et al.* Involvement of the CXCR7/CXCR4/CXCL12 axis in the malignant progression of human neuroblastoma. *PloS one* **7**, e43665, doi:10.1371/journal.pone.0043665 (2012).

123 Liu, Z. *et al.* Expression of stromal cell-derived factor 1 and CXCR7 in papillary thyroid carcinoma. *Endocrine pathology* **23**, 247-253, doi:10.1007/s12022-012-9223-x (2012).

124 Schutyser, E. *et al.* Hypoxia enhances CXCR4 expression in human microvascular endothelial cells and human melanoma cells. *European cytokine network* **18**, 59-70, doi:10.1684/ecn.2007.0087 (2007).

125 Williams, J. L., Patel, J. R., Daniels, B. P. & Klein, R. S. Targeting CXCR7/ACKR3 as a therapeutic strategy to promote remyelination in the adult central nervous system. *The Journal of experimental medicine* **211**, 791-799, doi:10.1084/jem.20131224 (2014).

126 Spear, M. A. *et al.* Isolation, characterization, and recovery of small peptide phage display epitopes selected against viable malignant glioma cells. *Cancer gene therapy* **8**, 506-511, doi:10.1038/sj.cgt.7700334 (2001).

127 Samoylova, T. I. *et al.* Phage probes for malignant glial cells. *Molecular cancer therapeutics* **2**, 1129-1137 (2003).

128 Romanov, V. I., Durand, D. B. & Petrenko, V. A. Phage display selection of peptides that affect prostate carcinoma cells attachment and invasion. *The Prostate* **47**, 239-251, doi:10.1002/pros.1068 (2001).

129 Jayanna, P. K., Bedi, D., Deinnocentes, P., Bird, R. C. & Petrenko, V. A. Landscape phage ligands for PC3 prostate carcinoma cells. *Protein engineering, design & selection : PEDS* **23**, 423-430, doi:10.1093/protein/gzq011 (2010).

130 Sun, J. *et al.* A novel mouse CD133 binding-peptide screened by phage display inhibits cancer cell motility in vitro. *Clinical & experimental metastasis* **29**, 185-196, doi:10.1007/s10585-011-9440-6 (2012).

131 Dong, J., Liu, W., Jiang, A., Zhang, K. & Chen, M. A novel peptide, selected from phage display library of random peptides, can efficiently target into human breast cancer cell. *Chin. Sci. Bull.* **53**, 860-867, doi:10.1007/s11434-008-0162-3 (2008).

132 Shukla, G. S. & Krag, D. N. Cancer cell-specific internalizing ligands from phage displayed beta-lactamase-peptide fusion libraries. *Protein engineering, design & selection : PEDS* **23**, 431-440, doi:10.1093/protein/gzq013 (2010).

133 Zhang, W. J. *et al.* Affinity peptide developed by phage display selection for targeting gastric cancer. *World journal of gastroenterology : WJG* **18**, 2053-2060, doi:10.3748/wjg.v18.i17.2053 (2012).

134 Soendergaard M, N.-N. J., Palmier MO, Deutscher SL. Peptide Phage Display for Discovery of Novel Biomarkers for Imaging and Therapy of Cell Subpopulations in Ovarian Cancer. *J Mol Biomark Diagn*, 7 (2011).

135 Bockmann, M. *et al.* Novel SRESPHP peptide mediates specific binding to primary medullary thyroid carcinoma after systemic injection. *Human gene therapy* **16**, 1267-1275, doi:10.1089/hum.2005.16.1267 (2005).

136 Bachmair, A., Finley, D. & Varshavsky, A. In vivo half-life of a protein is a function of its amino-terminal residue. *Science (New York, N.Y.)* **234**, 179-186 (1986).

137 Gonda, D. K. *et al.* Universality and structure of the N-end rule. *The Journal of biological chemistry* **264**, 16700-16712 (1989).

138 Tobias, J. W., Shrader, T. E., Rocap, G. & Varshavsky, A. The N-end rule in bacteria. *Science (New York, N.Y.)* **254**, 1374-1377 (1991).

139 Guruprasad, K., Reddy, B. V. & Pandit, M. W. Correlation between stability of a protein and its dipeptide composition: a novel approach for predicting in vivo stability of a protein from its primary sequence. *Protein engineering* **4**, 155-161 (1990).

140 Ikai, A. Thermostability and aliphatic index of globular proteins. *Journal of biochemistry* **88**, 1895-1898 (1980).

141 Idicula-Thomas, S. & Balaji, P. V. Understanding the relationship between the primary structure of proteins and its propensity to be soluble on overexpression in Escherichia coli. *Protein science : a publication of the Protein Society* **14**, 582-592, doi:10.1110/ps.041009005 (2005).

142 Kyte, J. & Doolittle, R. F. A simple method for displaying the hydropathic character of a protein. *Journal of molecular biology* **157**, 105-132 (1982).

143 Kalatskaya, I. *et al.* AMD3100 is a CXCR7 ligand with allosteric agonist properties. *Molecular pharmacology* **75**, 1240-1247, doi:10.1124/mol.108.053389 (2009).

144 Miao, Z. *et al.* CXCR7 (RDC1) promotes breast and lung tumor growth in vivo and is expressed on tumor-associated vasculature. *Proceedings of the National Academy of Sciences of the United States of America* **104**, 15735-15740, doi:10.1073/pnas.0610444104 (2007).

145 Stafford, R. J. & Ahrar, K. in *Interventional Magnetic Resonance Imaging Medical Radiology* (eds Thomas Kahn & Harald Busse) Ch. 629, 253-269 (Springer Berlin Heidelberg, 2012).

146 Rezler, E. M., Khan, D. R., Tu, R., Tirrell, M. & Fields, G. B. Peptide-mediated targeting of liposomes to tumor cells. *Methods in molecular biology (Clifton, N.J.)* **386**, 269-298, doi:10.1007/978-1-59745-430-8_10 (2007).

147 Tang, Q., Cao, B., Wu, H. & Cheng, G. Cholesterol-Peptide Hybrids to Form Liposome-Like Vesicles for Gene Delivery. *PloS one* **8**, e54460, doi:10.1371/journal.pone.0054460 (2013).

148 Zhou, Z. *et al.* Liposomal formulation of amphiphilic fullerene antioxidants. *Bioconjugate chemistry* **21**, 1656-1661, doi:10.1021/bc1001664 (2010).

149 Langereis, S., Geelen, T., Grull, H., Strijkers, G. J. & Nicolay, K. Paramagnetic liposomes for molecular MRI and MRI-guided drug delivery. *NMR in biomedicine* **26**, 728-744, doi:10.1002/nbm.2971 (2013).

150 van Woensel, M. *et al.* Formulations for Intranasal Delivery of Pharmacological Agents to Combat Brain Disease: A New Opportunity to Tackle GBM? *Cancers* **5**, 1020-1048, doi:10.3390/cancers5031020 (2013).

151 Grull, H. & Langereis, S. Hyperthermia-triggered drug delivery from temperature-sensitive liposomes using MRI-guided high intensity focused ultrasound. *Journal of controlled release : official journal of the Controlled Release Society* **161**, 317-327, doi:10.1016/j.jconrel.2012.04.041 (2012).

152 Gray, B. P., Li, S. & Brown, K. C. From phage display to nanoparticle delivery: functionalizing liposomes with multivalent peptides improves targeting to a cancer biomarker. *Bioconjugate chemistry* **24**, 85-96, doi:10.1021/bc300498d (2013).

153 Mikhaylov, G. *et al.* Ferri-liposomes as an MRI-visible drug-delivery system for targeting tumours and their microenvironment. *Nature nanotechnology* **6**, 594-602, doi:10.1038/nnano.2011.112 (2011).

154 Mohammad, F., Balaji, G., Weber, A., Uppu, R. M. & Kumar, C. S. Influence of Gold Nanoshell on Hyperthermia of Super Paramagnetic Iron Oxide Nanoparticles (SPIONs). *The journal of physical chemistry. C, Nanomaterials and interfaces* **114**, 19194-19201, doi:10.1021/jp105807r (2010).

155 Cho, S. K. *et al.* Functionalized gold nanorods for thermal ablation treatment of bladder cancer. *Journal of biomedical nanotechnology* **10**, 1267-1276 (2014).

156 Hattermann, K. *et al.* Effects of the chemokine CXCL12 and combined internalization of its receptors CXCR4 and CXCR7 in human MCF-7 breast cancer cells. *Cell and tissue research*, doi:10.1007/s00441-014-1823-y (2014).

157 Burns, J., Summers, B., Howard, M. & Schall, T. (Google Patents, 2004).

158 Heesen, M. *et al.* Cloning and chromosomal mapping of an orphan chemokine receptor: mouse RDC1. *Immunogenetics* **47**, 364-370, doi:10.1007/s002510050371 (1998).

159 Rapp, C., Snow, S., Laufer, T. & McClendon, C. L. The role of tyrosine sulfation in the dimerization of the CXCR4:SDF-1 complex. *Protein science : a publication of the Protein Society* **22**, 1025-1036, doi:10.1002/pro.2288 (2013).

160 Farzan, M. *et al.* The role of post-translational modifications of the CXCR4 amino terminus in stromal-derived factor 1 alpha association and HIV-1 entry. *The Journal of biological chemistry* **277**, 29484-29489, doi:10.1074/jbc.M203361200 (2002).

161 Choe, H. & Farzan, M. Chapter 7. Tyrosine sulfation of HIV-1 coreceptors and other chemokine receptors. *Methods in enzymology* **461**, 147-170, doi:10.1016/s0076-6879(09)05407-x (2009).

162 Altenburg, J. D. *et al.* A naturally occurring splice variant of CXCL12/stromal cell-derived factor 1 is a potent human immunodeficiency virus type 1 inhibitor with weak chemotaxis and cell survival activities. *Journal of virology* **81**, 8140-8148, doi:10.1128/jvi.00268-07 (2007).

163 Ma, W., Liu, Y., Ellison, N. & Shen, J. Induction of C-X-C chemokine receptor type 7 (CXCR7) switches stromal cell-derived factor-1 (SDF-1) signaling and phagocytic activity in macrophages linked to atherosclerosis. *The Journal of biological chemistry* **288**, 15481-15494, doi:10.1074/jbc.M112.445510 (2013).

164 Bianco, A. M. *et al.* CXCR7 and CXCR4 Expressions in Infiltrative Astrocytomas and Their Interactions with HIF1alpha Expression and IDH1 Mutation. *Pathology oncology research : POR*, doi:10.1007/s12253-014-9813-7 (2014).

165 Decaillot, F. M. *et al.* CXCR7/CXCR4 heterodimer constitutively recruits beta-arrestin to enhance cell migration. *The Journal of biological chemistry* **286**, 32188-32197, doi:10.1074/jbc.M111.277038 (2011).

166 Sánchez-Alcañiz, J. A. *et al.* Cxcr7 Controls Neuronal Migration by Regulating Chemokine Responsiveness. *Neuron* **69**, 77-90, doi:http://dx.doi.org/10.1016/j.neuron.2010.12.006 (2011).

167 Lee, S., Ashizawa, A. T., Kim, K. S., Falk, D. J. & Notterpek, L. Liposomes to target peripheral neurons and Schwann cells. *PloS one* **8**, e78724, doi:10.1371/journal.pone.0078724 (2013).

168 Nie, Y. *et al.* Cholesterol derivatives based charged liposomes for doxorubicin delivery: preparation, in vitro and in vivo characterization. *Theranostics* **2**, 1092-1103, doi:10.7150/thno.4949 (2012).

169 Tseng, L., Liang, H., Chung, T., Huang, Y. & Liu, D. Liposomes incorporated with cholesterol for drug release triggered by magnetic field. *Journal of Medical and Biological Engineering* **27**, 29 (2007).

170 Evjen, T. J. *et al.* In vivo monitoring of liposomal release in tumours following ultrasound stimulation. *European Journal of Pharmaceutics and Biopharmaceutics* **84**, 526-531 (2013).

General Reference Information, Protein PDB Structures, and Sequence Data

http://www.cancer.gov/

http://cancergenome.nih.gov/

http://www.cdc.gov/

http://www.genecards.org/

http://www.ncbi.nlm.nih.gov/

http://www.uniprot.org/uniprot/

http://www.rcsb.org/pdb/home/home.do

APPENDIX A

3D MOLECULAR MODELS OF THE LIPOSOME COMPONENTS (C-70 DERIVATIVE (ALM) AND EGG-PC) IN THIN-TUBE MODE AND CPK COLOR SCHEME

The C-70 fullerene model measured ~8.0Å long by ~6.5Å wide. This measurement is consistent with the elongated structure of C-70 fullerenes relative to the spherical shapes of C-60 fullerenes. The assembled ALM model measured ~20Å long by 6.5Å wide as was similar in size to the egg-PC model that measured 19.7Å long by 5.5Å wide.

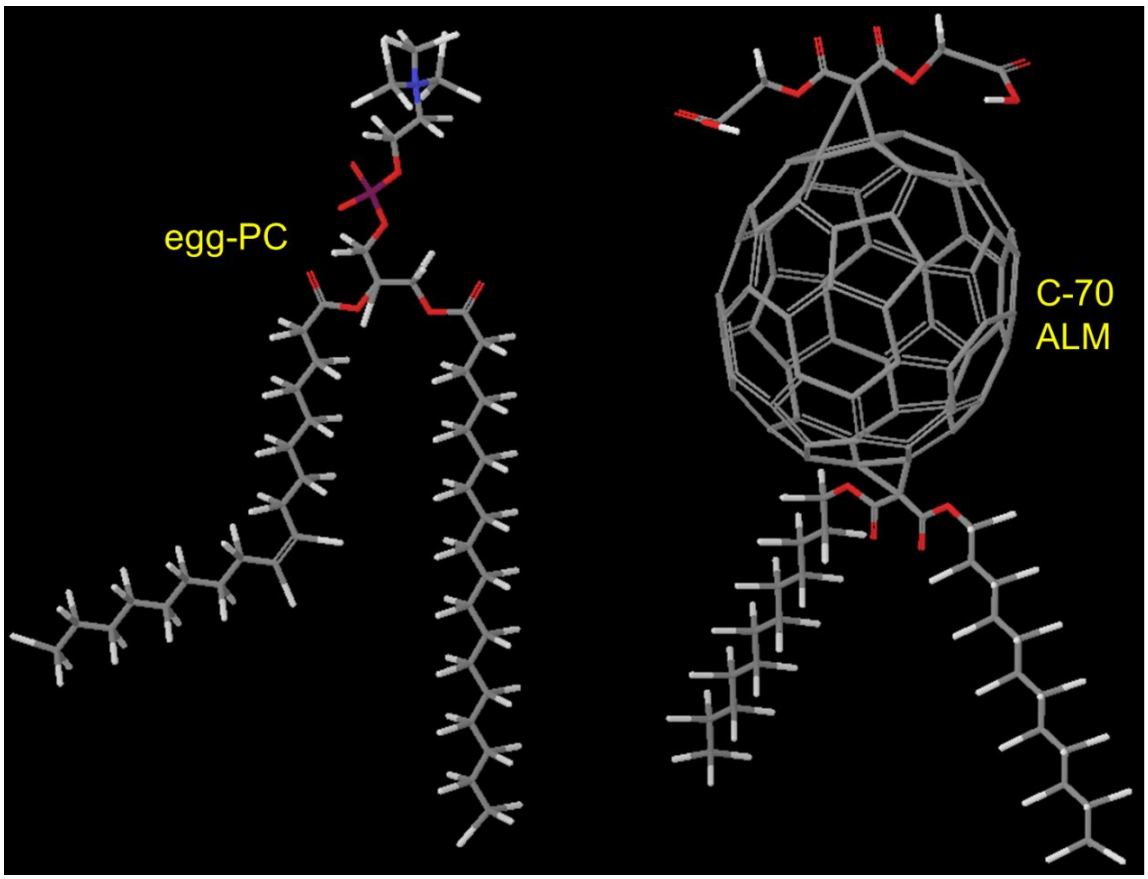

APPENDIX B

ALTERNATE VIEW OF THE 3D MOLECULAR MODELS OF THE LIPOSOME COMPONENTS IN APPENDIX A (C-70 DERIVATIVE (ALM) AND EGG-PC) IN SPACE-FILL MODE AND CPK COLOR SCHEME

The C-70 fullerene model measured ~8.0Å long by ~6.5Å wide. This measurement is consistent with the elongated structure of C-70 fullerenes relative to the spherical shapes of C-60 fullerenes. The assembled ALM model measured ~20Å long by 6.5Å wide as was similar in size to the egg-PC model that measured 19.7Å long by 5.5Å wide.

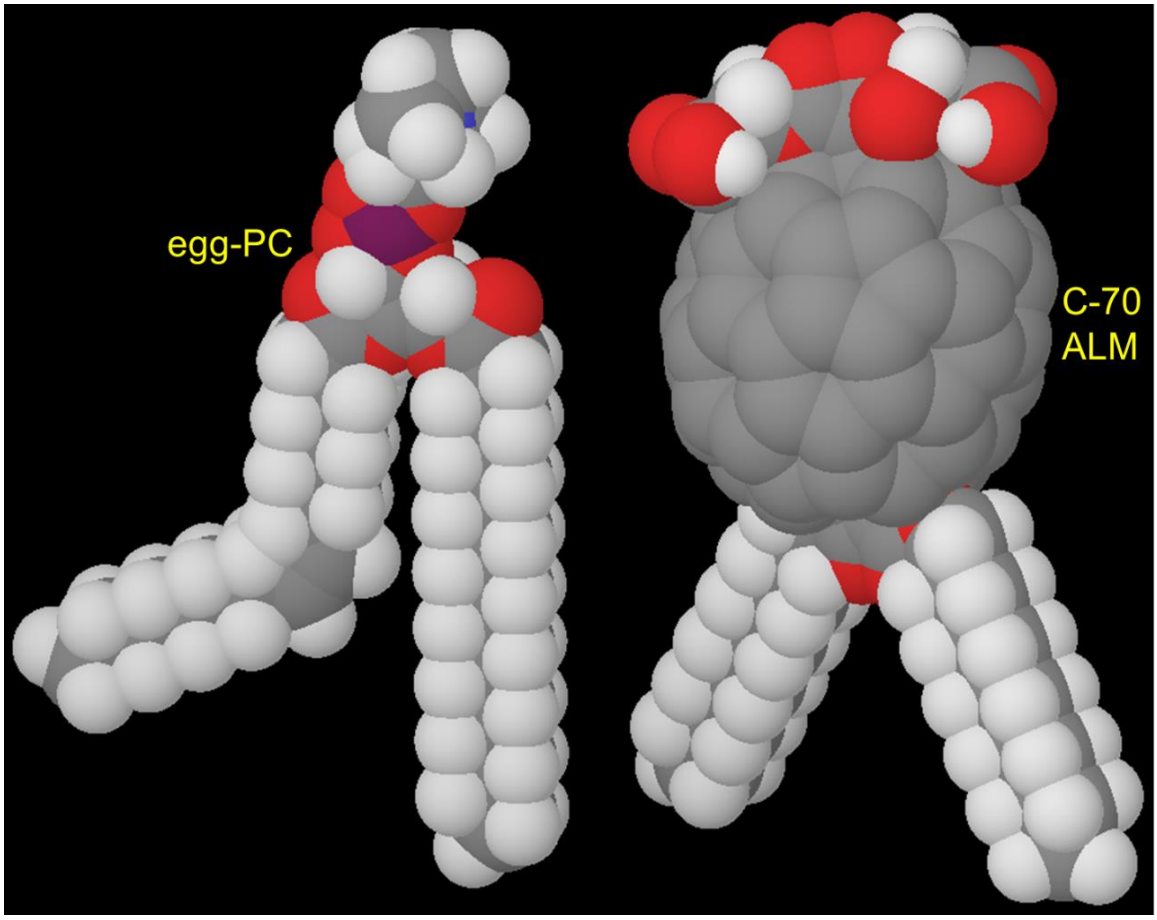

APPENDIX C

3D MOLECULAR MODELS OF THE LIPOSOME COMPONENTS IN APPENDIX A AND THE SELECTED PHAGE PEPTIDE SEQUENCES (P-3, P-9, AND P-20) IN THIN-TUBE MODE AND CPK COLOR SCHEME

The P-3 model measured ~28.5Å long by ~12.00Å wide. The P-9 model measured ~32.0Å long by ~10.00Å wide. The P-20 model measured ~27.5Å long by ~6.5Å wide. These measurements were similar to the ones observed for the assembled ALM model and the egg-PC model as seen in Appendix A.

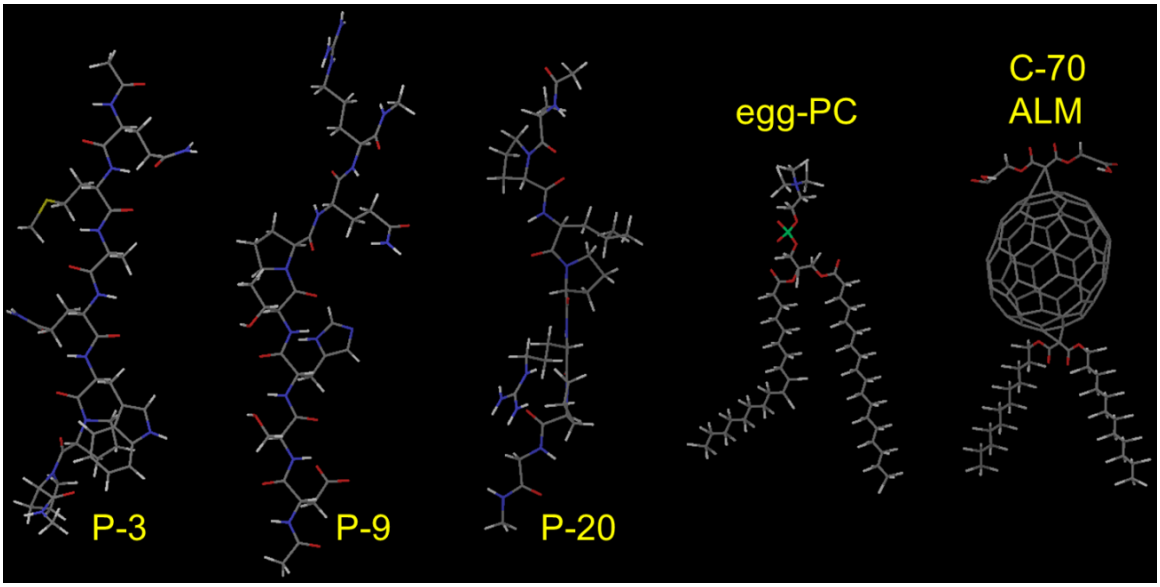

APPENDIX D

3D MOLECULAR MODELS OF THE LIPOSOME COMPONENTS IN APPENDIX A AND THE SELECTED PHAGE PEPTIDE SEQUENCES (P-3, P-9, AND P-20) IN APPENDIX C IN SPACE-FILL MODE AND CPK COLOR SCHEME

The P-3 model measured ~28.5Å long by ~12.00Å wide. The P-9 model measured ~32.0Å long by ~10.00Å wide. The P-20 model measured ~27.5Å long by ~6.5Å wide. These measurements were similar to the ones observed for the assembled ALM model and the egg-PC model as seen in Appendix A.